University of Eastern Piedmont
Department of Health Sciences
Ph.D. Program in Food, Health & Longevity
XXXVII Cycle

Leveraging Advanced Technologies to Optimize *In Vitro* Biophysical Stimulation Experiments

S.S.D. MED/50

Candidate: Farah Daou

Tutor: Dr. Andrea Cochis
Supervisor: Prof. Lia Rimondini
Coordinator: Prof. Antonia Follenzi

a.a. 2024/2025

Dedication

To Professor Lia Rimondini and Dr. Andrea Cochis, who gave me the opportunity to conduct research in the "T**i**ssue E**n**gineering a**n**d Bi**o**materials E**v**alu**ation (INNOVATION)"** laboratory at the Center of Excellence for Translational Research on Autoimmune and Allergic Diseases (CAAD), a research center of the University of Eastern Piedmont (UPO), Novara, Italy.

To my husband, Giuseppe Mento, whose patience, support, and encouragement were essential in helping me balance my personal and research lives. His belief in my abilities and his gentle nudges to keep going, even when I doubted myself, were invaluable throughout this journey.

To my cousins, Ziad Masri, Wael Masri, Mansour Daou, and Lara Masri, and to my friend, Raidan Alaridi, who guided me through this significant life transition, as I moved to a new country and embarked on a new scientific journey.

To my parents, especially my father, who ignited my curiosity.

To my family and friends for their unwavering love and support.

To my professors at the American University of Science & Technology (AUST), Beirut, Lebanon, especially Dr. Daniel Badro. I am indebted to them for nurturing the ethical and skilled scientist within me.

To my country, Lebanon, whose resilience in the face of great challenges has shaped me into a strong and persevering individual who values the simple joys of life.

Contents

Abstract 7

General Introduction 10

An automated 3D-printed perfusion bioreactor combinable with pulsed electromagnetic field stimulators for bone tissue investigations 19

1.1 Abstract 19

1.2 Introduction 19

1.3 Materials and Methods 22

1.3.1 Bioreactor design, components and working principle 22

1.3.2 CFD simulations and wall shear stress estimation 25

1.3.3 Electromagnetic field simulations 27

1.3.4 3D bone tissue-like model preparation and culture under perfusion 28

1.3.5 Assessments of 3D bone tissue-like models cultured under perfusion 28

1.3.6 Combined bi-directional perfusion and PEMF stimulation culture and quantitative PCR analysis 29

1.3.7 Statistical analysis 30

1.4 Results 30

1.4.1 Preliminary bioreactor performance tests 30

1.4.2 CFD simulations and wall shear stress estimation 30

1.4.3 Electromagnetic field simulations 33

1.4.4 Assessments of 3D bone tissue-like models cultured under perfusion 34

1.4.5 Combined bi-directional perfusion and PEMF stimulation culture and quantitative PCR analysis 36

1.5 Discussion 37

1.6 Conclusions 41

1.7 Acknowledgments 42

1.8 References 43

In Vitro Reproduction of Trabecular Bone Microenvironment for Investigating the Effects of Pulsed Electromagnetic Field Stimulation on Human Mesenchymal Stem Cells 49

2.1 Abstract 49

2.2 Introduction 49
2.3 Materials and Methods 54
2.3.1 3D printing and characterization of the trabecular bone-like polylactic acid (PLA) scaffolds resembling the morphological features of the iliac crest (referred to as PLA600) 54
2.3.2 Parallelized, automated perfusion bioreactor equipped with PEMF stimulator 54
2.3.3 Trabecular bone-like tissue preparation and evaluation 55
2.3.4 Trabecular bone-like tissue stimulation using PEMF 57
2.4 Results 59
2.4.1 3D trabecular, bone-like tissues 59
2.4.2 The set-up of cell culture conditions 63
2.5 Discussion 65
2.6 Conclusions 67
2.7 Fundings 68
2.8 Acknowledgments 68
2.9 References 68
Unraveling the Transcriptome Profile of Pulsed Electromagnetic Field Stimulation in Bone Regeneration Using a Bioreactor-Based Investigation Platform 73
3.1 Abstract 73
3.2 Introduction 73
3.3 Materials and Methods 78
3.3.1 Trabecular bone-like tissue preparation using PLA600 scaffolds 78
3.3.2 Trabecular bone-like tissue culturing under three conditions 78
3.3.3 Transcriptomic studies: RNA-Sequencing (RNA-Seq) 78
3.3.4 Gene expression analyses 79
3.4 Results 81
3.4.1 Read processing and alignment 81
3.4.2 Differential expression analysis 82
3.4.3 Immune potential of PEMF stimulation 84
3.4.4 Angiogenic potential of PEMF stimulation 88
3.4.5 Osteoinductive potential of PEMF stimulation 88
3.4.6 Secondary pathways altered by PEMF stimulation 89
3.4.3 Validation of raw expression signals and differential gene expression 90
3.5 Discussion 92

3.6 Conclusions 94
3.7. Fundings 95
3.8 Acknowledgments 95
3.9 References 95
Upgrading the Automated Perfusion Bioreactor with Hydrostatic Pressure to Better Mimic Bone's Mechanical Environment 101
4.1 Abstract 101
4.2 Introduction 101
4.3 Materials and Methods 103
4.3.1 Parallelized, automated perfusion bioreactor equipped with pinch valves 103
4.3.2 PLA600 trabecular bone-like tissue culturing within the perfusion bioreactor equipped with pinch valves 105
4.4.3. Statistical analysis 106
4.4 Results 107
4.4.1 Hydrostatic pressure characterization using collagen-loaded PLA600 scaffolds 107
4.4.2 Cell viability and infiltration within the PLA600 scaffolds under three culture conditions 108
4.5 Discussion 111
4.6 Conclusions 112
4.7. Fundings 112
4.8 Acknowledgments 112
4.9 References 112
Synergistic Effects of Various Mechanical Cues on Mesenchymal Stem Cell Behavior in Engineered 3D Microenvironments 115
5.1 Abstract 115
5.2 Introduction 115
5.3 Materials and Methods 118
5.3.1 3D printing and characterization of the trabecular bone-like polylactic acid (PLA) scaffolds resembling the morphological features of bones, specifically the ulna, tibia, and femur (referred to as P3S3) 118
5.3.2 Parallelized, automated perfusion bioreactor equipped with pinch valves 118
5.3.3 P3S3 trabecular bone-like tissue preparation and evaluation within the perfusion bioreactor 118
5.3.4 P3S3 trabecular bone-like tissue culturing within the perfusion bioreactor equipped with pinch valves under a simulated rehabilitation program 120

5.3.4. Statistical analysis 122
5.4 Results 123
5.4.1 Cell viability and infiltration within the P3S3 scaffolds under dynamic culture conditions 123
5.4.2 Hydrostatic pressure characterization using collagen-loaded P3S3 scaffolds 126
5.4.3 Cell viability and infiltration within the P3S3 scaffolds under dynamic culture conditions simulating a rehabilitation program 126
5.4.4 Gene expression analysis of cells within the P3S3 under dynamic culture conditions simulating a rehabilitation program 128
5.5 Discussion 131
5.6 Conclusions 134
5.7. Fundings 134
5.8 Acknowledgments 134
5.9 References 134
Conclusion & Future Prospective 138
Fundings 140
Acknowledgments 141

Chapter I

Abstract

This thesis explores the application of advanced technologies to optimize *in vitro* experiments examining cellular responses to biophysical stimuli, particularly those involved in bone biology research. The first chapter introduces a novel automated perfusion bioreactor that integrates both fluid flow-induced shear stress and pulsed electromagnetic field (PEMF) stimulation for cultivating 3D bone tissue-like constructs. Computational simulations were employed to optimize the culture chamber design and predict the distribution of shear stress and magnetic fields within the commercial Bio-Oss scaffold. Preliminary biological experiments using human bone marrow-derived mesenchymal stem cells (BM-MSCs) evaluated the osteogenic potential of these stimuli. The second chapter describes the development of trabecular bone tissue-like models using 3D-printed polylactic acid (PLA) scaffolds and human BM-MSCs. The scaffolds, designed to mimic the morphological features of the iliac crest (referred to as PLA600), were subjected to fluid flow-induced shear stress and pulsed electromagnetic field (PEMF) stimulation. This chapter aimed to optimize the stability of BM-MSCs within the scaffolds and their sensitivity to PEMF stimulation by evaluating various cell seeding methods and culture media, respectively. The third chapter presents the employment of the optimal cell seeding method and cell culture medium to investigate the molecular and cellular effects of PEMF stimulation on BM-MSCs cultured under fluid flow-induced shear stress via transcriptomic studies. This chapter aimed to improve the understanding of the signaling pathways involved in the PEMF-induced bone healing. The fourth chapter presents an upgraded version of the automated perfusion bioreactor that provides intermittent hydrostatic pressure (simulating physiological loading and unloading), in addition to fluid flow-induced shear stress. PLA600 scaffolds seeded with BM-MSCs using the optimized experimental conditions described in Chapter two were also employed. This chapter aimed to evaluate cell viability under bone-tissue-like mechanical stimuli simulating physiological unloading. The fifth chapter presents the employment of a second type of 3D-printed biomimetic PLA scaffolds, designed to mimic the human trabecular bone architecture in physiological conditions and to resemble the morphological features of bones, specifically the ulna, tibia, and femur (referred to as P3S3). This chapter aims to evaluate cell viability within these new scaffolds under fluid flow-induced shear stress, both with and without intermittent hydrostatic pressure, using the automated perfusion bioreactor described in the previous Chapters. Additionally, the study investigated changes in gene expression levels induced by the introduction of intermittent hydrostatic pressure,

mimicking physiological loading experienced during an in-patient rehabilitation program. This multidisciplinary research offers novel insights into leveraging *in vitro* investigation platforms to explore the cellular and molecular effects of biophysical stimulation, enhancing the outcomes of *in vitro* studies and contributing to a reduction in animal use in research.

Sommario

Questa tesi esplora l'applicazione di tecnologie avanzate per ottimizzare esperimenti in vitro che esaminano le risposte cellulari agli stimoli biofisici, in particolare quelli coinvolti nella ricerca sulla biologia ossea. Il primo capitolo introduce un nuovo bioreattore di perfusione automatizzato che integra sia lo stress da taglio indotto dal flusso di fluido sia la stimolazione con campo elettromagnetico pulsato (PEMF) per coltivare costrutti simili a tessuto osseo 3D. Sono state impiegate simulazioni computazionali per ottimizzare la progettazione della camera di coltura e prevedere la distribuzione dello stress da taglio e dei campi magnetici all'interno dello scaffold commerciale Bio-Oss. Esperimenti biologici preliminari che utilizzano cellule staminali mesenchimali derivate dal midollo osseo umano (BM-MSC) hanno valutato il potenziale osteogenico di questi stimoli. Il secondo capitolo descrive lo sviluppo di modelli simili a tessuto osseo trabecolare utilizzando scaffold in acido polilattico (PLA) stampati in 3D e BM-MSC umane. Gli scaffold, progettati per imitare le caratteristiche morfologiche della cresta iliaca (denominati PLA600), sono stati sottoposti a sollecitazione di taglio indotta dal flusso di fluido e stimolazione con campo elettromagnetico pulsato (PEMF). Questo capitolo mirava a ottimizzare la stabilità delle BM-MSC all'interno degli scaffold e la loro sensibilità alla stimolazione PEMF valutando rispettivamente vari metodi di semina cellulare e terreni di coltura. Il terzo capitolo presenta l'impiego del metodo di semina cellulare ottimale e del terreno di coltura cellulare per studiare gli effetti molecolari e cellulari della stimolazione PEMF sulle BM-MSC coltivate sotto sollecitazione di taglio indotta dal flusso di fluido tramite studi trascrittomici. Questo capitolo mirava a migliorare la comprensione dei percorsi di segnalazione coinvolti nella guarigione ossea indotta da PEMF. Il quarto capitolo presenta una versione aggiornata del bioreattore di perfusione automatizzato che fornisce pressione idrostatica intermittente (simulando carico e scarico fisiologici), oltre alla sollecitazione di taglio indotta dal flusso di fluido. Sono stati impiegati anche scaffold PLA600 seminati con BM-MSC utilizzando le condizioni sperimentali ottimizzate descritte nel Capitolo due. Questo capitolo mirava a valutare la vitalità cellulare sotto stimoli meccanici simili a quelli del tessuto osseo che simulavano lo scarico fisiologico. Il quinto capitolo presenta l'impiego di un secondo tipo di scaffold PLA biomimetici stampati in 3D, progettati per imitare l'architettura ossea trabecolare umana in condizioni fisiologiche e per assomigliare alle caratteristiche morfologiche delle ossa, in particolare ulna, tibia e femore (denominati P3S3). Questo capitolo mira a valutare la vitalità cellulare all'interno di questi nuovi scaffold sotto stress di taglio indotto dal flusso di fluido, sia con che senza pressione idrostatica intermittente, utilizzando il bioreattore di perfusione automatizzato descritto nei capitoli precedenti. Inoltre, lo studio ha esaminato i cambiamenti nei livelli di espressione genica indotti dall'introduzione di pressione idrostatica intermittente, imitando il carico fisiologico sperimentato durante un programma di riabilitazione ospedaliera. Questa ricerca multidisciplinare offre nuove intuizioni sullo sfruttamento delle piattaforme di indagine in vitro per esplorare gli effetti cellulari e molecolari della stimolazione biofisica, migliorando i risultati degli studi in vitro e contribuendo a ridurre l'uso di animali nella ricerca.

Chapter II

General Introduction

The use of animals in science has been a complex subject, sparkling philosophical and ethical debates. For instance, René Descartes (1596-1650) famously viewed animals as mere machines, lacking consciousness or sentience. In contrast, Baruch Spinoza (1632–1677) argued that while animals are sentient, humans have a right to use them for their benefit since their nature is different from that of humans. Voltaire (1694–1778), Jean-Jacques Rousseau's (1712–1778), Jeremy Bentham's (1748–1832), and Arthur Schopenhauer's (1788–1860) countered that animals are capable of suffering, despite lacking reason or speech, and should not be treated as mere means to an end [1]. The Cruelty to Animals Act passed in Great Britain in 1876 marked a pivotal milestone as it established the world's first legislation regulating the use of animals in scientific research [2]. However, the utilitarian principle, aiming for the greatest good for the greatest number, has been invoked to justify animal use in scientific research on the grounds of potential human benefit. This perspective continues to underpin the ethical framework today in many parts of the world where scientific research using animals is subject to effective regulation [2].

Public concerns about animal experimentation first emerged at the Annual Meeting of the British Medical Association (BMA) in 1874. This ignited the antivivisection movement, leading to calls for legislation to ban animal experimentation and the formation of antivivisection organizations within months. Similar movements began in the United States, culminating in the establishment of the American Anti-Vivisection Society in 1883. While the First World War temporarily dampened this debate, it did not extinguish it. In the 1970s, antivivisection and animal welfare groups united to advocate for new legislation governing animal research and testing. These organizations can be categorized into three primary groups: legitimate animal welfare organizations, mainstream antivivisection groups, and animal rights activists [3]. The escalating incidents against researchers by animal rights activists, from 6-27 events per year (1993–1997) to 76-103 per year (2003–2006), underscore the urgent need to integrate a comprehensive understanding of biomedical research into the educational system [4]. The scientific community and some pharmaceutical trade associations responded by establishing organizations to represent their perspectives in public and political debates. In response, the campaigns of the animal rights movement have ranged from peaceful and legitimate protests to illegal and dangerous acts, such as the sending of letter bombs. These campaigns have had some successes: a small laboratory dog breeder near Hereford, UK, closed in 1997, followed by Hillgrove Farm (a cat breeder) in 1999, as well as Shamrock Farm (a primate supplier) and Regal Rabbits in 2000. However, various political

factors have prevented them from achieving their ultimate goal of shutting down Huntingdon Life Sciences (HLS), Europe's largest contract research company [5]. Understanding public perceptions of animal use in scientific research requires delving into two central arguments: the ethical considerations surrounding animal welfare and the necessity of animal research.

Regarding animal welfare, it is worth noting that scientists have developed alternative methods to replace, reduce, or refine animal use, and have implemented welfare improvements, such as the use of anesthetics, analgesics, humane endpoints, and environmental enrichment [5]. A prime example is the 3Rs principles (Replacement, Reduction, and Refinement) introduced in 1959 by English biologists William Russell and Rex Burch in their book "The Principles of Humane Experimental Technique." [6] Aligned with the 3Rs principles, the Center for Alternatives to Animal Testing (CAAT) was established in 1981 at Johns Hopkins University in Baltimore, USA, primarily focused on finding methods to replace animals in cosmetics safety testing. Acknowledging the difficulty of completely replacing animals in research, CAAT emphasized the importance of reduction and refinement. In 1993, they organized the First World Conference on the 3Rs, which has been held every 2-3 years since. Recognizing the need for further action, the British Government launched the National Centre for the 3Rs (NC3Rs – www.nc3rs.org.uk) in 2004, aiming to encourage scientists to adopt the 3Rs. This was followed by the establishment of similar national centers, mainly in European countries [2]. These efforts culminated in the passage of Directive 2010/63 on the Protection of Animals Used for Scientific Purposes by the European Parliament in 2010 which sets out strict guidelines related to animal welfare in research [7]. The directive aimed to elevate and standardize animal welfare and use practices across Europe [8].

While it may appear that the 3Rs principle inherently opposes the use of animals in research, its primary goal is to mitigate animal suffering by reducing or eliminating unnecessary or avoidable pain, fear, stress, anxiety, bodily discomfort, and other significant negative experiences inflicted on research animals [9]. Russel and Burch defined the 3Rs as follows: "*Replacement means the substitution for conscious living higher animals of insentient material. Reduction means reduction in the numbers of animals used to obtain information of a given amount and precision. Refinement means any decrease in the incidence or severity of inhumane procedures applied to those animals which still have to be used (p 64)*." [6] Although Russell and Burch emphasized that the primary objective of replacement is to minimize animal distress rather than to abolish animal use entirely, as argued also by Tannenbaum and Bennett (2015), critical questions persist [9]. Can animal models emulate specific features of human physiology and pathology? Do findings from animal studies reliably translate to humans? Given recent technological advancements, do the original definitions of the 3Rs accurately reflect the current landscape of scientific research?

To address these questions, we must first examine the data. The European Commission's 2019 report provides statistics on animal use for scientific purposes in the Member States of the European Union in 2015-2017. According to the report, in 2017, approximately 9.39 million animals were used for the first time in research and testing. Of these, around 1.3

million were employed for the creation and maintenance of genetically altered (GA) animal lines. Mice constituted the most used species (61%), followed by fish (13%), rats (12%), other mammals (8%), and birds (6%). Amphibians, cephalopods, and reptiles accounted for less than 0.3% of the total, as did dogs, cats, and non-human primates, which are of particular public concern. The main areas of animal use were basic research (45%), translational/applied research (23%), and regulatory use to satisfy the requirements of certain legislations (23%). Severity assessment revealed that 51% of all uses were classified as ‘mild’, 32% as ‘moderate’, 11% as ‘severe’, and 6% involved ‘non-recovery procedures’. Notably, only 2% of all animals used were reused [10]. To determine the justifiability of these relatively high numbers, we can examine the translational impact.

Several studies have reported low animal-to-human translational success rates, a phenomenon often termed "translational failure." A recent umbrella review revealed that surprisingly 50% of therapies across various biomedical fields (range: 34% to 100%) transitioned from animal studies to early-phase human clinical trials. Furthermore, 40% of these therapies progressed to the more rigorous randomized controlled trial (RCT) stage (range: 29% to 62%). However, a strikingly low proportion, only 5% overall (range: 0% to 20%), achieved regulatory approval. Factors hindering translation include biological discrepancies between animals and humans, poor methodological quality in both animal and human studies, a disconnect between animal studies and clinical trials, the stringent requirements of RCTs and regulatory approval [11], as well as publication bias and insufficient reporting of details of animals, methods, and materials [12]. A previous narrative review highlighted that in drug development the translation failure is over 92%. This high rate of failure has been attributed to the limitations of animal models in accurately replicating human diseases. The authors advocate for a paradigm shift in biomedical research, urging researchers and regulatory agencies to adopt alternatives to animal testing for predicting human responses[13]. The field of tissue engineering follows the same pattern in terms of clinical translation [14,15].

These numbers raise serious questions about the necessity of animal research. High rates of translational failure suggest that current animal research methods may not be as effective as intended for biomedical research, particularly in drug development and medical device innovation. However, researchers often choose animal studies for reasons beyond scientific necessity. This phenomenon is known as "animal methods bias" in research and publishing. While the publishing process is essential for scientific advancement, it can be influenced by biases, such as a preference for animal-based experiments. This bias can affect the likelihood of a study being published and a grant application being accepted. It can also hinder the adoption of non-animal research methods, which offer potential benefits for preclinical studies [16]. A recent survey found that researchers frequently feel pressured to include animal experiments in their studies, even when they believe it was unnecessary, due to reviewer requests and potential career consequences [17]. To address this issue, editors, peer reviewers, and the scientific community must be educated about animal methods bias, trained in evaluating non-animal research, and encouraged to adopt a more inclusive research environment that values diverse methodologies. Funding agencies should prioritize non-animal research and provide adequate resources to support its development and validation.

Researchers should also be empowered to say no to animal experiments when they believe they are unnecessary. Public advocacy for animal-free research can play a crucial role in driving change by demanding cruelty-free cosmetics, for instance, and supporting the shift towards animal-free research [16].

The high number of animals used in research and animal methods bias, coupled with limited clinical translation, has led regulatory agencies to partner with academia and industry to develop new approach models (NAMs). These NAMs encompass a range of alternatives to animal testing, including computational models (*in silico*), advanced cell culture techniques (such as cell and tissue cultures, organoids, organs-on-chip, and microphysiological systems), and the use of alternative organisms (such as lower vertebrates and invertebrates) [18,19].

There are numerous examples of NAMs that have received regulatory approval and contributed to the decrease in the use of animals in science. Notably, NAMs have been widely adopted in industrial chemical safety assessments, particularly for cosmetic ingredients. In the EU, Regulation (EC) No 1223/2009, enacted in 2009, prohibited the sale of new cosmetic products tested on animals [20]. While animal studies remain necessary for industrial chemical testing, growing concerns about the variability of animal data, time, cost, and ethical implications are driving stakeholders to embrace NAMs. This is especially true for compounds that are often not designed to be biologically active and for exposures that are generally unintentional and at lower levels [21]. One prominent example is the replacement of the Draize test with NAMs based on human cornea epithelium to assess eye irritation caused by chemicals and cosmetics [22]. Additionally, NAMs have been developed for skin sensitization testing [23]. The NAMs developed for cosmetic ingredients and industrial chemicals can also be applied for pesticide testing [24]. Computational models are another valuable tool, and several have been developed. For example, models that can predict interactions with the estrogen receptor or identify chemical-induced biological effects in human cells have been developed [21].

Similar to industrial practices, research is increasingly focused on minimizing animal testing. Given the known limitations of animal models in predicting human responses, there is a strong demand for rigorous evaluation of *in vitro* experiments. Technological advancements have led to the development of numerous preclinical *in vitro* assays that can contribute to the 3Rs: replacement, reduction, and refinement of animal use. The quality of *in vitro* models is based on their ability to accurately replicate the complexity of real physiological or pathological states, as this directly affects the value of the obtained data. While there is no single solution that satisfies all requirements, the development and application of these models can contribute to advancing research and reducing animal use in science. One significant advancement has been the transition from 2D cell cultures to 3D cell cultures and co-cultures to create *in vitro* tissue-like structures. 3D cell cultures can be broadly categorized into scaffold-free or scaffold-based culture systems, with scaffolds made from either natural or synthetic materials [25]. These models have been further refined by considering the mechanical cues that cells experience in their natural environments. Cells are physical entities that can sense and respond to local and global physical stimuli [26]. These physical stimuli

are tissue-specific and include compression, tension, and shear stress, yet cells can also respond to non-native stimuli, such as acoustic waves [27]. By combining efforts and technological tools, researchers have developed a wide range of engineered models for various diseases, including those of the heart, lung, intestine, liver, kidney, cartilage, skin, vascular, endocrine, musculoskeletal, and nervous systems, as well as models of infectious diseases and cancer [28]. These complex systems have also been employed for drug development and precision medicine [29]. Therefore, the development of advanced technologies, particularly those incorporating 3D cell culture and physical stimuli, offers a promising avenue for reducing animal use while ensuring scientific validity.

— THE PRIMARY AIM OF THIS THESIS IS TO INVESTIGATE THE INFLUENCE OF DIVERSE PHYSICAL STIMULI ON CELLULAR BEHAVIOR THROUGH ADVANCED *IN VITRO* MODELS INCORPORATING 3D TISSUE CONSTRUCTS, BIOREACTORS, AND CONTROLLED EXTERNAL PHYSICAL STIMULATION —

The main specific objectives are:

- Develop a novel automated perfusion bioreactor that integrates both fluid flow-induced shear stress and pulsed electromagnetic field (PEMF) stimulation to culture 3D bone tissue-like constructs.
- Optimize the culture conditions of trabecular bone tissue-like models resembling the morphological features of the iliac crest within the developed bioreactor-based technology to investigate the effects of PEMF stimulation on bone marrow-derived mesenchymal stem cells (BM-MSCs) behavior.
- Uncover the molecular and cellular mechanisms underlying BM-MSC responses to PEMF stimulation when cultured under fluid flow-induced shear stress.
- Investigate the response of BM-MSCs to the addition of intermittent hydrostatic pressure as an additional physical stimulus in the bioreactor-based technology.
- Implement the developed bioreactor-based technology to culture trabecular bone tissue-like models resembling the morphological features of human bones, specifically the ulna, tibia, and femur.

The present doctoral thesis begins by addressing the urgent need for advanced technologies capable of accurately replicating the complex features of native tissues. Bioreactor-based technologies represent invaluable tools for researchers to study specific tissues under physiological and pathological states, as well as to investigate therapeutic interventions.

- In **Chapter 1**, I introduce a novel automated perfusion bioreactor that integrates both fluid flow-induced shear stress and PEMF stimulation to cultivate 3D bone tissue-like constructs. Computational simulations were employed to optimize the culture chamber design and predict the distribution of shear stress and magnetic fields within the commercial Bio-Oss scaffold. Preliminary biological experiments using human BM-MSCs were conducted to evaluate the osteogenic potential of these stimuli.

While developing an advanced bioreactor-based technology is essential, it is equally crucial to cultivate 3D bone tissue-like constructs that closely mimic the intricate architectural features of native bone tissue within the bioreactor environment.

- In **Chapter 2**, I present the development of the first trabecular bone tissue-like constructs. These engineered tissues consist of 3D-printed biomimetic polylactic acid (PLA) scaffolds, designed to mimic the human trabecular bone architecture in physiological conditions and to resemble the morphological features of the iliac crest (referred to as PLA600). Various cell seeding methods (suspension seeding, cell-releasing 2% alginate, and 0.5% cell-releasing collagen) and culture media (basal medium and osteogenic medium) were tested to optimize BM-MSC attachment and facilitate the detection of BM-MSC responses to PEMF stimulation, respectively.

The precise signaling pathways underlying the clinical benefits of PEMF stimulation on bone healing remain largely unexplored. As we investigate our innovative bioreactor-based technology, it is essential to ascertain whether it can shed light on the modified signaling pathways within BM-MSCs residing in trabecular bone tissue-like scaffolds.

- In **Chapter 3**, I explore how PEMF stimulation influences BM-MSCs cultured under fluid flow-induced shear stress at the molecular and cellular levels through transcriptomic studies. By analyzing the transcriptomic profiles of cells cultured under diverse physical stimuli, we can elucidate the signaling pathways involved in PEMF-induced bone healing.

To accurately mimic the *in vivo* microenvironment of bone cells, it is essential to recapitulate the complex interplay of mechanical stimuli, including compression, tension, shear stress, and hydrostatic pressure.

- In **Chapter 4**, I investigate the utilization of PLA600 trabecular bone-like tissues within an upgraded automated perfusion bioreactor. This enhanced system provides intermittent hydrostatic pressure (simulating physiological loading and unloading) alongside fluid flow-induced shear stress. The objective of this chapter was to assess

cell viability under these combined bone-tissue-like mechanical stimuli.

Bone tissue, particularly trabecular bone, exhibits significant morphological heterogeneity. This variation includes differences in porosity, trabecular thickness, connectivity, and orientation. These morphological characteristics directly influence the mechanical properties and biological functions of the bone tissue.

- In **Chapter 5**, I introduce a novel 3D-printed biomimetic PLA scaffold, designed to mimic the human trabecular bone architecture in physiological conditions and to resemble the morphological features of bones, specifically the ulna, tibia, and femur (referred to as P3S3). This chapter aimed to evaluate cell viability and changes in gene expression within the new scaffolds under fluid flow-induced shear stress with and without intermittent hydrostatic pressure, mimicking physiological loading experienced during an in-patient rehabilitation program.

References

1. Henrique Franco, N. (2013) Animal Experiments in Biomedical Research: A Historical Perspective. *Animals (Basel)*, **3** (1), 238.
2. MacArthur Clark, J. (2018) The 3Rs in research: a contemporary approach to replacement, reduction and refinement. *British Journal of Nutrition*, **120** (s1), S1–S7.
3. Matfield, M. (2002) Animal experimentation: the continuing debate. *Nature Reviews Drug Discovery 2002 1:2*, **1** (2), 149–152.
4. Beversdorf, D.Q., Roos, R.P., Hauser, W.A., Lennon, V.A., and Mehler, M.F. (2015) Animal extremists' threats to neurologic research continue: Neuroreality II. *Neurology*, **85** (8), 730.
5. Matfield, M. (2002) Animal experimentation: the continuing debate. *Nature Reviews Drug Discovery 2002 1:2*, **1** (2), 149–152.
6. Principles - The Johns Hopkins Center for Alternatives to Animal Testing.
7. Animals in science - European Commission.
8. Legal and ethical aspects of using animals in research in the EU | HSTalks.
9. Tannenbaum, J., and Bennett, B.T. (2015) Russell and Burch's 3Rs Then and Now: The Need for Clarity in Definition and Purpose. *J Am Assoc Lab Anim Sci*, **54** (2), 120.
10. EUR-Lex - 52020DC0016 - EN - EUR-Lex.
11. Ineichen, B. V., Furrer, E., Grüninger, S.L., Zürrer, W.E., and Macleod, M.R. (2024) Analysis of animal-to-human translation shows that only 5% of animal-tested therapeutic interventions obtain regulatory approval for human applications. *PLoS Biol*, **22** (6), e3002667.
12. Hooijmans, C.R., and Ritskes-Hoitinga, M. (2013) Progress in Using Systematic Reviews of Animal Studies to Improve Translational Research. *PLoS Med*, **10** (7), e1001482.
13. Marshall, L.J., Bailey, J., Cassotta, M., Herrmann, K., and Pistollato, F. (2023) Poor Translatability of Biomedical Research Using Animals — A Narrative Review. *Alternatives to Laboratory Animals*, **51** (2), 102–135.
14. Yano, K., Speidel, A.T., and Yamato, M. (2018) Four Food and Drug Administration draft guidance documents and the REGROW Act: A litmus test for future changes in human cell- and tissue-based products regulatory policy in the United States? *J Tissue Eng Regen Med*, **12** (7), 1579.
15. Hoffman, T., Khademhosseini, A., and Langer, R. (2019) Chasing the Paradigm: Clinical Translation of 25 Years of Tissue Engineering. *Tissue Eng Part A*, **25** (9–10), 679.
16. Krebs, C.E., and Herrmann, K. (2024) Confronting the bias towards animal experimentation (animal methods bias). *Frontiers in Drug Discovery*, **4**, 1347798.
17. Krebs, C.E., Lam, A., McCarthy, J., Constantino, H., and Sullivan, K. (2023) A survey to assess animal methods bias in scientific publishing. *ALTEX - Alternatives to animal experimentation*, **40** (4), 665–676.
18. Grimm, H., Biller-Andorno, N., Buch, T., Dahlhoff, M., Davies, G., Cederroth, C.R., Maissen, O., Lukas, W., Passini, E., Törnqvist, E., Olsson, I.A.S., and Sandström, J.

(2023) Advancing the 3Rs: innovation, implementation, ethics and society. *Front Vet Sci*, **10**, 1185706.
19. Doke, S.K., and Dhawale, S.C. (2013) Alternatives to animal testing: A review. *Saudi Pharmaceutical Journal : SPJ*, **23** (3), 223.
20. Consolidated TEXT: 32009R1223 — EN — 13.08.2019.
21. Kaplan, B.L.F., Hoberman, A.M., Slikker, W., Smith, M.A., Corsini, E., Knudsen, T.B., Marty, M.S., Sobrian, S.K., Fitzpatrick, S.C., Ratner, M.H., and Mendrick, D.L. (2024) Protecting Human and Animal Health: The Road from Animal Models to New Approach Methods. *Pharmacol Rev*, **76** (2), 251.
22. Doucet, O., Lanvin, M., Thillou, C., Linossier, C., Pupat, C., Merlin, B., and Zastrow, L. (2006) Reconstituted human corneal epithelium: A new alternative to the Draize eye test for the assessment of the eye irritation potential of chemicals and cosmetic products. *Toxicology in Vitro*, **20** (4), 499–512.
23. Hoffmann, S., Alépée, N., Gilmour, N., Kern, P.S., van Vliet, E., Boislève, F., Bury, D., Cloudet, E., Klaric, M., Kühnl, J., Lalko, J.F., Mewes, K., Miyazawa, M., Nishida, H., Tam Brami, M.T., Varçin, M., Api, A.M., and Europe, C. (2022) Expansion of the Cosmetics Europe skin sensitisation database with new substances and PPRA data. *Regul Toxicol Pharmacol*, **131**.
24. Stucki, A.O., Barton-Maclaren, T.S., Bhuller, Y., Henriquez, J.E., Henry, T.R., Hirn, C., Miller-Holt, J., Nagy, E.G., Perron, M.M., Ratzlaff, D.E., Stedeford, T.J., and Clippinger, A.J. (2022) Use of new approach methodologies (NAMs) to meet regulatory requirements for the assessment of industrial chemicals and pesticides for effects on human health. *Frontiers in Toxicology*, **4**, 964553.
25. Knight, E., and Przyborski, S. (2015) Advances in 3D cell culture technologies enabling tissue-like structures to be created in vitro. *J Anat*, **227** (6), 746–756.
26. Bukoreshtliev, N. V., Haase, K., and Pelling, A.E. (2012) Mechanical cues in cellular signalling and communication. *Cell and Tissue Research 2012 352:1*, **352** (1), 77–94.
27. Ambattu, L.A., and Yeo, L.Y. (2023) Sonomechanobiology: Vibrational stimulation of cells and its therapeutic implications. *Biophys Rev*, **4** (2).
28. Benam, K.H., Dauth, S., Hassell, B., Herland, A., Jain, A., Jang, K.J., Karalis, K., Kim, H.J., MacQueen, L., Mahmoodian, R., Musah, S., Torisawa, Y.S., Van Der Meer, A.D., Villenave, R., Yadid, M., Parker, K.K., and Ingber, D.E. (2015) Engineered in vitro disease models. *Annu Rev Pathol*, **10**, 195–262.
29. Wang, L., Hu, D., Xu, J., Hu, J., and Wang, Y. (2024) Complex in vitro model: A transformative model in drug development and precision medicine. *Clin Transl Sci*, **17** (2), e13695.

Chapter 1

An automated 3D-printed perfusion bioreactor combinable with pulsed electromagnetic field stimulators for bone tissue investigations

1.1 Abstract

In bone tissue engineering research, bioreactors designed for replicating the main features of the complex native environment represent powerful investigation tools. Moreover, when equipped with automation, their use allows reducing user intervention and dependence, increasing reproducibility and the overall quality of the culture process. In this study, an automated uni-/bi-directional perfusion bioreactor combinable with pulsed electromagnetic field (PEMF) stimulation for culturing 3D bone tissue models is proposed. A user-friendly control unit automates the perfusion, minimizing the user dependency. Computational fluid dynamics simulations supported the culture chamber design and allowed the estimation of the shear stress values within the construct. Electromagnetic field simulations demonstrated that, in combination with a PEMF stimulator, the construct can be exposed to uniform magnetic fields. Preliminary biological tests on 3D bone tissue models showed that perfusion promotes the release of the early differentiation marker alkaline phosphatase. The histological analysis confirmed that perfusion favors cells to deposit more extracellular matrix (ECM) with respect to the static culture and revealed that bi-directional perfusion better promotes ECM deposition across the construct with respect to unidirectional perfusion. Lastly, the Real-time PCR results of 3D bone tissue models cultured under bi-directional perfusion without and with PEMF stimulation revealed that the only perfusion induced a ~ 40-fold up-regulation of the expression of the osteogenic gene collagen type I with respect to the static control, while a ~ 80-fold up-regulation was measured when perfusion was combined with PEMF stimulation, indicating a positive synergic pro-osteogenic effect of combined physical stimulations.

1.2 Introduction

Nowadays, due to the population aging coupled with rising of obesity and decreased physical activities, bone fractures and their clinical management represent a heavy socio-economic burden [1,2] complemented by a dramatically growing need for bone replacement worldwide

[3,4]. In fact, although bone can usually regain functionality by self-healing, there are pathological conditions such as nonunion or large bone defects due to trauma, infections, tumors or osteoporosis in which self-healing fails, causing severe pain and immobility to patients[5,6]. Besides the conventional surgical procedures adopted for managing critical-sized bone defects, bone tissue engineering (BTE) is emerging as a promising strategy for generating in vitro functional bone tissue substitutes to be implanted for promoting *in vivo* bone regeneration[7]. BTE approaches are based on the effective interplay among osteogenic cells, three-dimensional (3D) porous scaffolds, and physiological chemical and physical stimuli[8,9]. Currently, a direct translation of BTE strategies to clinical use still remains challenging due to scientific, technical, and regulatory limitations[10–12], and BTE substitutes are mostly adopted as 3D bone tissue models for in vitro bone research and pre-clinical studies[13,14]. For example, it has been demonstrated that mechanical forces, such as compression and fluid flow-induced shear stress, influence or even drive stem cells differentiation into mature bone lineages[15–17]. Therefore, for a clear understanding of the mechanotransduction mechanisms driving bone tissue development, homeostasis, and regeneration, the in vitro modelling and analysis of 3D bone tissue models exposed to controlled native-like physical stimuli would be essential [18]

In this context, several bioreactors have been developed and adopted as powerful investigation tools for providing in vitro defined native-like physical stimuli [19–27]. Technically, bioreactors imposing hydrostatic pressure were developed to mimic the native-like compression [28–31]. Along with this approach, a variety of studies showed that direct perfusion, by guaranteeing continuous medium flow through the 3D cultured constructs, ensures efficient mass transport during both cell seeding and tissue culture[32,33] and exposes the constructs to fluid flow-induced shear stress profiles that can promote proliferation and differentiation of osteoblasts and foster bone mineralization [31,34–36]. For example, Bancroft and colleagues developed a direct unidirectional perfusion bioreactor (total medium volume = 200 mL) based on a peristaltic pump and observed increased deposition of mineral extracellular matrix (ECM) produced by marrow stromal osteoblasts seeded on titanium fiber mesh scaffolds, when cultured under perfusion for 16 days [34,37]. Moreover, adopting the same setup and constructs, the combination of unidirectional perfusion and osteogenic medium resulted in enhanced proliferation and differentiation of mesenchymal stem cells [38]. Subsequently, the bi-directional/oscillating perfusion mode, which was at first introduced to improve cell seeding efficiency [39–42], has emerged as an effective strategy to stimulate the constructs more uniformly by better recapitulating the multi-directional movement of the interstitial fluid within the native bone [43,44], promoting osteogenic differentiation as well [45–47]. In 2018, Beşkardeş et al. developed a bi-directional perfusion bioreactor based on a syringe pump and found that bi-directional perfusion, combined with osteogenic culture medium, enhanced osteogenic differentiation of pre-osteoblasts seeded on chitosan-hydroxyapatite scaffolds after 21 days of culture [47]. However, only one study compared the effects of uni- and bi-directional perfusion on 3D bone constructs, demonstrating that after 6 days bi-directional flow promoted more uniform cell proliferation and increased early osteogenic effects with respect to unidirectional flow [48]. This result was obtained by using two different non-automated perfusion systems: a

unidirectional perfusion bioreactor (total culture medium volume = 250 mL) based on a pump for chromatography, and a bi-directional perfusion device based on a syringe pump acting on a flexible membrane (total culture medium volume = 1.5 mL). Moreover, due to their peculiar architectures and to the lack of automated control, the two perfusion devices needed different manual operating procedures. For overcoming the intrinsic limitations of manual procedures, a further crucial feature in advanced bioreactors is automation, which allows enhancing environmental control and reducing user intervention, thus increasing process reproducibility and standardization. In 2018, Schmid and co-workers developed a perfusion bioreactor with automated cell seeding and active control of oxygen concentration during the culture, facilitating the investigation of BTE constructs with high homogeneity and viability [33].

Besides the well-known mechanical stimuli characterizing the bone tissue environment *in vivo*, in the last decades further physical stimuli, clinically applied for boosting bone tissue regeneration, have been investigated. In particular, the non-invasive pulsed electromagnetic field (PEMF) stimulation was demonstrated to foster bone cell proliferation, differentiation, and ECM protein expression, with evident beneficial effects in promoting endogenous bone healing [49–52]. PEMF stimulation induces a secondary electric field in the exposed tissue, like the one generated in native bone during the transduction of mechanical energy into electrical energy (bone piezoelectric behavior) [53], which can trigger the cell membrane depolarization and consequently stimulate ion currents [54]. However, due to the variety of PEMF stimulators and setups adopted, a complete understanding of the biological mechanisms induced by PEMF is yet missing and PEMF stimulation is empirically applied in the orthopedic clinical practice [53,55,56]. Thus, new investigation tools and approaches are required for performing in-depth studies that could lead to defining optimal standardized PEMF protocols for treating the different pathological conditions.

Inspired by this scenario, we developed a novel automated perfusion bioreactor that allows culturing 3D constructs under tunable, automated uni- or bi-directional perfusion and that can be combined with PEMF stimulators. Computational modelling supported the design optimization of the bioreactor culture chamber, allowing characterizing the fluid dynamics and the magnetic field across it. Rapid, flexible and cost-effective 3D-printing techniques were adopted for the manufacturing phase. A user-friendly control unit was appositely developed for enabling setting and automated control of the perfusion unit, with the final aim of reducing the user dependency and increasing process reproducibility. For assessing the bioreactor performances in terms of perfusion, preliminary biological tests were performed on 3D bone tissue models, obtained by seeding human mesenchymal stem cells (hMSCs) on commercial bone substitutes, cultured under uni- or bi-directional perfusion. The biological effects of the different imposed culture conditions were evaluated in terms of cell viability, release of the early osteogenic differentiation marker alkaline phosphatase (ALP), and ECM deposition. Lastly, to verify the performances of the combined platform and to investigate the potential pro-osteogenic effect of combining bi-directional perfusion and PEMF stimulation, a real-time PCR-based test was performed culturing 3D bone tissue models for 14 days under three defined conditions: static condition, bi-directional perfusion, and bi-directional

perfusion combined with PEMF stimulation. The expression of the osteogenic genes ALP and collagen type I were evaluated at the end of the culture by Real-time PCR.

1.3 Materials and Methods

1.3.1 Bioreactor design, components and working principle

The proposed bioreactor was designed for providing, in a controlled manner, tunable direct perfusion and to be combinable with a PEMF generator. In detail, the bioreactor is composed of: (1) a culture chamber, for housing the cultured 3D construct; (2) a perfusion unit, for providing uni- or bi-directional perfusion; (3) a control unit, for setting and automatically controlling the perfusion unit from outside the incubator **(Figure 1.1A)**.

The perfusion unit is composed of: (1) a culture medium reservoir with an inlet port, an outlet port, a medium sampling port, and air filters; (2) oxygen permeable platinum-cured silicone tubing (Darwin Microfluidics, France); (3) luer fittings (IDEX Health & Science, United States); and (4) a peristaltic pump (G100-1 J, Longer Precision Pump, China. All suitable for incubation and for connection to the control unit. The flow rate ranges from 0.006 to 6 mL/min (for tubing with an internal diameter of 1.0 mm) and 0.024 to 24 mL/min (for tubing with an internal diameter of 2.4 mm).

The control unit, connected to the pump via RS-485 serial communication, is enclosed in a compact box ($135 \times 130 \times 60$ mm^3) and equipped with a microcontroller board (Arduino Micro, Arduino, Italy) that runs a purpose-built software. A user-friendly interface, based on four push buttons and one LCD display (Arduino, Italy), allows setting the perfusion parameters. In unidirectional mode, the flow direction can be set by selecting the direction of rotation of the pump head; however, in order to promote the outflow of possible air bubbles, a bottom-to-top flow is recommended. In bi-directional mode, the user can set the cycle duration, i.e., the time interval after which the flow direction is automatically inverted. The bi-directional cycle duration can be adjusted from 1 second to 24 hours. Preliminary tests for assessing the bioreactor's performance in terms of watertightness and reliability were also performed.

The bioreactor is combinable with a PEMF generator **(Figure 1.1B)** to deliver individual or combined physical stimulations (uni- or bi-directional perfusion and/or PEMF stimulation) to the cultured constructs. To deliver PEMF stimulation to the cultured constructs, a commercial PEMF generator composed of a generator and two solenoids was selected (magnetic field intensity = 1.5 mT, frequency = 75 Hz, IGEA Clinical Biophysics, Italy) and the bioreactor culture chamber can be placed between the solenoids.

A

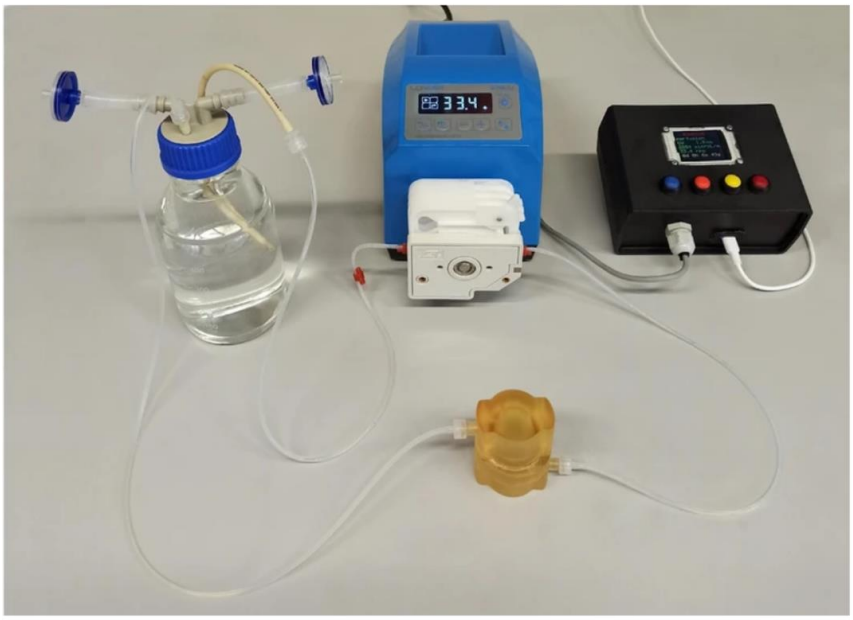

B

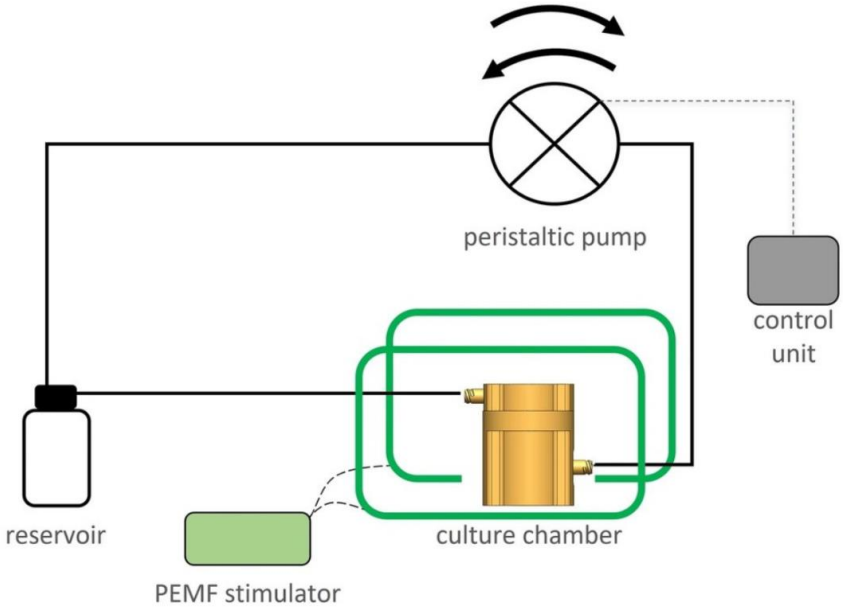

Figure 1.1. Bioreactor setup. **(A)** Photograph of the bioreactor components: culture chamber, perfusion unit, and control unit, positioned outside the incubator. **(B)** Schematic representation of the bioreactor system, illustrating the interconnection between the culture chamber, perfusion unit, and control unit, as well as the integration of pulsed electromagnetic field (PEMF) stimulation.

The culture chamber is connected to the perfusion unit. By applying computational fluid dynamics (CFD) simulations, two versions of the culture chamber (identified as “CC1” and “CC2”) were designed (SOLIDWORKS, Dassault Systèmes, France). Both chamber layouts consist of two cylindrical screwable parts, equipped with inlet and outlet channels and luer threads **(Figure 1.2A)**. CC1 is characterized by a cylindrical geometry with external diameter of 48 mm and height of 61 mm, and an internal diameter of 20 mm and a height of 42 mm. For CC1, the culture chamber working volume is 10 mL, the inlet and outlet channels connect laterally to the internal volume, and watertightness is achieved by combining an interlocking mechanism and an O-ring inserted in the bottom part of the chamber for axial sealing. CC2 layout was designed to improve the flow field distribution within the chamber and to reduce the working volume. In detail, CC2 has an external cylindrical geometry with a diameter of 48 mm and a height of 65 mm), while internally it is characterized by a truncated cone geometry upstream and downstream of the cylindrical central part with a diameter of 24 mm and a height of 15 mm). For CC2, the working volume is 2.5 mL, the inlet and outlet channels connect co-axially to the internal volume due to curved paths, and an O-ring is located on the top part of the chamber for radial sealing. Based on CFD outcomes, CC2 was selected as the optimal layout that was then 3D-printed by stereolithography (SLA) using the biocompatible Dental SG Resin (Form 3, Formlabs, United States), setting a layer thickness of 50 μm **(Figure 1.2B)**. To place the 3D constructs within these culture chambers, tailored flexible cylindrical holders that can be press-fit inserted within the culture chamber. Four cylindrical holders with internal diameters of 7, 8, 9, or 10 mm, external diameter of 24 mm, and a height of 15 mm were manufactured by casting biocompatible silicone (SYLGARD 184, Dow Corning, United States) into modular acrylonitrile butadiene styrene (ABS) molds. The molds were 3D-printed by fused deposition modeling (uPrint SE Plus, Stratasys, United States) and cured at 60 °C for 5 h.

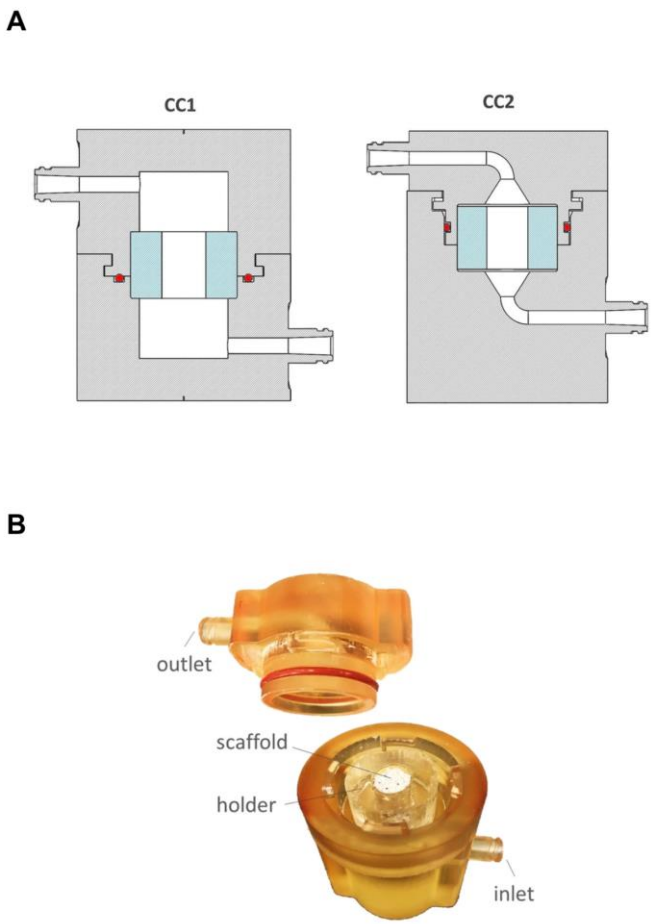

Figure 1.2. 3D-printed bioreactor culture chambers. **(A)** Cross-sectional views of the 3D-printed culture chambers, "CC1" and "CC2." The chambers are shown in gray, with the silicone holder in blue and the o-ring in red. **(B)** The 3D-printed culture chamber "CC2" consists of a top section with an o-ring and flow outlet, and a bottom section containing the silicone holder and a representative scaffold.

1.3.2 CFD simulations and wall shear stress estimation

For supporting the optimization of the culture chamber design, CFD simulations were performed. In detail, the 3D geometries of CC1 and CC2 were discretized with 3.41×10^6 and 4.99×10^5 elements, respectively, using tetrahedral elements for the bulk and hexahedral elements for the boundary layer (COMSOL Multiphysics 5.3, COMSOL Inc., Sweden). The 3D construct, assumed as a reference cylinder (diameter = 10 mm, height = 15 mm), was modeled as a homogeneous and isotropic porous medium with the properties (permeability $k = 3 \times 10^{-10}$ m^2, porosity $\varphi = 60\%$ [57]) of the commercial Bio-Oss scaffold (Geistlich Pharma AG, Switzerland), and was adopted for the preliminary biological tests. The culture

medium was modeled as an incompressible, Newtonian fluid (density $\rho = 9.94 \times 10^2$ kg/m^3, dynamic viscosity $\mu = 6.89 \times 10^{-4}$ Pa.s at 37 °C). The governing equations of fluid motion were solved in their discretized form in the fluid domain, while the Brinkman equation [58] in its discretized form was adopted for describing perfusion in the porous domain. Four steady-state simulations were performed for each culture chamber layout, with and without the 3D construct and prescribing unidirectional perfusion with flow rate values of 0.3 and 1.0 mL/min (imposing a parabolic velocity profile) at the inlet of the culture chamber bottom. A reference pressure was imposed at the outlet, and the no-slip condition was applied at the internal walls of the culture chambers. Moreover, in order to investigate the development of the flow upstream of the construct within CC1 and CC2, the velocity field distributions were analyzed at three different horizontal sections of the culture chamber bottom **(Figure 1.3)**.

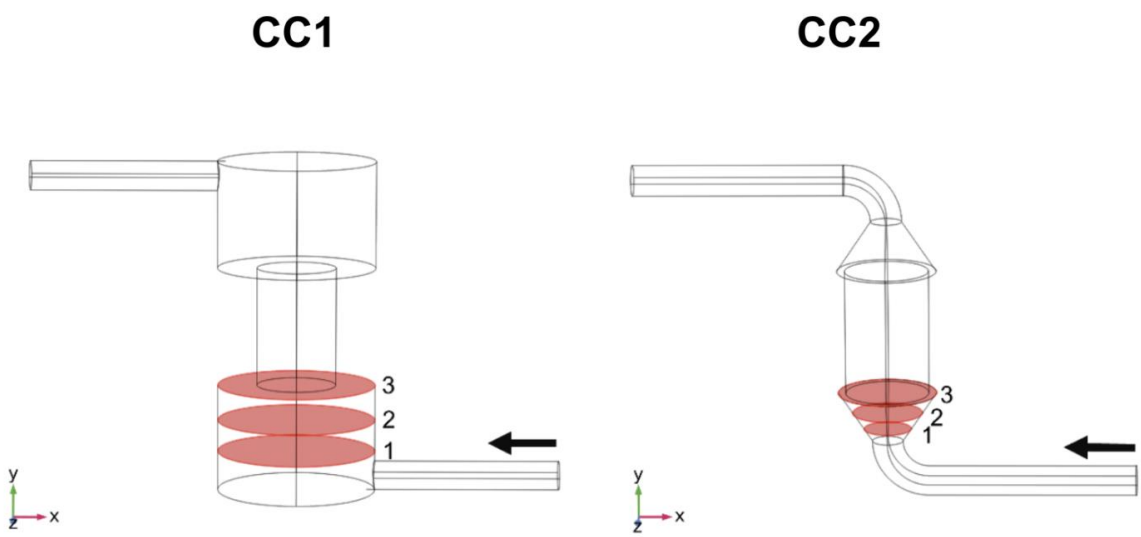

Figure 1.3. 3D view of the internal geometry of CC1 and CC2 highlighting the direction of flow perfusion and the 3 horizontal sections where the fluid velocity field distributions were analyzed: 1) at 0.5 mm above the end of the inlet channel; 2) at midway between the construct and the end of the inlet channel (i.e., 4.5 mm below the construct for CC1 and 2.5 mm below the construct for CC2); 3) tangent to the construct.

The simulated flow regimes within CC1 and CC2, expressed in terms of Reynolds number (Re) calculated considering the internal diameter of the inlet channel (3.7 mm) as the characteristic length, resulted to be laminar (Re = 2.48 for 0.3 mL/min; Re = 8.28 for 1.0 mL/min). Following the adoption of the Brinkman equation, the wall shear stress (τ_w) in the porous construct was evaluated using the expression obtained by Wang and Tarbell[59,60], which provides an accurate estimation for constructs with permeability higher than 10^{-10} m^2:

$$\tau_w = \frac{4}{\pi} \frac{\mu}{\sqrt{k}} v_{avg}$$

where μ is the dynamic viscosity of the culture medium, v_{avg} is the average velocity of the culture medium within the construct as obtained from CFD simulations, *k* is the construct permeability, and a null cell density was assumed.

1.3.3 Electromagnetic field simulations

Electromagnetic field simulations were conducted to evaluate the compatibility of the proposed bioreactor with the PEMF generator [61]. Specifically, a 3D steady-state simulation was performed using a commercial finite element-based software (COMSOL Multiphysics 5.3, COMSOL Inc., Sweden) to analyze the magnetic field distribution within the CC2 when positioned between the two solenoids of the PEMF generator **(Figure 1.4)**.

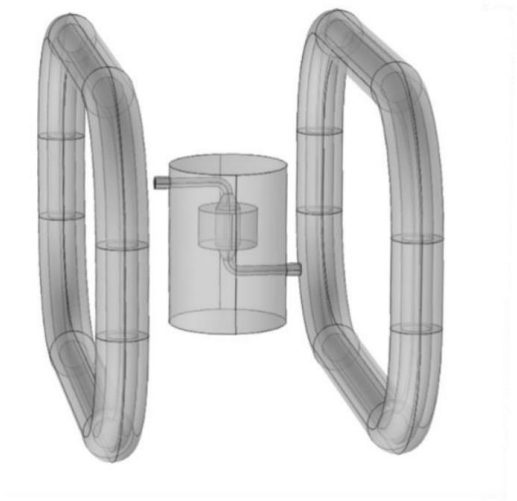

Figure 1.4. 3D geometry considered for the stationary electromagnetic field modeling.

The CC2's internal geometry was discretized using 2.25×10^6 tetrahedral and 1.61×10^5 triangular elements. The Ampere's Law was solved in its discretized form, applying a current of 160 mA at each solenoid. A magnetic insulation condition ($n \times A = 0$, where A is the magnetic potential) was imposed on the domain boundaries. Each component was modeled according to its electromagnetic properties **(Table 1.1)**.

Table 1.1. Electromagnetic properties of the modelled domains (when the properties were unknown, an analogous material was considered)

Domain	**Electric conductivity (S/m)**	**Relative permittivity**	**Relative permeability**
Culture chamber (photopolymer)	1×10^{-14}	3.1	1
Holder (PDMS)	2.5×10^{-14}	2.4	1
Construct (glass ceramic) [62]	1×10^{-7}	24.5	1
Culture medium [63,64]	1.45	80	1
Coils (copper)	5.998×10^{7}	1	1

Coils' cover (PVC) [65]	1.33×10^{-13}	4.46	1
Air	0	1	1

1.3.4 3D bone tissue-like model preparation and culture under perfusion

Primary human bone marrow-derived human mesenchymal stem cells (hBM-MSCs) were obtained from Merck (C-12974 PromoCell GmbH, Germany) were cultivated in low-glucose Dulbecco's modified Eagle's medium (low-glucose DMEM, gibco, Thermo Fisher Scientific, Inc.) supplemented with 15% fetal bovine serum (FBS, gibco Thermo Fisher Scientific, Inc.) and 1% antibiotics (penicillin/streptomycin, gibco Thermo Fisher Scientific, Inc.). Cells were incubated in a humidified atmosphere with 5% CO_2 at 37°C. The 3D bone tissue-like models were obtained by seeding 4×10^6 cells into a pre-molded cylinder (diameter = 10 mm, height = 6 mm) of commercial bone substitute Bio-Oss (Geistlich Pharma AG, Switzerland), as previously described [66]. The 3D constructs were then cultured under static conditions for 48 h to allow full cell adhesion and spread.

The 3D bone tissue-like models were inserted in the tailored flexible cylindrical holders, which were transferred into the bioreactor culture chamber (CC2), previously filled with 1 mL of culture medium. The bioreactor setup was then placed in the incubator. Using the control unit, the flow rate was set to 0.3 mL/min under unidirectional perfusion mode or under bi-directional perfusion mode (cycle duration = 2 h). The 3D bone tissue-like models were dynamically cultured for 3 or 6 days with a total culture medium volume of 50 mL. Control tests were performed with analogous 3D bone tissue-like models cultured in static conditions, with a total culture medium volume of 3 mL that was changed every 3 days. All experiments were conducted in triplicate (n = 3).

1.3.5 Assessments of 3D bone tissue-like models cultured under perfusion

The effects of uni- or bi-directional perfusion were investigated in terms of cell viability, alkaline phosphatase (ALP) release, and extracellular matrix (ECM) deposition. Cell viability was evaluated at days 3 and 6 by assessing cell metabolic activity using the alamarBlue™ Cell Viability Reagent (Life Technologies, Italy) according to the manufacturer's instructions. Briefly, the 3D bone tissue-like models cultured under static and dynamic conditions were collected, submerged in the alamarBlue™ solution, and incubated for 4 h. Then, 100 µL aliquots were transferred to a black 96-well plate, and fluorescence signals were measured with a spectrophotometer (Spark, Tecan Trading AG, Switzerland) at excitation and emission wavelengths of 530 and 590 nm, respectively. The early osteogenic marker ALP, released by constructs cultured under static and dynamic conditions, was measured at days 3 and 6 using a colorimetric assay (ab83369 from AbCam, United Kingdom) according to the manufacturer's instructions. Briefly, 80 µL of each supernatant was collected and mixed with 50 µL of the pNPP solution and 10 µL of the ALP enzyme. After 60 min, the optical density was evaluated by spectrophotometry (Spark, Tecan Trading

AG, Switzerland) using a 405 nm wavelength. Finally, on day 6, the deposition of ECM was verified by histology. The 3D bone tissue-like models cultured under static and dynamic conditions were collected, fixed with 10% formalin, dehydrated with a series of 70%, 90%, and 100% alcohol solutions, and embedded in resin (Tecnovit 7200, Kulzer, Germany). The constructs were then sliced horizontally parallel to the flow direction (top-down) to a final thickness of 80 µm. Histological analysis was performed on the central slices representative of the scaffold core using Toluidine Blue O (Merck, Italy). Images were acquired using an optical digital scanner (NanoZoomer S60, Hamamatsu, Japan).

1.3.6 Combined bi-directional perfusion and PEMF stimulation culture and quantitative PCR analysis

To assess the combined effects of bi-directional perfusion and pulsed electromagnetic field (PEMF) stimulation on 3D bone tissue-like models, we cultured constructs for 14 days under the following conditions: (i) static culture (control); (ii) bi-directional perfusion (flow rate = 0.3 mL/min, cycle duration = 2 h); and (iii) bi-directional perfusion (flow rate = 0.3 mL/min, cycle duration = 2 h) combined with PEMF stimulation (magnetic field intensity = 1.5 mT, frequency = 75 Hz, exposure time = 24 h/day. To minimize biochemical interference, constructs were maintained in low-glucose DMEM supplemented with 15% FBS. At the end of the culture period, we evaluated the expression of the early osteogenic gene ALP and the late osteogenic gene collagen type I alpha 1 chain (COL1A1) using reverse transcription-quantitative PCR (RT-qPCR). Total RNA was extracted using TRIzol (Invitrogen Life Technologies, Italy) according to the manufacturer's instructions. RNA yield and quality were assessed using a NanoDrop spectrophotometer (NanoDrop One, Thermo Fisher Scientific Inc.). 1 µg of total RNA was treated with DNase I to remove genomic DNA contamination and was reverse transcribed using the iScriptTM gDNA Clear cDNA Synthesis Kit (Bio-Rad Laboratories) and a thermal cycler (Mastercycler X50s, Eppendorf). Third, the genes of interest and the reference gene were analyzed via qPCR which was performed on 1 ng/µL of cDNA using a master mix of SsoAdvancedTM Universal SYBR® Green Supermix (Bio-Rad Laboratories) and primers at a concentration of 2.5 µM, and the reactions were performed and monitored using a thermal cycler (CFX96TM Real-Time System, Bio-Rad Laboratories) according to the standard protocol. The cycle threshold for each gene of interest was normalized against the reference gene that is the ribosomal protein L34 (RPL34), and relative gene expression levels were determined using the Livak's using the $2^{-\Delta\Delta Ct}$ method [67,68], and the reference gene was used to normalize the results. Experiments were performed in triplicate. The primer pairs of the analyzed genes are listed in **Table 1.2**.

Table 1.2. Description of the designed primers.

Gene	Forward Primer	Reverse Primer
Alkaline phosphatase (ALP)	5'- GAG TAT GAG AGT GAC GAG AAA G -3'	5'- GAA GTG GGA GTG CTT GTA TC -3'

Collagen type I alpha 1 chain (COL1A1)	5'- GGA TTC CAG TTC GAG TAT GG -3'	5'- CAG TGG TAG GTG ATG TTC TG -3'
Ribosomal protein L34 (RPL34)	5'- GAC GTA GGC TTT CCT ACA ATA C -3'	5'- GTG CTT TCC CAA CCT TCT T -3'

1.3.7 Statistical analysis

All biological experiments were performed in triplicate and results were statistically analyzed using the SPSS software (v.20.0, IBM, United States). Data normal distribution and homogeneity of variance were confirmed by the Shapiro–Wilk's and the Levene's test, respectively; then, groups were compared by the one-way ANOVA using the Tukey's test as post-hoc analysis. Significant differences were established at $p < 0.05$.

1.4 Results

1.4.1 Preliminary bioreactor performance tests

The watertightness and reliability of the bioreactor were preliminarily tested in-house. Firstly, the CC2 underwent 5 autoclave cycles, to assess the maintenance of geometry and functionality. No deformations were observed in the CC2 components. Secondly, the CC2 was connected to the perfusion unit and tested in unidirectional perfusion mode with and without a reference scaffold (Bio-Oss, Geistlich Pharma AG, Switzerland), using distilled water at room temperature and imposing the highest flow rate provided by the pump (24 mL/min) for 58 h. No leakage was observed both with and without the reference scaffold inserted. Moreover, in the case of scaffold inserted, the applied bottom-to-top unidirectional perfusion efficiently promoted the outflow of air, preventing the residence of air bubbles that could impair the culture process. Lastly, the control unit was connected to the pump and the bi-directional perfusion mode was tested setting different cycle durations and checking the inversion timing using a stopwatch. The control unit timing respected the prescribed conditions.

1.4.2 CFD simulations and wall shear stress estimation

The CFD simulations allowed characterizing the hydrodynamics within CC1 and CC2 layouts at the imposed flow rates of 0.3 mL/min and 1 mL/min **(Figure 1.5)** for defining the optimal layout. In detail, the flow streamlines developing within CC1 reveal recirculation regions in the bottom and top parts of culture chamber, both without and with the construct inserted. Differently, within CC2 the flow streamlines follow the internal geometry of the culture chamber avoiding recirculation regions, both without and with the construct inserted.

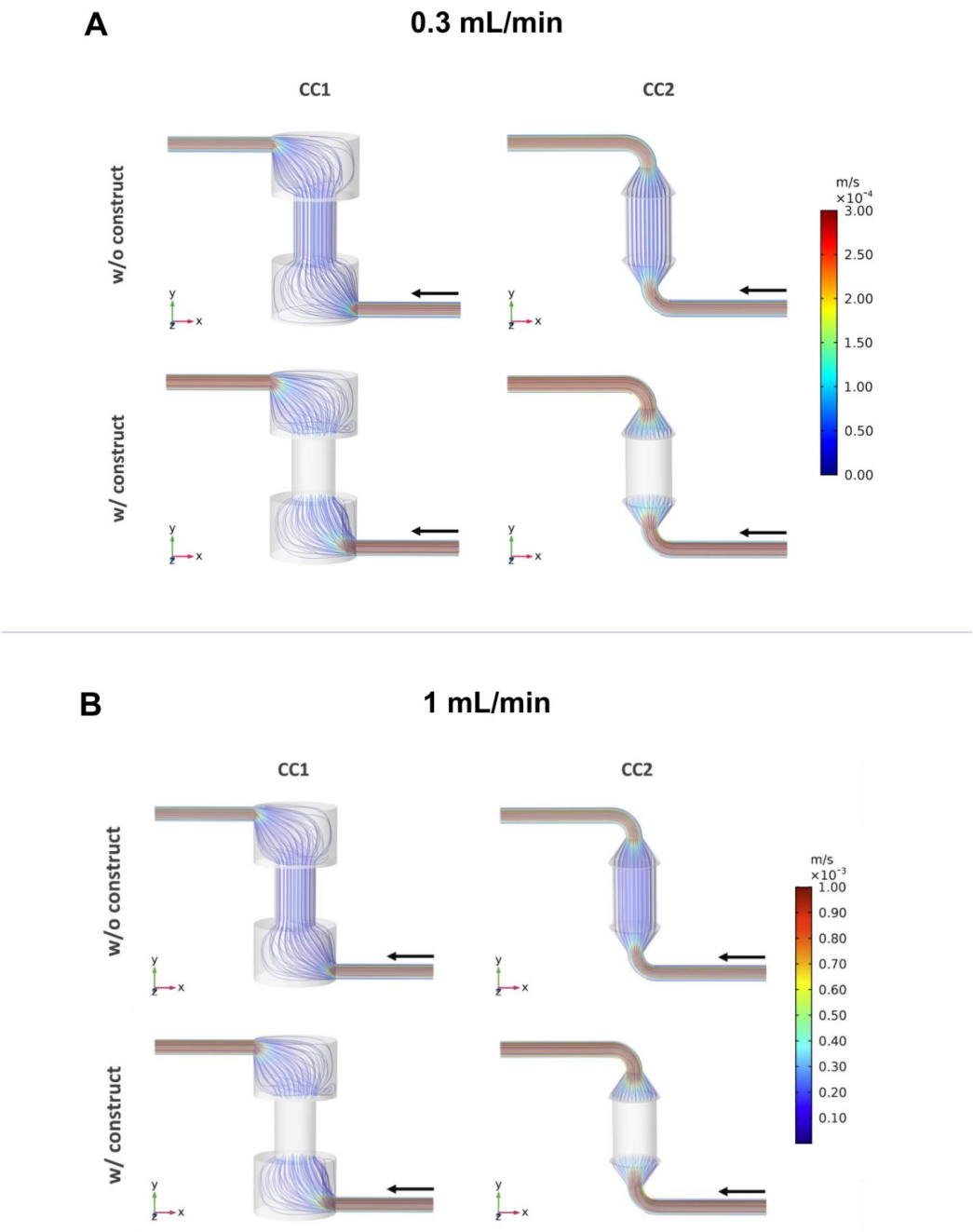

Figure 1.5. Flow streamlines developing within CC1 and CC2. The flow streamlines developed without construct and with an inserted construct modelled as porous medium in CC1 and CC2 while imposing a modeled flow rate of **(A)** 0.3 mL/min and **(B)** 1 mL/min and color-coded compared with velocity values (m/s).

Upstream of the construct **(Figure 1.6)**, the longitudinal velocity component within CC1 exhibits an uneven distribution, with the maximum velocity misaligned from the longitudinal axis near the inlet and a flattened profile at the entrance. In-plane velocity vectors show a

diverging pattern near the inlet and a converging pattern approaching the construct. Additionally, within CC1, large regions of low or zero velocity, particularly at the bottom of the culture chamber **(Figure 1.6A)**, indicate potential flow stagnation. In contrast, CC2 demonstrates a symmetric, parabolic velocity profile throughout the upstream region. Only near the walls of CC2 are low or zero velocities observed **(Figure 1.6B)**. Consequently, CC2 was chosen as the optimal design for manufacturing.

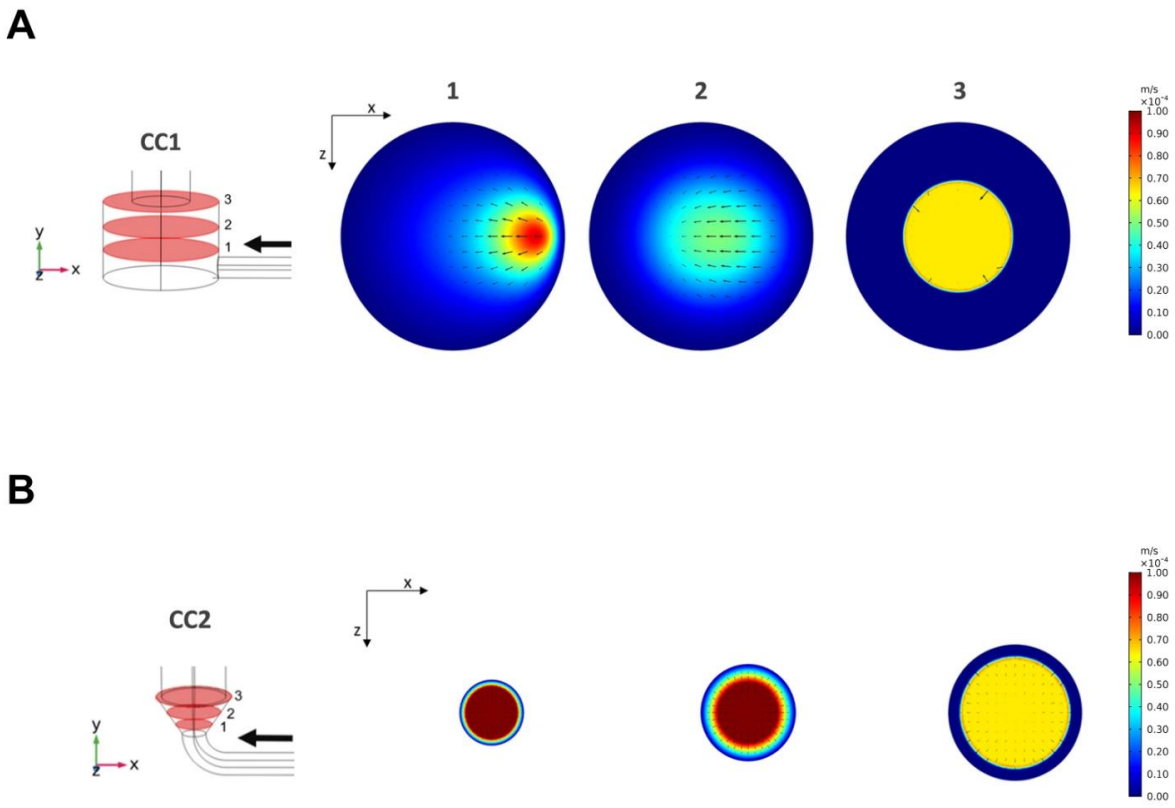

Figure 1.6. Flow development upstream of the construct in CC1 and CC2, analyzed at three horizontal sections. **(A)** Bottom portion of CC1 with horizontal sections and the contour plots of longitudinal velocity component (color) and in-plane velocity vectors (arrows) for the three horizontal sections. **(B)** Bottom portion of CC2 with horizontal sections and the contour plots of longitudinal velocity component (color) and in-plane velocity vectors (arrows) for the three horizontal sections.

Development of the flow upstream of the construct within CC1 and CC2, analyzed at three different horizontal sections. (a) Bottom part of CC1 with horizontal sections. (b) Bottom part of CC2 with horizontal sections. Contour plots of the velocity component along the longitudinal axis of the culture chamber with vectors of in-plane velocity components for the three horizontal sections of CC1 (c) and of CC2 (d).

The wall shear stress values within the construct, calculated from the average velocity values obtained from the CFD analysis, turn out to be 3.23 or 10.75 mPa for both CC1 and CC2, depending on the imposed flow rates, 0.3 and 1.0 mL/min, respectively **(Table 1.3)**.

Table 1.3. Mean velocity and wall shear stress values within the construct calculated for the different modelled conditions.

Chamber layout	**Flow rate (mL/min)**	**Mean velocity within the construct (m/s)**	**Wall shear stress (mPa)**
CC1	0.3	6.37×10^{-5}	3.23
	1	2.12×10^{-4}	10.75
CC2	0.3	6.37×10^{-5}	3.23
	1	2.12×10^{-4}	10.75

1.4.3 Electromagnetic field simulations

The electromagnetic field simulations confirmed that positioning the bioreactor culture chamber between the two solenoids of the PEMF generator does not affect the magnetic field distribution, neither on the xy **(Figure 1.7A)** or xz **(Figure 1.7B)** cross planes. Additionally, the simulations clearly showed that the construct housed in the bioreactor culture chamber is exposed to a uniform magnetic field, as testified by the magnetic field magnitude isolines and the contour plots on the longitudinal **(Figure 1.7C)** and transverse **(Figure 1.7D)** sections of the culture chamber. The magnetic field intensity resulting on the region occupied by the construct is 1.5 mT, in accordance with the nominal value specified by the stimulator manufacturer.

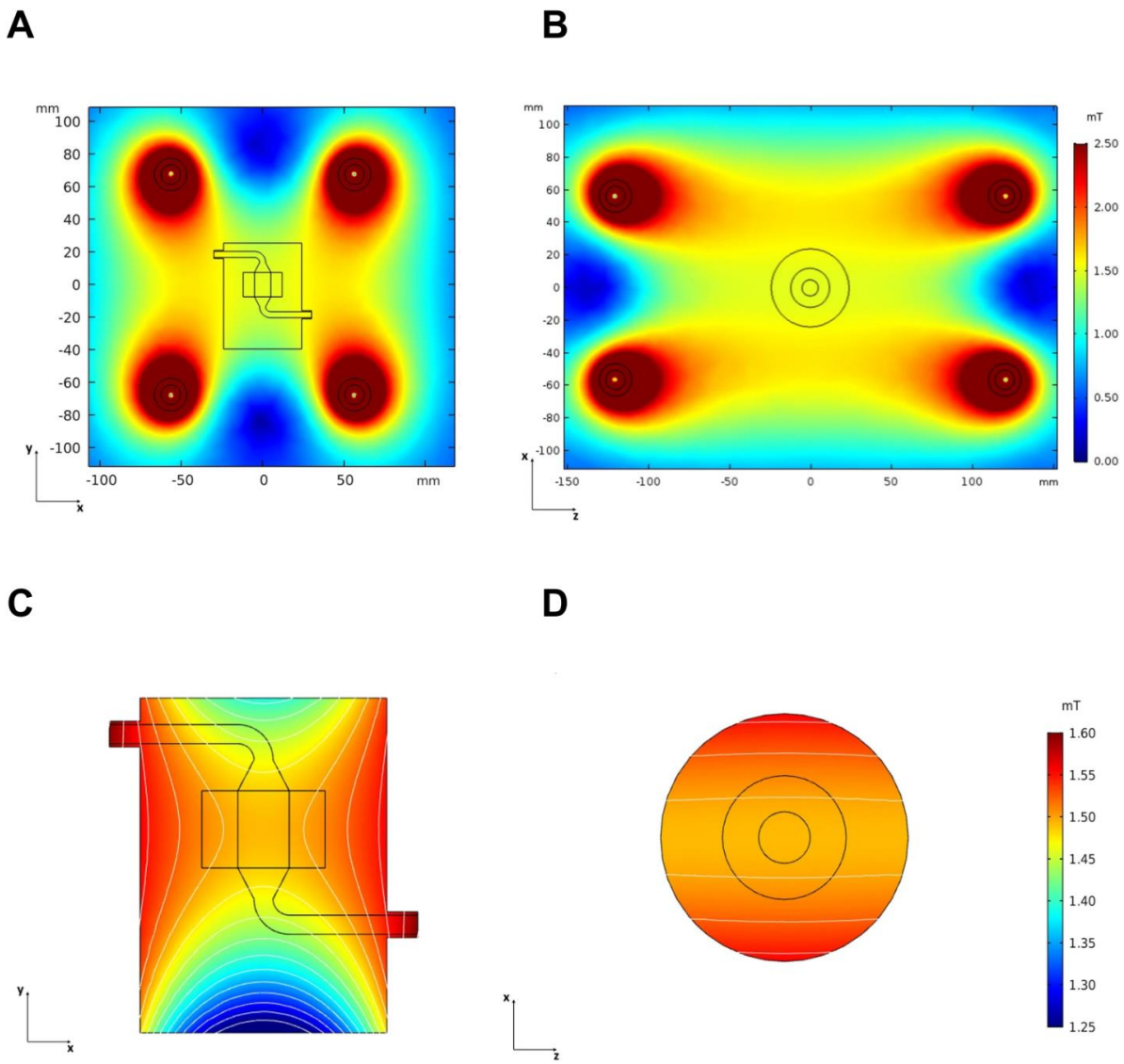

Figure 1.7. Contour plots with isolines of the magnetic field magnitude developing around and within the bioreactor culture chamber located between the PEMF stimulator solenoids. **(A)** Distribution of the magnetic field on the xy cross plane. **(B)** Distribution of the magnetic field on the xz cross plane. **(C)** Distribution of the magnetic field within the longitudinal section of the culture chamber. **(D)** Distribution of the magnetic field within the transverse section of the culture chamber.

1.4.4 Assessments of 3D bone tissue-like models cultured under perfusion

To evaluate the bioreactor's suitability for 3D bone tissue culture, models were cultivated under uni- or bi-directional perfusion and static conditions. The metabolic activity of cells exposed to uni- or bi-directional perfusion was comparable (> 90%, $p > 0.05$) to that of

statically cultured constructs at both days 3 and 6 **(Figure 1.8A)**. Notably, in line with previous studies, both uni- and bi-directional perfusion conditions led to a significant increase in the release of the early osteogenic marker ALP into the supernatant compared to static controls ($p < 0.05$, indicated by §, **Figure 1.8B**). Specifically, after 3 days, dynamic culture increased ALP release by approximately 10-12%, and after 6 days, this rose to 20-21%, as summarized in **Table 1.4**. No significant differences were observed between uni- and bi-directional perfusion ($p > 0.05$).

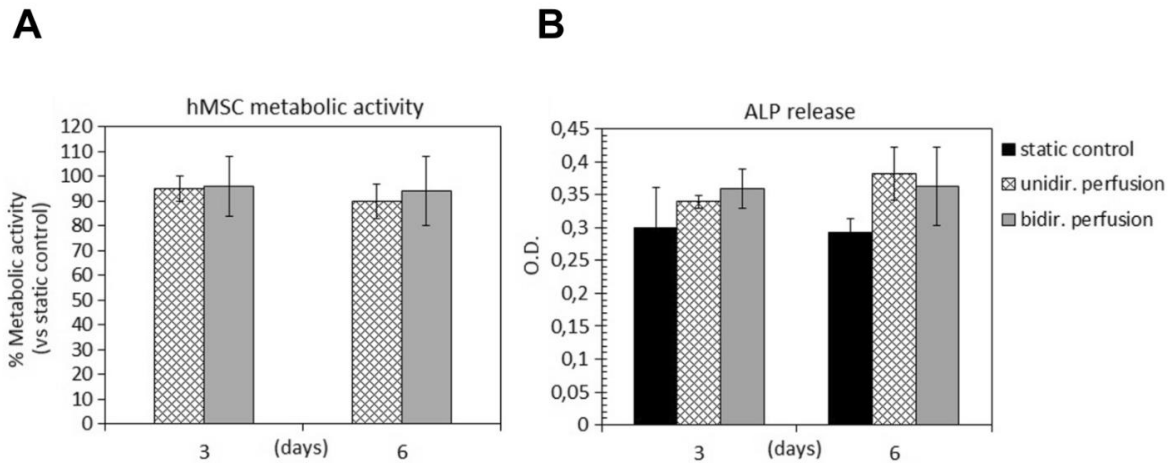

Figure 1.8. Biological assessments of 3D bone tissue-like models cultured under perfusion. **(A)** metabolic activity of the 3D models cultured under unidirectional and bi-directional perfusion, evaluated at days 3 and 6 using alamarBlue™ assay. Results were expressed as a percentage of the static culture control (100% viability). **(B)** ALP release from the 3D models cultured under static conditions (control), unidirectional perfusion, and bi-directional perfusion, assessed at days 3 and 6 ($p < 0.05$ indicated by §). Bars represent the means of three biological replicates +/− standard deviation (SD).

Table 1.4. Enhanced alkaline phosphatase (ALP) release by cells in perfused 3D bone tissue-like models (% vs static control).

Bioreactor setup	**Day 3**	**Day 6**
Unidirectional perfusion	+ 10.82%	+ 21.23%
Bidirectional perfusion	+ 12.23%	+ 20.72%

Regarding ECM deposition and distribution, histological analysis of day 6 constructs revealed that both uni- and bi-directional perfusion effectively stimulated adherent cells to produce ECM compared to static control **(Figure 1.9)**. ECM deposits (stained blue and indicated by arrows) were significantly more abundant in perfused constructs **(Figure 1.9B,C)** than in statically cultured ones **(Figure 1.9A)**, as evident in both 10x and 20x magnification images. Moreover, comparing uni- and bi-directional perfusion, a more homogeneous and consistent ECM deposition was observed with bi-directional perfusion

(Figure 1.9C), suggesting its superior efficiency in stimulating ECM secretion by adherent cells.

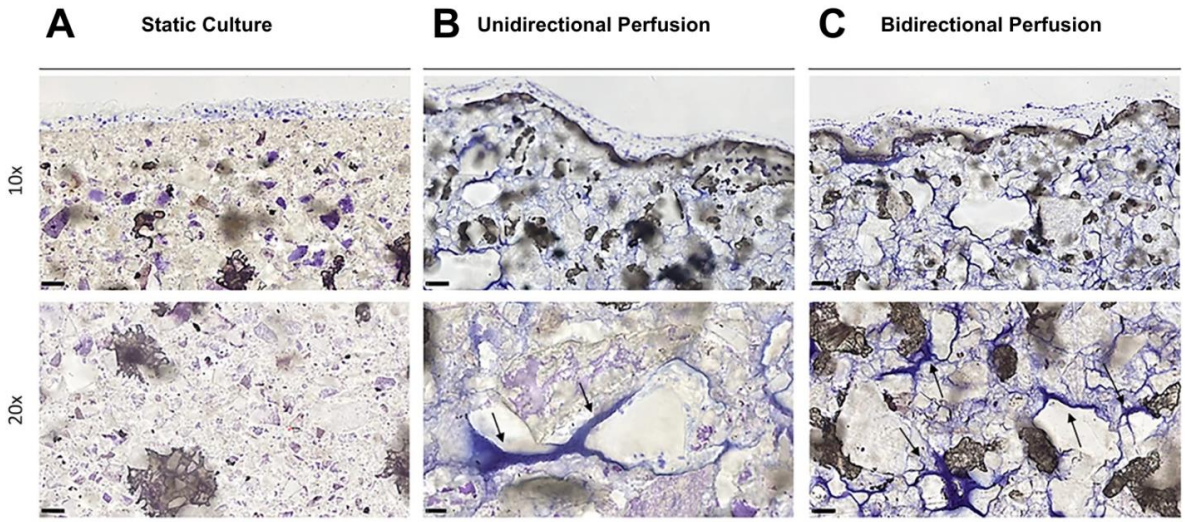

Figure 1.9. Toluidine blue-stained histological sections of 3D bone tissue-like models after 6 days of cultivation. **(A)** 3D bone tissue-like models in static culture. **(B)** 3D bone tissue-like models under unidirectional perfusion. **(C)** 3D bone tissue-like models under bidirectional perfusion. Black arrows highlight extracellular matrix (ECM) deposition. Scale bars represent 100 μm (10x) and 50 μm (20x).

1.4.5 Combined bi-directional perfusion and PEMF stimulation culture and quantitative PCR analysis

To evaluate the combined effects of bi-directional perfusion and PEMF stimulation on 3D bone tissue-like models, cultures were maintained for 14 days under three conditions: static culture (control), bi-directional perfusion, and bi-directional perfusion with PEMF stimulation. To minimize biochemical interference, constructs were maintained in low-glucose DMEM supplemented with 15% FBS. At the end of the culture period, the expressions of the early ALP and late COL1 osteogenic genes were assessed **(Figure 1.10)**. At the end of the culture period, the expression of the early ALP and late COL1 osteogenic genes was assessed (Fig. 8). Specifically, when normalized to static culture **(Figure 1.10A)**, bi-directional perfusion resulted in a ~40-fold increase in COL1 gene expression, demonstrating the significant role of fluid flow-induced shear stress in promoting collagen type I expression, even in the absence of biochemical stimulation. Interestingly, the combination of bi-directional perfusion and PEMF stimulation led to an even more pronounced pro-osteogenic effect, with an almost 80-fold increase in COL1 expression compared to the control. This suggests that the additional ~40-fold increase observed with PEMF stimulation could be attributed to the secondary electric field induced in the constructs by the PEMF. In contrast to the significant effects on COL1 expression, less pronounced differences were observed in the expression of the early osteogenic marker ALP among the

three culture conditions **(Figure 1.10B)**. Bi-directional perfusion resulted in a ~1-fold increase in ALP expression, while the combination of bi-directional perfusion and PEMF stimulation led to a ~1.5-fold increase compared to the control.

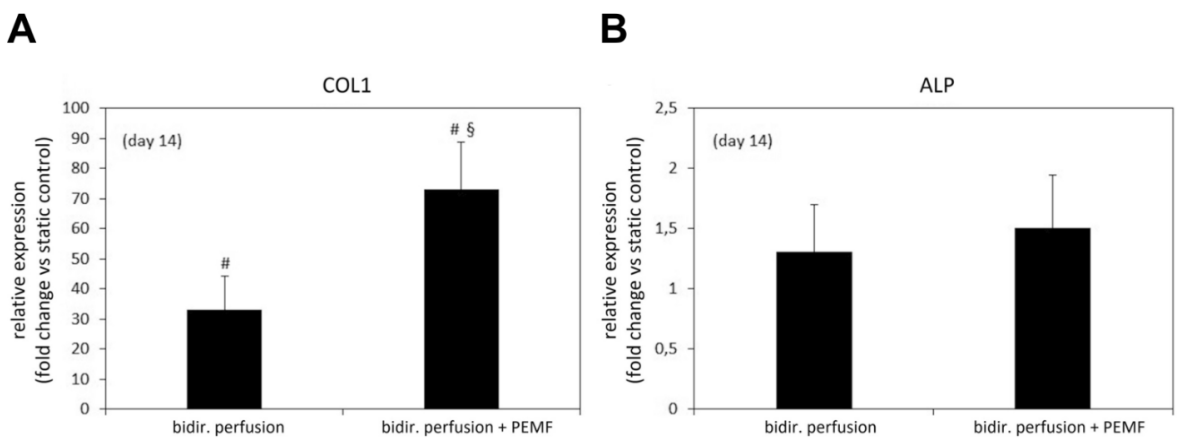

Figure 1.10. Quantitative PCR analysis of 3D bone tissue-like models cultured for 14 days under static condition (control), bidirectional perfusion, and bidirectional perfusion with pulsed electromagnetic field (PEMF) stimulation. **(A)** Expression level of collagen type I (COL1). **(B)** Expression level of alkaline phosphatase (ALP). Bars represent the mean fold change of three biological replicates +/− standard deviation (SD). Significant differences compared to the control (#) and bi-directional perfusion (§) are indicated at $p < 0.05$.

1.5 Discussion

In the emerging and multidisciplinary research field of mechanobiology, it is clearly recognized that physical stimuli arising from the surrounding microenvironment or externally applied play a crucial role in influencing cell fate [69,70] and, at the tissue scale, tissue development, homeostasis, and even disease pathogenesis could be strictly dependent on physical forces [71]. In particular, bone and cartilage are among the tissues mostly influenced by mechanical stimuli *in vivo*: being deputed to the body support and mechanical stress dissipation, osteochondral tissues are highly exposed to compression and fluid flow-induced shear stress. In parallel, further physical stimuli, such as the non-invasive PEMF stimulation, are increasingly adopted in clinical practice for promoting endogenous bone healing [55]. However, a full understanding of the biological mechanisms induced in bone tissue by defined physical stimuli is still missing and the influence of different stimulation parameters and combinations is unknown [72], leading to empirical treatments.

Inspired by the need of unrevealing how physical stimuli regulate cell and tissue functions, we developed a versatile automated perfusion bioreactor combinable with PEMF stimulation devices. As regards the bioreactor culture chamber, two layouts were designed and compared

in terms of hydrodynamic performances. The outcomes of the computational analysis confirmed that the internal geometry of the CC2 layout allows the development of a symmetric flow profile within the culture chamber and minimizes the regions with low or null longitudinal velocity, reducing the risk of recirculation and stagnation zones. For these reasons and due to the limited working volume (2.5 mL), CC2 design was selected as the optimal geometry and was then manufactured by the SLA 3D-printing technique, which allowed fabricating the bioreactor following a single-step procedure, reducing complexity, costs and lead time [42,73–77]. To provide controlled uni- or bi-directional perfusion, the closed-loop perfusion unit was equipped with a peristaltic pump suitable to be incubated and to be externally controlled. For the control unit, the selection of a low-cost open-source microcontroller board allowed combining control accuracy and reliability with compactness, flexibility, and cost-efficiency. Placed outside the incubator, the user-friendly control unit allows externally setting and automatically controlling the perfusion unit, while keeping constant the incubator conditions and reducing the contamination risk.

The automated perfusion control, which enables selecting uni- or bi-directional perfusion mode within the same platform and without user intervention along the culture, is the first significant advantage and novelty of the proposed bioreactor. Indeed, conventional bioreactors providing unidirectional perfusion are either non-automated [34,38] or exploit automation strategies for regulating the flow rate, but do not allow reverting the flow direction [33]. On the other side, bioreactors delivering bi-directional perfusion are commonly based on syringe pumps [46,47,78], which are unsuitable for providing continuous unidirectional perfusion. The only study that compared uni- and bi-directional perfusion on 3D bone tissue-like models adopted two non-automated perfusion systems characterized by different total culture medium volumes (250 mL vs 1.5 mL, respectively) [48]. Differently, our bioreactor allows comparing uni- and bi-directional perfusion modes using the same device and total culture medium volume of 50 mL.

As concerns the shear stress values induced by direct perfusion, several studies investigated the optimal range for *in vitro* dynamic culture of 3D bone tissue-like models [20,79]. In detail, shear stress values ranging from 0.55 mPa to 24 mPa were shown to stimulate osteogenic differentiation of hMSCs and to promote ECM mineralization in both β-tricalcium phosphate [80] and silk fibroin [81] scaffolds. Differently, values exceeding 60 mPa were shown to result in cell death or detachment [82], while values below 0.1 mPa did not stimulate any ECM mineralization [83]. In our study, the shear stress values developing within the construct under unidirectional perfusion were estimated to be 3.23 or 10.75 mPa, depending on the imposed flow rate (0.3 and 1.0 mL/min, respectively), thus confirming the suitability of the bioreactor for *in vitro* bone tissue culture and maturation.

As proof of concept, biological experiments imposing uni- or bi-directional perfusion mode on 3D bone tissue-like models, based on hBM-MSCs seeded on Bio-Oss scaffolds, were performed. Being a pre-validated therapeutic product applied in clinic for small bone defects repair, Bio-Oss allowed specifically correlating the biological results with the applied perfusion conditions (uni- or bi-directional mode compared with the static control). To our

knowledge, this is the first time that, thanks to automation, uni- and bi-directional perfusion modes were compared using the same platform and total culture medium volume. Firstly, it was demonstrated that the bioreactor perfusion culture does not introduce any disturbance for the cells in comparison to the static control in terms of metabolic activity. Actually, the imposed flow rate (0.3 mL/min) was appositely selected to mimic the interstitial fluid features in the native tissue [84], providing native-like flow-induced shear stress to the cells. Moreover, no significant differences were observed between uni- and bi-directional perfusion conditions in terms of cell viability. The biological effect of the perfusion culture emerged from the evaluation of the early osteogenic marker ALP. In fact, just providing direct uni- or bi-directional perfusion for a short-term culture (6 days), without the use of osteogenic medium, a general increase of the ALP release was observed for the constructs cultured under perfusion compared with the static controls (+ 10–12% at day 3 and + 20–21% at day 6). This is in accordance with previous findings, showing that flow-induced shear stress alone is crucial for boosting osteogenic differentiation [48,85]. No significant differences were observed by comparing the uni- and the bi-directional perfusion modes in terms of ALP release. However, histological assessment enabled revealing the effect of the perfusion mode in terms of stimulation of cells in secreting and depositing ECM within the construct pores. Indeed, it is well known that flow-induced shear stress can influence ECM deposition [86,87]. In particular, in literature it was shown that unidirectional perfusion can induce a homogeneous ECM deposition within the construct, due to the different fluid transport and consequent shear stress values experienced by the cells located in the proximal and distal parts of the construct compared with the main fluid direction [48]. Conversely, bi-directional perfusion has been reported as an effective strategy to provide uniform mechanical stimulation over time to the construct, promoting osteogenesis in a more effective manner and inducing homogeneous ECM deposition along the whole 3D bone tissue-like models [48]. In our study, the histological images of the 3D constructs harvested after 6 days of uni- or bi-directional perfusion and stained with Toluidine blue confirmed that perfusion favors cells to better penetrate the scaffold structure as well as to deposit more ECM compared with static conditions. Notably, the ECM deposition was more marked for the constructs exposed to bi-directional perfusion, confirming the hypothesis that a bi-directional flow can represent a more efficient culture condition for 3D constructs mimicking physiological tissues. In particular, Toluidine blue was selected for the staining of the 3D bone tissue-like models as it specifically visualizes the proteoglycan content in a tissue [88]. Proteoglycans and glycoproteins represent the majority of the non-collagenous proteins of the bone matrix. During the bone healing process, proteoglycans such as decorin, biglycan, and osteoadherin play a pivotal role in promoting and supporting the early mineralization of the matrix in the first stages of osteogenesis. Therefore, it can be speculated that the regions positive to the Toluidine blue staining showing a dark-blue pigmentation are representative of early mineralization occurring in the pores of the constructs cultured under perfusion. These experiments were performed for a short culture time (6 days) to assess the suitability of the developed bioreactor to culture 3D bone tissue-like models under a physiological condition such as perfusion. Moreover, the analysis of the ALP release and the histology of the deposited ECM allowed determining the optimal perfusion mode (i.e., bi-directional

perfusion) to be applied for further tests dealing with the investigation of the combined stimulation (bi-directional perfusion + PEMF stimulation).

Indeed, the results from the electromagnetic field modelling showed that the proposed bioreactor is in principle suitable to be combined with a commercial PEMF stimulator for exposing 3D bone tissue-like models to uni-/bi-directional flow-induced shear stress and uniform pulsed electromagnetic field. Based on the preliminary biological results, dedicated biological tests were then performed for verifying the performances of the combined platform and for investigating the potential pro-osteogenic effect on 3D bone tissue models of combining bi-directional perfusion and PEMF stimulation. The constructs were cultured for 14 days under three different conditions (i.e., static culture (control), bi-directional perfusion, and bi-directional perfusion combined with PEMF stimulation) and, for all experiments, the maintenance medium was adopted for avoiding the interference of biochemical stimulation that could lead to misleading interpretation of the effects of the applied physical stimulations. On day 14, the expression of the early osteogenic gene ALP and the late osteogenic gene COL1 were evaluated by qPCR to provide a quantitative evaluation of the effect of individual or combined applied stimuli in terms of pro-osteogenic boost. Results revealed that bi-directional perfusion per se induced a ~ 40-fold up-regulation of COL1 in comparison to the control, and the further combination with PEMF stimulation boosted the up-regulation of COL1 up to ~ 80-fold. This result represents promising evidence that the combination of bi-directional perfusion and PEMF stimulation leads to a positive synergic contribution in promoting the expression of COL1, which is a fundamental component of the bone matrix. Indeed, COL1 represents the 90–95% of the organic components of the bone tissue and is one of the key factors in determining the bone mechanical properties (particularly elasticity and flexibility) [89]. At the cellular and subcellular level, this synergic effect is due to the combination of the fluid flow-induced shear stress and the PEMF secondary electric field induced in the constructs. Fluid flow-induced shear stress acts on the cell membrane and can deform it, leading to alteration of membrane proteins and causing mechano-activated ion channels to open and allow the influx of cations, such as Ca^{2+}, Na^{+}, and K^{+}, into the cell [36,90]. In parallel, PEMF stimulation can trigger the depolarization of the cell membrane and consequently stimulate ion currents, such as opening the Ca^{2+} channels and leading to an intracellular Ca^{2+} ion accumulation [91,92]. Such ions unbalance can activate specific cascades, such as the nuclear factors of activated cells (NFAT), enabling the transcription and the synthesis of osteogenic proteins [93]. Regarding the less evident effect of up-regulation observed for the ALP expression, although present, it should be noted that several studies reported ALP to be upregulated within 2 days of osteogenic induction [94]; therefore, 14 days could represent a too long culture time for appreciating the effect of physical stimulation on ALP expression.

In literature, only the study of Wang and colleagues combined a perfusion bioreactor with a sinusoidal electromagnetic field (EMF) generator [52]. In detail, rabbit MSCs were seeded on hydroxyapatite/collagen scaffolds and the constructs were cultured for 14 days under unidirectional perfusion (10 mL/min) and EMF stimulation (magnetic field intensity = 1 mT, frequency = 15 Hz, exposure time = 4 h/day) with and without osteogenic culture medium,

obtaining enhanced osteogenic differentiation at the end of the culture, similarly to our results. However, the system proposed by Wang et al. allowed delivering only unidirectional perfusion with no automated control of the pump [52]. Therefore, a further advantage and novelty of the presented platform is related to its versatility to combine automated uni-/bi-directional perfusion and PEMF stimulation, which was demonstrated to be crucial for boosting pro-osteogenic differentiation in 3D bone tissue models.

Some limitations could affect this study. In the CFD modelling the construct was assumed as a homogeneous and isotropic porous medium, lacking the information about the real microarchitecture of the Bio-Oss scaffold and neglecting the presence of the cells. Moreover, the simulations did not consider that along the culture the construct geometry is modified by cell proliferation and ECM deposition, which cause a decrease of the mean pore size and an increase of shear stress values over time. For these reasons, the computed shear stress values can be considered as a reasonable estimation for the early culture stage and in the future micro-computed tomography imaging of the constructs will be performed at day 0 and at different time points in order to precisely characterize the flow dynamics within the construct along its maturation [95–97]. As regards the electromagnetic field modelling, it was performed in steady-state conditions. Although this approach neglects the temporal evolution of the magnetic field occurring during a PEMF pulse, the results were sufficiently accurate for describing the conditions occurring at the pulse peak while allowing a significant reduction of the computational costs. Concerning the biological tests, it should be noted that for the perfusion condition a higher culture medium volume was used to compare with the static condition (50 mL vs 3 mL changed every 3 days, respectively). A higher culture medium volume provides a higher amount of nutrients, and it could be speculated that this aspect, rather than fluid flow-induced shear stress, could favor the metabolic activity of the cells cultivated under perfusion compared with the statically cultured ones. However, the fact that the ECM deposition was more marked for the constructs exposed to bi-directional perfusion compared with the ones cultured under unidirectional perfusion (same culture medium volume) confirms that perfusion plays a beneficial role in ECM deposition. Lastly, the adopted Bio-Oss scaffold probably further contributed to stimulating osteogenesis due to its chemical composition. However, since all the constructs cultured under either static or dynamic conditions were based on Bio-Oss scaffolds and were cultured using the same basal medium (DMEM), the observed differences can be directly ascribed to the applied culture conditions.

1.6 Conclusions

In this study, we developed, characterized, and tested a tunable perfusion bioreactor based on automated control that can be combined with PEMF stimulation devices to be used as a powerful tool for in vitro BTE production and investigations. The bioreactor is highly versatile as it allows housing constructs of different sizes and delivers individual or combined flow-induced shear stress and PEMF stimulations. Moreover, the adopted automation strategy

enables providing uni- or bi-directional perfusion within the same platform and using the same total culture medium volume, significantly reducing the user intervention and dependence along the culture and increasing robustness and reproducibility of the culture process. The preliminary biological tests on perfusion demonstrated that the only application of perfusion was crucial for promoting osteogenic differentiation in the cultured constructs, even without the use of biochemical stimulation. In fact, uni- and bi-directional perfusion conditions were effective in stimulating the osteogenic differentiation of the cultured 3D bone tissue models, and highlighted that bi-directional perfusion better promoted the ECM deposition throughout the construct. Lastly, as regards PEMF stimulation, biological results demonstrated the synergic pro-osteogenic effect of combining bi-directional perfusion and PEMF stimulation and confirmed that the proposed platform could be used for both the production of BTE constructs and as a powerful investigation tool. In the next future, an advanced investigation approach, based on the proposed bioreactor and high-throughput analyses, could lead to unravel molecular mechanisms activated by biophysical stimulation applied in clinic and to define the precise combinations of parameters inducing specific biological effects, paving the way for optimized orthopedic clinical protocols.

This chapter was published as a "research article" in the scientific journal *Scientific reports* from *Nature*:

Gabetti, S., Masante, B., Cochis, A., Putame, G., Sanginario, A., Armando, I., Fiume, E., Scalia, A. C., ***Daou, F.***, Baino, F., Salati, S., Morbiducci, U., Rimondini, L., Bignardi, C., & Massai, D. **(2022)**. An automated 3D-printed perfusion bioreactor combinable with pulsed electromagnetic field stimulators for bone tissue investigations. *Scientific reports*, 12(1), 13859. https://doi.org/10.1038/s41598-022-18075-1

1.7 Acknowledgments

The authors would like to express their sincere gratitude to Prof. Diana Massai, Dr. Stefano Gabetti, Dr. Beatrice Masante, and Dr. Govanni Putame from Polytechnic University of Turin for the design, fabrication, and optimization of the bioreactor culture chamber. The preliminary biological evaluations conducted at the University of Eastern Piedmont (UPO) provided the foundational input for this development.

I would also like to thank Prof. Lia Rimondini and Prof. Andrea Cochis for their supervision. A sincere thank you to my colleagues, Dr. Ajay Reddy Kumar and Dr. Alessandro Calogera Scalia, for their invaluable assistance with the experiments.

1.8 References

1. El-Rashidy, A.A., Roether, J.A., Harhaus, L., Kneser, U., and Boccaccini, A.R. (2017) Regenerating bone with bioactive glass scaffolds: A review of in vivo studies in bone defect models. *Acta Biomater.*, **62**.
2. Suryani, L. (2019) Effects of electromagnetic field on proliferation, differentiation, and mineralization of MC3T3 cells. *Tissue Eng. C Methods*, **25**.
3. Borgström, F. (2020) Fragility fractures in Europe: Burden, management and opportunities. *Arch. Osteoporos.*, **15**.
4. Kanis, J.A. (2021) SCOPE 2021: a new scorecard for osteoporosis in Europe. *Arch. Osteoporos.*, **16**.
5. Nauth, A., Schemitsch, E., Norris, B., Nollin, Z., and Watson, J.T. (2018) Critical-size bone defects: Is there a consensus for diagnosis and treatment? *J. Orthop. Trauma*, **32**.
6. Migliorini, F. (2021) Strategies for large bone defect reconstruction after trauma, infections or tumour excision: A comprehensive review of the literature. *Eur. J. Med. Res.*, **26**.
7. Pedrero, S.G., Llamas-Sillero, P., and Serrano-López, J. (2021) A Multidisciplinary journey towards bone tissue engineering. *Materials*, **14**.
8. Amini, A.R., Laurencin, C.T., and Nukavarapu, S.P. (2012) Bone tissue engineering: Recent advances and challenges. *Crit. Rev. Biomed. Eng.*, **40**.
9. Kargozar, S. (2019) Bone tissue engineering using human cells: A comprehensive review on recent trends, current prospects, and recommendations. *Appl. Sci.*, **9**.
10. Evans, C.H. (2011) Barriers to the clinical translation of orthopedic tissue engineering. *Tissue Eng. B Rev.*, **17**.
11. Campana, V. (2014) Bone substitutes in orthopaedic surgery: from basic science to clinical practice. *J. Mater. Sci. Mater. Med.*, **25**.
12. Mittwede, P.N., Gottardi, R., Alexander, P.G., Tarkin, I.S., and Tuan, R.S. (2018) Clinical applications of bone tissue engineering in orthopedic trauma. *Curr. Pathobiol. Rep.*, **6**.
13. Quarto, R., and Giannoni, P. (2016) Bone tissue engineering: Past-present-future. *Methods Mol. Biol.*, **1416**.
14. Vunjak Novakovic, G., Eschenhagen, T., and Mummery, C. (2014) Myocardial tissue engineering: In vitro models. *Cold Spring Harbor Perspect. Med.*, **4**.
15. Frost, H.M. (2004) A 2003 update of bone physiology and Wolff's Law for clinicians. *Angle Orthod.*, **74**.
16. Manokawinchoke, J. (2021) Mechanical loading and the control of stem cell behavior. *Arch. Oral Biol.*, **125**.
17. Wan, X., Liu, Z., and Li, L. (2021) Manipulation of stem cells fates: The master and multifaceted roles of biophysical cues of biomaterials. *Adv. Func. Mater.*, **31**.
18. Duval, K. (2017) Modeling physiological events in 2D vs 3D cell culture. *Physiology*, **32**.
19. Wendt, D., Riboldi, S.A., Cioffi, M., and Martin, I. (2009) Bioreactors in tissue engineering: scientific challenges and clinical perspectives. *Adv. Biochem. Eng. Biotechnol.*, **112**.
20. Yeatts, A.B., and Fisher, J.P. (2011) Bone tissue engineering bioreactors: Dynamic culture and the influence of shear stress. *Bone*, **48**.
21. Salter, E. (2012) Bone tissue engineering bioreactors: A role in the clinic? *Tissue Eng. B Rev.*, **18**.

22. Martin, I., Wendt, D., and Heberer, M. (2004) The role of bioreactors in tissue engineering. *Trends Biotechnol.*, **22**.
23. Martin, I., Smith, T., and Wendt, D. (2009) Bioreactor-based roadmap for the translation of tissue engineering strategies into clinical products. *Trends Biotechnol.*, **27**.
24. Hambor, J.E. (2012) Bioreactor design and bioprocess controls for industrialized cell processing: Bioengineering strategies and platform technologies. *BioProcess Int.*, **10**.
25. Massai, D. (2016) A versatile bioreactor for dynamic suspension cell culture: Application to the culture of cancer cell spheroids. *PLoS One*, **11**.
26. Massai, D. (2020) Bioreactor platform for biomimetic culture and in situ monitoring of the mechanical response of in vitro engineered models of cardiac tissue. *Front. Bioeng. Biotechnol.*, **8**.
27. Lim, D. (2021) Bioreactor design and validation for manufacturing strategies in tissue engineering. *Bio-des. Manuf.*
28. Thorpe, S.D. (2010) The response of bone marrow-derived mesenchymal stem cells to dynamic compression following TGF-β3 induced chondrogenic differentiation. *Ann. Biomed. Eng.*, **38**.
29. Steward, A.J., Wagner, D.R., and Kelly, D.J. (2014) Exploring the roles of integrin binding and cytoskeletal reorganization during mesenchymal stem cell mechanotransduction in soft and stiff hydrogels subjected to dynamic compression. *J. Mech. Behav. Biomed. Mater.*, **38**.
30. Zhao, Y.-. H. (2015) Hydrostatic pressure promotes the proliferation and osteogenic/chondrogenic differentiation of mesenchymal stem cells: The roles of RhoA and Rac1. *Stem Cell Res.*, **14**.
31. Sart, S., Agathos, S.N., Li, Y., and Ma, T. (2016) Regulation of mesenchymal stem cell 3D microenvironment: From macro to microfluidic bioreactors. *Biotechnol. J.*, **11**.
32. Alvarez-Barreto, J.F., Linehan, S.M., Shambaugh, R.L., and Sikavitsas, V.I. (2007) Flow perfusion improves seeding of tissue engineering scaffolds with different architectures. *Ann. Biomed. Eng.*, **35**.
33. Schmid, J. (2018) A perfusion bioreactor system for cell seeding and oxygen-controlled cultivation of three-dimensional cell cultures. *Tissue Eng. C Methods*, **24**.
34. Bancroft, G.N. (2002) Fluid flow increases mineralized matrix deposition in 3D perfusion culture of marrow stromal osteoblasts in a dose-dependent manner. *Proc. Natl. Acad. Sci. USA*, **99**.
35. Carpentier, B., Layrolle, P., and Legallais, C. (2011) Bioreactors for bone tissue engineering. *Int. J. Artif. Org.*, **34**.
36. Wittkowske, C., Reilly, G.C., Lacroix, D., and Perrault, C.M. (2016) In vitro bone cell models: Impact of fluid shear stress on bone formation. *Front. Bioeng. Biotechnol.*, **4**.
37. Bancroft, G.N., Sikavitsas, V.I., and Mikos, A.G. (2003) Technical note: Design of a flow perfusion bioreactor system for bone tissue-engineering applications. *Tissue Eng.*, **9**.
38. Datta, N. (2006) In vitro generated extracellular matrix and fluid shear stress synergistically enhance 3D osteoblastic differentiation. *Proc. Natl. Acad. Sci. USA*, **103**.
39. Wendt, D., Marsano, A., Jakob, M., Heberer, M., and Martin, I. (2003) Oscillating perfusion of cell suspensions through three-dimensional scaffolds enhances cell seeding efficiency and uniformity. *Biotechnol. Bioeng.*, **84**.

40. Du, D., Furukawa, K., and Ushida, T. (2008) Oscillatory perfusion seeding and culturing of osteoblast-like cells on porous beta-tricalcium phosphate scaffolds. *J. Biomed. Mater. Res.*, **86A**.
41. Koch, M.A., Vrij, E.J., Engel, E., Planell, J.A., and Lacroix, D. (2010) Perfusion cell seeding on large porous PLA/calcium phosphate composite scaffolds in a perfusion bioreactor system under varying perfusion parameters. *J. Biomed. Mater. Res.*, **95A**.
42. Engel, N. (2021) An optimized 3D-printed perfusion bioreactor for homogeneous cell seeding in bone substitute scaffolds for future chairside applications. *Sci. Rep.*, **11**.
43. Knothe Tate, M.L. (2003) Whither flows the fluid in bone? An osteocyte's perspective. *J. Biomech.*, **36**.
44. Fritton, S.P., and Weinbaum, S. (2009) Fluid and solute transport in bone: Flow-induced mechanotransduction. *Annu. Rev. Fluid Mech.*, **41**.
45. Tseng, C.-. L., Chang, K.-. M., Wu, C.-. C., Wang, Y.-. K., and Wang, I.-. K. (2014) Rabbit mesenchymal stem cells cultured in a dynamic culture system displayed superior cell proliferation and osteogenetic induction. *J. Exp. Clin. Med.*, **6**.
46. Chen, G., Xu, R., Zhang, C., and Lv, Y. (2017) Responses of MSCs to 3D scaffold matrix mechanical properties under oscillatory perfusion culture. *ACS Appl. Mater. Interfaces*, **9**.
47. Beşkardeş, I.G., Aydın, G., Bektaş, Ş., Cengiz, A., and Gümüşderelioğlu, M. (2018) A systematic study for optimal cell seeding and culture conditions in a perfusion mode bone-tissue bioreactor. *Biochem. Eng. J.*, **132**.
48. Du, D., Furukawa, K.S., and Ushida, T. (2009) 3D culture of osteoblast-like cells by unidirectional or oscillatory flow for bone tissue engineering. *Biotechnol. Bioeng.*, **102**.
49. Ceccarelli, G. (2013) A comparative analysis of the in vitro effects of pulsed electromagnetic field treatment on osteogenic differentiation of two different mesenchymal cell lineages. *BioRes. Open Access*, **2**.
50. Cadossi, R., Massari, L., Racine-Avila, J., and Aaron, R.K. (2020) Pulsed electromagnetic field stimulation of bone healing and joint preservation: Cellular mechanisms of skeletal response. *J. Am. Acad. Orthop. Surg. Glob. Res. Rev.*, **4**.
51. Daish, C., Blanchard, R., Fox, K., Pivonka, P., and Pirogova, E. (2018) The application of pulsed electromagnetic fields (PEMFs) for bone fracture repair: Past and perspective findings. *Ann. Biomed. Eng.*, **46**.
52. Wang, H. (2019) Enhanced osteogenesis of bone marrow stem cells cultured on hydroxyapatite/collagen I scaffold in the presence of low-frequency magnetic field. *J. Mater. Sci.*, **30**.
53. Varani, K. (2021) Pulsed electromagnetic field stimulation in osteogenesis and chondrogenesis: signaling pathways and therapeutic implications. *IJMS*, **22**.
54. Markov, M.S. (2007) Pulsed electromagnetic field therapy history, state of the art and future. *Environmentalist*, **27**.
55. Hu, H. (2020) Promising application of pulsed electromagnetic fields (PEMFs) in musculoskeletal disorders. *Biomed. Pharmacother.*, **131**.
56. Zhang, B., Xie, Y., Ni, Z., and Chen, L. (2020) Effects and mechanisms of exogenous electromagnetic field on bone cells: A review. *Bioelectromagnetics*, **41**.

57. Zhang, X., Tiainen, H., and Haugen, H.J. (2019) Comparison of titanium dioxide scaffold with commercial bone graft materials through micro-finite element modelling in flow perfusion. *Med. Biol. Eng. Comput.*, **57**.
58. Brinkman, H.C. (1949) A calculation of the viscous force exerted by a flowing fluid on a dense swarm of particles. *Appl. Sci. Res.*, **1**.
59. Wang, D.M., and Tarbell, J.M. (1995) Modeling interstitial flow in an artery wall allows estimation of wall shear stress on smooth muscle cells. *J. Biomech. Eng.*, **117**.
60. Vossenberg, P., Higuera, G.A., Straten, G., Blitterswijk, C.A., and Boxtel, A.J.B. (2009) Darcian permeability constant as indicator for shear stresses in regular scaffold systems for tissue engineering. *Biomech. Model. Mechanobiol.*, **8**.
61. Fassina, L. (2006) Effects of electromagnetic stimulation on calcified matrix production by SAOS-2 cells over a polyurethane porous scaffold. *Tissue Eng.*, **12**.
62. Pisitpipathsin, N., Kantha, P., Eitsayeam, S., Rujijanakul, G., Guo, R., Bhalla, A.S., and Pengpat, K. (2013) Effect of BCZT on Electrical Properties and Bioactivity of 45S5 Bioglass. *Integrated Ferroelectrics*, **142** (1), 144–153.
63. Chen, M.-T., Jiang, C., Vernier, P.T., Wu, Y.-H., and Gundersen, M.A. (2009) Two-dimensional nanosecond electric field mapping based on cell electropermeabilization. *PMC Biophysics 2009 2:1*, **2** (1), 1–16.
64. Tandon, N., Marsano, A., Maidhof, R., Wan, L., Park, H., and Vunjak-Novakovic, G. (2011) Optimization of Electrical Stimulation Parameters for Cardiac Tissue Engineering. *J Tissue Eng Regen Med*, **5** (6), e115.
65. Mukherjee, A.K., and Patri, M. (1990) Electrical properties of chlorinated atactic polypropylene (CAPP) and PVC–DOP–CAPP system. *J Appl Polym Sci*, **39** (7), 1485–1493.
66. Sohrabi, M. (2020) Enhancing mechanical properties and biological performances of injectable bioactive glass by gelatin and chitosan for bone small defect repair. *Biomedicines*, **8**.
67. Livak, K.J., and Schmittgen, T.D. (2001) Analysis of Relative Gene Expression Data Using Real-Time Quantitative PCR and the 2−ΔΔCT Method. *Methods*, **25** (4), 402–408.
68. Schmittgen, T.D., and Livak, K.J. (2008) Analyzing real-time PCR data by the comparative CT method. *Nature Protocols 2008 3:6*, **3** (6), 1101–1108.
69. Martino, F., Perestrelo, A.R., Vinarský, V., Pagliari, S., and Forte, G. (2018) Cellular mechanotransduction: From tension to function. *Front. Physiol.*, **9**.
70. Kim, M.-. H., and Kino-oka, M. (2021) Mechanobiological conceptual framework for assessing stem cell bioprocess effectiveness. *Biotechnol. Bioeng.*, **118**.
71. Ethier, C.R., and Simmons, C.A. (2007) *Introductory Biomechanics from Cells to Organisms*, Cambridge University Press.
72. Zhou, J. (2014) Different electromagnetic field waveforms have different effects on proliferation, differentiation and mineralization of osteoblasts in vitro: Effects of electromagnetic fields on osteoblasts. *Bioelectromagnetics*, **35**.
73. Smith, L.J., Li, P., Holland, M.R., and Ekser, B. (2018) FABRICA: A bioreactor platform for printing, perfusing, observing, & stimulating 3D tissues. *Sci. Rep.*, **8**.
74. Putame, G. (2019) Application of 3D printing technology for design and manufacturing of customized components for a mechanical stretching bioreactor. *J. Healthc. Eng.*, **2019**.

75. Wendt, D., Riboldi, S.A., Cioffi, M., and Martin, I. (2009) Potential and bottlenecks of bioreactors in 3D cell culture and tissue manufacturing. *Adv. Mater.*, **21**.
76. Hansmann, J., Groeber, F., Kahlig, A., Kleinhans, C., and Walles, H. (2013) Bioreactors in tissue engineering-principles, applications and commercial constraints. *Biotechnol. J.*, **8**.
77. Putame, G. (2020) Compact and tunable stretch bioreactor advancing tissue engineering implementation: Application to engineered cardiac constructs. *Med. Eng. Phys.*, **84**.
78. Stavenschi, E., Labour, M.-. N., and Hoey, D.A. (2017) Oscillatory fluid flow induces the osteogenic lineage commitment of mesenchymal stem cells: The effect of shear stress magnitude, frequency, and duration. *J. Biomech.*, **55**.
79. Zhao, F., Rietbergen, B., Ito, K., and Hofmann, S. (2018) Flow rates in perfusion bioreactors to maximise mineralisation in bone tissue engineering in vitro. *J. Biomech.*, **79**.
80. Li, D., Tang, T., Lu, J., and Dai, K. (2009) Effects of flow shear stress and mass transport on the construction of a large-scale tissue-engineered bone in a perfusion bioreactor. *Tissue Eng. A*, **15**.
81. Vetsch, J.R., Betts, D.C., Müller, R., and Hofmann, S. (2017) Flow velocity-driven differentiation of human mesenchymal stromal cells in silk fibroin scaffolds: A combined experimental and computational approach. *PLoS One*, **12**.
82. McCoy, R.J., Jungreuthmayer, C., and O'Brien, F.J. (2012) Influence of flow rate and scaffold pore size on cell behavior during mechanical stimulation in a flow perfusion bioreactor. *Biotechnol. Bioeng.*, **109**.
83. Olivares, A.L., Marsal, È., Planell, J.A., and Lacroix, D. (2009) Finite element study of scaffold architecture design and culture conditions for tissue engineering. *Biomaterials*, **30**.
84. Najmi, Z. (2020) Evaluation of nisin and LL-37 antimicrobial peptides as tool to preserve articular cartilage healing in a septic environment. *Front. Bioeng. Biotechnol.*, **8**.
85. Holtorf, H.L., Jansen, J.A., and Mikos, A.G. (2005) Flow perfusion culture induces the osteoblastic differentiation of marrow stromal cell-scaffold constructs in the absence of dexamethasone. *J. Biomed. Mater. Res. A*, **72A**.
86. Ding, C.-. M., Zhou, Y., He, Y.-. N., and Tan, W.-. S. (2008) Perfusion seeding of collagen–chitosan sponges for dermal tissue engineering. *Process. Biochem.*, **43**.
87. Seddiqi, H. (2020) Inlet flow rate of perfusion bioreactors affects fluid flow dynamics, but not oxygen concentration in 3D-printed scaffolds for bone tissue engineering: Computational analysis and experimental validation. *Comput. Biol. Med.*, **124**.
88. Bergholt, N.L., Lysdahl, H., Lind, M., and Foldager, C.B. (2019) A standardized method of applying toluidine blue metachromatic staining for assessment of chondrogenesis. *Cartilage*, **10**.
89. Lehmann, T.P. (2021) The regulation of collagen processing by miRNAs in disease and possible implications for bone turnover. *Int. J. Mol. Sci.*, **23**.
90. McMahon, L.A., Campbell, V.A., and Prendergast, P.J. (2008) Involvement of stretch-activated ion channels in strain-regulated glycosaminoglycan synthesis in mesenchymal stem cell-seeded 3D scaffolds. *J. Biomech.*, **41**.
91. Murillo, G. (2017) Electromechanical Nanogenerator-cell interaction modulates cell activity. *Adv. Mater.*, **29**.
92. More, N., and Kapusetti, G. (2017) Piezoelectric material: A promising approach for bone and cartilage regeneration. *Med. Hypotheses*, **108**.

93. Jacob, J., More, N., Kalia, K., and Kapusetti, G. (2018) Piezoelectric smart biomaterials for bone and cartilage tissue engineering. *Inflamm. Regener.*, **38**.
94. Golub, E.E., and Boesze-Battaglia, K. (2007) The role of alkaline phosphatase in mineralization. *Curr. Opin. Orthop.*, **18**.
95. Massai, D. (2014) Image-based three-dimensional analysis to characterize the texture of porous scaffolds. *Biomed. Res. Int.*, **2014**.
96. Zermatten, E. (2014) Micro-computed tomography based computational fluid dynamics for the determination of shear stresses in scaffolds within a perfusion bioreactor. *Ann. Biomed. Eng.*, **42**.
97. Pecci, R., Baiguera, S., Ioppolo, P., Bedini, R., and Gaudio, C. (2020) 3D printed scaffolds with random microarchitecture for bone tissue engineering applications: Manufacturing and characterization. *J. Mech. Behav. Biomed. Mater.*, **103**.

Chapter 2

In Vitro Reproduction of Trabecular Bone Microenvironment for Investigating the Effects of Pulsed Electromagnetic Field Stimulation on Human Mesenchymal Stem Cells

2.1 Abstract

Bone tissue possesses a complex hierarchical structure and serves crucial mechanical and biological functions. To advance bone biology research and regenerative therapies, *in vitro* models replicating the *in vivo* environment are essential. This study employed an advanced *in vitro* bioreactor-based platform to investigate the impact of biophysical stimuli on bone regeneration and healing. Human bone marrow-derived mesenchymal stem cells (BM-MSCs) were seeded onto 3D-printed polylactic acid (PLA) scaffolds mimicking the architecture of trabecular bone (referred to as PLA600) using three cell seeding methods: suspension seeding, cell-releasing alginate, and cell-releasing collagen. The seeded scaffolds were cultured in the perfusion bioreactor, providing fluid flow-induced shear stress, as previously described in Chapter 1. Cell-releasing collagen proved optimal for cell infiltration and distribution, enabling the generation of trabecular bone-like tissues *in vitro*. To further enhance bone tissue regeneration, pulsed electromagnetic field (PEMF) stimulation was integrated into the bioreactor-based platform, as previously described in Chapter 1. BM-MSCs were cultured in either basal medium or osteogenic medium under fluid flow-induced shear stress with and without PEMF stimulation. Our findings revealed that the combined application of PEMF stimulation and fluid flow-induced shear stress significantly promoted BM-MSC osteogenic differentiation, only in the absence of the biochemical stimuli of the osteogenic medium. Thus, this bioreactor-based platform offers a promising approach for studying bone biology and exploring non-invasive therapeutic strategies for bone regeneration.

2.2 Introduction

A total of 213 bones, excluding the sesamoid bones, make up the adult human skeleton. These bones serve diverse mechanical, chemical, and biological functions. They provide the body's framework necessary to support the body, facilitate movement and locomotion by acting as attachment points for muscles, and offer a shield that protects the vital organs from injury. Moreover, they maintain the mineral balance within the body, regulate acid-base

equilibrium, serve as storage sites for growth factors and cytokines, as well as house the bone marrow, where blood cells are produced [1] and mesenchymal stem cells reside [2].

Bone is a calcified tissue, generally composed of 60% inorganic component (primarily crystalline hydroxyapatite: $[Ca_3(PO_4)_2]_3Ca(OH)_2$), 10% water and 30% organic component (comprises more than 30 proteins with type I collagen being the most abundant, around 90%) by weight [3]. The cells inhabiting this tissue are osteoclasts (bone-resorbing cells) and osteoblasts (bone-forming cells), in addition to osteocytes and bone lining cells that are both involved in bone remodeling, among other functions. While osteoclasts originate from hematopoietic stem cells, osteoblasts originate from mesenchymal stem cells that are in turn transformed to osteocytes and bone-lining cells [4].

Bones can be categorized by shape (long, short, flat, and irregular bones) and porosity (cortical bone, also known as compact bone or dense bone, with 5-15% porosity, and trabecular bone, also known as cancellous bone or spongy bone, with 40-95% porosity) [5]. There are various levels of hierarchical structural organization of bone tissue, which are: (1) the macrostructure: cortical and trabecular bone; (2) the microstructure (from 10 to 500 μm): Haversian systems, osteons, and single trabeculae; (3) the sub-microstructure (1–10 μm): lamellae; (4) the nanostructure (from a few hundred nanometers to 1 μm): fibrillar collagen and embedded mineral; and (5) the sub-nanostructure (below a few hundred nanometers): molecular structure of constituent elements, such as mineral, collagen, and non-collagenous organic proteins [6]. The mechanical properties of bone are depicted by its composition and the various levels of hierarchical structural organization [7].

Thus, the cellular microenvironment of bone tissue is complex and dynamic, significantly influencing cellular behavior. Consequently, *in vitro* experiments should strive to replicate the *in vivo* niche as faithfully as possible to yield accurate and reliable results. Researchers have been incorporating tissue engineering concepts and tools into biomedical research to facilitate the transition toward more elaborate *in vitro* tissue models for studying cell behavior in healthy or diseased states [8]. Bone tissue engineering (BTE) has focused on developing engineered constructs to induce the regeneration of functional bone tissues via three components (i.e., biomaterials, cells, and signaling molecules). It offers a potential alternative to conventional bone grafts [9]. Although only a few bone tissue-engineered constructs have been translated from bench to bedside due to technical, business, and philosophical challenges [10], recent advancements have transformed this field, with bone tissue-engineered constructs serving as *in vitro* models for studying bone physiology and pathology [11]. These novel *in vitro* tissue models exhibit unique attributes that set them apart from the traditional *in vitro* ones, primarily their 3D architecture and the application of biomechanical stimuli. However, to maximize their effectiveness, it is essential to understand their limitations and strengths.

The transition from 2D to 3D cell culture in BTE [12] requires careful consideration of several factors, including pore size (commonly ranging from 100 to 800 μm) to mimic the microarchitecture of trabecular bone and provide stem cells with geometrical cues for

osteogenic differentiation [13]. 3D cell cultures are increasingly favored over 2D cell cultures for several valid reasons. While 2D cell cultures are cost-effective and easy to manipulate, they do not accurately replicate the physiological cellular microenvironment. In contrast, 3D cell cultures offer a more faithful representation of the physiological cellular microenvironment by preserving cell shape, cell-to-cell interactions, cell-to-extracellular matrix (ECM) interactions, proliferation rates, as well as gene and protein expression levels, allowing for better modeling of physiological and pathological conditions. As a result, 3D cell cultures became widely used in drug discovery, cell therapy, tissue engineering, regenerative medicine, and modeling pathologies [12].

The various 3D cell culture techniques can be grouped into non-scaffold-based methods (e.g., hanging drop, low attachment plate, magnetic levitation), scaffold-based approaches utilizing natural and synthetic biomaterials, and specialized platforms (e.g., microfluidic devices, micropatterned plates) [14]. However, each technique has its own set of advantages and disadvantages, with the most significant challenges lying in the complex workflow and the final analyses [15]. It is essential to note that 3D cultures, while more physiologically relevant than 2D cultures, do not fully capture the complexity of the *in vivo* niche. They often lack the relevant cell types, growth factors, and long-distance signaling from other organ systems (e.g. the immune and endocrine systems), and their static nature prevents them from replicating the dynamic perfusion and other mechanical stresses experienced *in vivo* [16]. Despite the challenges, 3D cell cultures offer greater utility than 2D cell cultures, as evidenced by the discrepancies in the results obtained using these two cell culture techniques [17–19].

Additionally, scaling up the size of bone tissue-engineered constructs poses a significant challenge due to the limitations of passive diffusion. This restricts the transfer of nutrients and gasses within the 3D scaffolds, often leading to the formation of a necrotic core inside the constructs [20]. To improve mass transfer to cells, dynamic cell cultures using bioreactors can be employed. The use of bioreactors can help in mimicking the supply of nutrients and gasses, the continuous waste removal, as well as the mechanical stimulation of cells. Notable examples include the spinner-flask bioreactor, rotating wall vessels, and perfusion bioreactors (including Quasi Vivo® (QV) system and microfluidics). However, there is also a lack of established guidelines regarding the optimal flow rates, culture medium volume, and the implementation of non-invasive, real-time *in situ* monitoring [21], and thus, the utilization of bioreactors in various fields of research is still not standardized.

Beyond mass transfer, bioreactors are crucial for providing tissue-specific biophysical stimuli [22]. Mechanical stresses play a crucial role in *in vivo* environments. This has prompted researchers to introduce similar stimuli into *in vitro* ones. Cells are constantly and cyclically subjected to cyclic mechanical cues, both intrinsic (e.g., changes in cell density, shape, ECM elasticity, and topography) and extrinsic (e.g., shear stress from fluid flow, hydrostatic pressure, compression, and tension) [23]. Their ability to respond to mechanical stimuli within milliseconds is known as “mechanotransduction”. This process comprises three key stages: first, the cells sense the stimuli (mechanosensing); second, signals are transmitted

across the cells (mechanotransmission); and finally, the cells respond to the stimuli by altering cellular activities (mechanoresponse) [24]. Given the sensitivity of bone cells to biophysical stimuli, accurately identifying the specific stimuli they encounter during cell culture is essential. This knowledge can bridge the gap between in vitro applications and the biophysical conditions prevalent in native tissues [22].

As such, bone tissue-engineered constructs offer unprecedented opportunities to study bone development, fracture healing, and the pathogenesis of bone diseases, such as osteoporosis and osteoarthritis. While these models can more accurately replicate the spatial and biomechanical complexity observed *in vivo*, their clinical relevance should be interpreted with caution, as they lack the full complexity of an *in vivo* environment. As more researchers adopt 3D cell cultures, new methodologies will emerge, further advancing the development and validation of these models. Moreover, even if only a few aspects of the *in vivo* environment can be replicated *in vitro*, novel *in vitro* models often exhibit higher predictive values compared to conventional ones. This strengthens the correlation between these models and animal studies. Consequently, these *in vitro* tissue models can contribute to reducing the use of animals in research, aligning with the principles of the European Directive 2010/63/EC. This directive emphasizes the "3Rs" strategy (reduction, refinement, and replacement) to reinforce the importance of using alternative *in vitro* and *in silico* methods for obtaining the essential information prior to clinical trials [25].
The biophysical stimuli that cells in the body are exposed to extend to electrical fields (EF), magnetic fields (MF) and electromagnetic fields (EMF) ones. The frequency range of such stimuli is extremely low (0-300 Hz), encompassing the action potentials of nerves and heart tissue, skeletal muscle vibrations and frequencies elicited by rhythmic activities within other body tissues [26]. Bone tissue is particularly responsive to these stimuli due to its inherent piezoelectric properties, primarily derived from the highly organized and aligned structure of collagen fibers within the bone matrix [27]. Thus, bone is an electromechanically responsive tissue, responding to external stimuli under two different configurations. The first is the direct piezoelectric effect, which converts mechanical energy (compressive stress, tensile stress, and applied vibration) to electrical energy. The second is the converse piezoelectric effect, which converts electrical energy to mechanical energy, and can produce contraction, elongation, and vibration [27]. Both direct and converse piezoelectric effects can promote bone healing and regeneration; however, it is highly challenging, even in tissues or cells studied *in vitro*, to determine which responses directly result from piezoelectric effects.

Biophysical intrinsic stimulation, often occurring in the form of pulsed EMFs (PEMFs), is known to induce osteogenesis. Consequently, extrinsic PEMF stimulation has been applied to stimulate bone healing and regeneration [26]. To harness the beneficial effects of these bioelectric signals, researchers have explored the use of smart piezoelectric biomaterials, which can mimic natural bone bioelectric signals through direct and converse piezoelectric effects. Examples include inorganic piezoceramics (lead-based, lead-free, or titanates), organic piezoelectric polymers (synthetic and natural), and composites combining inorganic piezoceramics and organic piezoelectric polymers [27]. Polylactic acid (PLA), a bio-based piezoelectric polymer, is permitted for the use in several biomedical applications by the Food

and Drug Administration (FDA). Additionally, the FDA and European regulatory bodies have allowed the use of PLA resin in food and drug delivery systems [28]. As an FDA-approved biomaterial, PLA has been widely applied due to its unique properties, including biocompatibility, biodegradability, and piezoelectricity (piezoelectric constant is approximately -10 pico Coulombs/N [pC/N]) [29].

The primary objective of our study was to develop an advanced *in vitro* bioreactor-based technology for bone biology research. We used a recently proposed advanced technology, described in Chapter 1, based on an automated perfusion bioreactor that provides bone-tissue-like mechanical stimulation (i.e., fluid flow-induced shear stress) and can be equipped with a custom-made PEMF stimulator. We initially constructed trabecular bone-like tissues by seeding human bone marrow-derived mesenchymal stem cells (BM-MSCs) on 3D-printed biomimetic PLA scaffolds, designed to mimic the human trabecular bone architecture in physiological conditions and to resemble the morphological features of the iliac crest (referred to as PLA600). To optimize BM-MSC attachment and culturing under fluid flow-induced shear stress, we compared various cell-seeding methods including suspension seeding, cell-releasing 2% alginate, and 0.5% cell-releasing collagen. Next, we cultured the most promising trabecular bone tissues in both basal and osteogenic media while applying PEMF stimulation. This allowed us to identify the culture medium that best facilitated the detection of BM-MSC responses to PEMF stimulation under fluid flow-induced shear stress.

2.3 Materials and Methods

2.3.1 3D printing and characterization of the trabecular bone-like polylactic acid (PLA) scaffolds resembling the morphological features of the iliac crest (referred to as PLA600)

The design and fabrication of the 3D-printed, biomimetic PLA600 scaffolds have been carried out according to a previously reported procedure [30]. Briefly, a random 3D distribution of spheres, as virtual porogens with a diameter of 600 μm, was created by means of a custom-made script to be subtracted from a cylindrical volume (10 mm diameter, 5 mm height) to prepare the scaffold computer-aided design (CAD) models. The resulting files were imported to ideaMaker (Raise3D Inc., Irvine, CA, USA) and sliced in the Z direction at 0.25 mm. Scaffolds were then fabricated by processing a PLA filament (FormFutura BV, The Netherlands) using a Raise 3D N2 printer (Raise 3D Inc., Irvine, CA, USA), setting the nozzle temperature at 205 °C and the build plate temperature at 60 °C. The resulting scaffolds had a trabecular spacing of 531 μm, a trabecular thickness of 350 μm, and a total porosity of 60.34%. The scaffolds were previously characterized and tested for bioactivity [31]. The resulting scaffolds have a mean permeability value of 2.36×10^{-10} m^2 [32]. The scaffolds were submerged in phosphate-buffered saline (PBS, 1X) and agitated on an orbital shaker for 2 h to remove polymeric residues. Subsequently, they were sterilized by immersion in 70% ethanol for 4 h, followed by air drying.

2.3.2 Parallelized, automated perfusion bioreactor equipped with PEMF stimulator

An automated perfusion bioreactor equipped with a custom-made PEMF stimulator, previously developed and described in Chapter 1, was parallelized here. Briefly, the parallelized, automated perfusion bioreactor consists of three independent 3D-printed culture chambers (CCs) connected to three independent closed-loop hydraulic circuits controlled by a custom control unit, designed for housing and culturing the 3D bone-like tissues under direct perfusion **(Figure 2.1)**. Direct perfusion guarantees continuous medium flow through the cultured constructs, ensuring efficient mass transport and exposing the constructs to fluid flow-induced shear stress, which is known to promote proliferation and differentiation of osteoblasts and favor bone mineralization [33,34].

Each CC (Dental SG Resin, Formlabs, United States) is composed of two screwable parts that allow housing constructs of different sizes, which are in turn press-fit in a tailored polydimethylsiloxane (PDMS) holder (SYLGARD 184, Dow Corning, United States). Each closed loop hydraulic circuit is composed of oxygen-permeable tubing (Darwin Microfluidics, France) and a culture medium reservoir, and is connected to a multichannel peristaltic pump (G100-1 J, Longer Precision Pump, China) suitable to be incubated at 37oC. The pump is controlled by a custom control unit, equipped with a microcontroller board (Arduino Micro, Arduino, Italy), that allows setting the pump's parameters and guarantees the same perfusion conditions in each CC. Finally, the custom-made PEMF stimulator (IGEA

Clinical Biophysics, Italy) consists of a generator and two solenoids among which the bioreactor CCs can be placed (magnetic field intensity = 1.5 mT, frequency = 75 Hz).

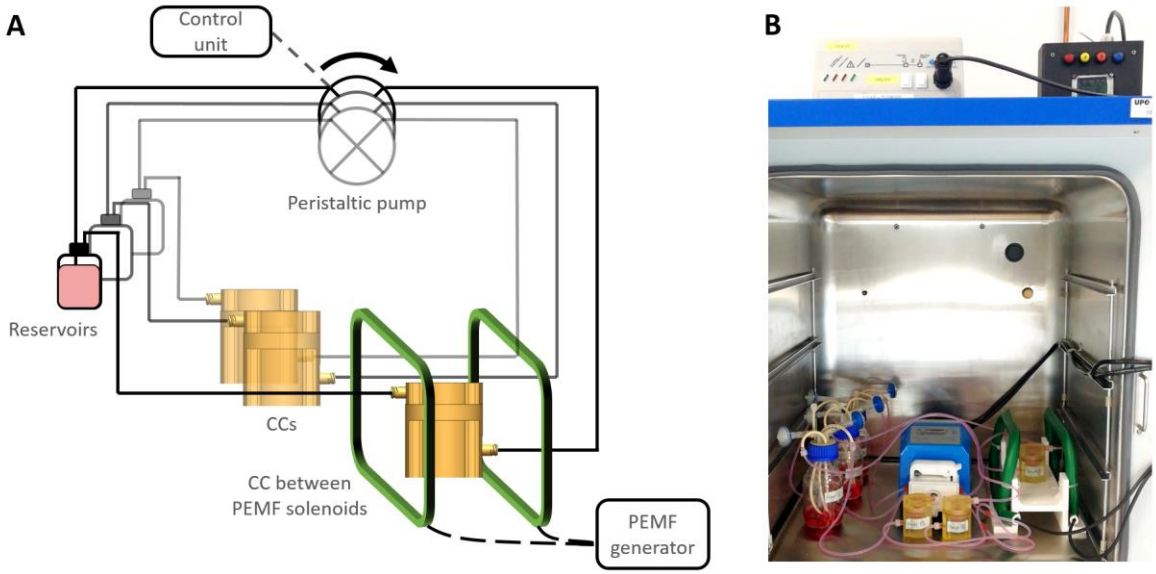

Figure 2.1. The bioreactor-based investigation platform. **(A)** Schematic representation of the parallelized, automated perfusion bioreactor and the custom-made pulsed electromagnetic field (PEMF) stimulator set-up, with three independent culture chambers and hydraulic circuits; **(B)** Parallelized, automated perfusion bioreactor and PEMF stimulator set-up within the incubator.

2.3.3 Trabecular bone-like tissue preparation and evaluation

2.3.3.1 Cell culture conditions

Human telomerase reverse transcriptase (hTERT)-immortalized BM-MSCs of clonal line Y201, which was generated by James et al. [35], were cultivated in basal medium (BM) that is low-glucose Dulbecco's modified Eagle's medium (DMEM, gibco, Thermo Fisher Scientific, Inc.) supplemented with 15% fetal bovine serum (FBS, gibco Thermo Fisher Scientific, Inc.) and 1% antibiotics (penicillin/streptomycin, gibco Thermo Fisher Scientific, Inc.) and incubated in a humidified atmosphere with 5% CO_2 at 37°C. The cells were passaged once they reached 80-90% confluency by enzymatic digestion using trypsin/ethylenediamine tetraacetic acid (trypsin/EDTA, gibco Thermo Fisher Scientific, Inc.) before each assay.

2.3.3.2 Cell seeding and culturing under two conditions

Cells were directly seeded on the top of the PLA600 scaffolds inserted in the PDMS holders of the automated bioreactor placed in a 6-well cell culture plate either by suspension seeding or by using cell-releasing hydrogels at a defined density of 3x106 cells and a defined volume of 200 µL. For suspension seeding, cells were resuspended in 200 µL of BM; for cell-

releasing 2% alginate, 4% (40 mg/mL) alginate solution was prepared using alginic acid sodium salt from brown algae (Medium viscosity, Merck, Italy), and then mixed in a 1:1 ratio with the cell suspension; and for cell-releasing 0.5% collagen, cells were resuspended in 200 µL of 5 mg/mL PureCol EZ Gel solution (Merck, Italy). Samples were incubated for 4-6 h to allow cell infiltration and adhesion. Then, samples seeded by suspension seeding and cell-releasing 0.5% collagen were covered by BM and incubated overnight; whereas samples seeded by cell-releasing 2% alginate were incubated overnight in 150 µL of 0.2 M calcium chloride ($CaCl_2$) solution, and then washed once with PBS (1X) to remove the $CaCl_2$ solution. After the overnight incubation, the samples were cultured in two different culture conditions for 21 days: static culture, in which the samples were kept in the cell culture plate, and BM was changed every 3-4 days; and direct perfusion, in which samples were placed in the automated perfusion bioreactor under unidirectional, direct perfusion at 0.3 mL/min with 50 mL of BM pumped from the reservoir, and the medium was changed every 7 days. Samples were evaluated in triplicates (n = 3).

2.3.3.3 Cell viability assay

On day 21 of culture, the viability of BM-MSCs seeded on the biomimetic PLA600 scaffolds using the three different cell seeding methods and cultured under the two different culture conditions was evaluated via the live/dead cell assay (LIVE/DEAD™ Viability/Cytotoxicity Kit for mammalian cells, Invitrogen Life Technologies). Briefly, the scaffolds were removed from the CCs of the bioreactor, placed in a 24-well cell culture plate, washed with PBS (1X), and then incubated in a BM containing 2 µM calcein-AM and 2 µM ethidium homodimer-1 (EthD-1). After 15 min of incubation at 37°C and 5% CO_2 atmosphere, cells were imaged using a fluorescence microscope (THUNDER Imager 3D Cell Culture, Leica Microsystems) to visualize the green calcein AM that stains live cells and the red EthD-1 that stains dead cells.

2.3.3.4 Cell infiltration and distribution assessment

On day 21 of culture, the infiltration and distribution of BM-MSCs were examined using a scanning electron microscope (SEM) (JSM-IT500, JEOL, Italy). For SEM analysis, the scaffolds were removed from the CCs of the bioreactor, placed in a 24-well cell culture plate, and gently washed with PBS (1X). Then, cells were fixed with 2.5% glutaraldehyde at 4°C overnight, and after cell fixation, the 2.5% glutaraldehyde was dispensed, and samples were washed with PBS (1X), dehydrated in graded alcohol of 30%, 50%, 70%, 90%, and 100% (twice) for 30 min each, covered by hexamethydisilazane (HMDS) for 30 min, and then air-dried in a chemical fume hood. Finally, samples were coated with gold using a sputter coating machine (DII-29030SCTR Smart Coater, JEOL, Italy).

2.3.4 Trabecular bone-like tissue stimulation using PEMF

Following the selection of the optimal cell seeding method, which is cell-releasing 0.5% collagen, the bioreactor-based investigation platform was used to perform preliminary studies on PEMF stimulation for bone healing.

2.3.4.1 Trabecular bone-like tissue culturing under six conditions

Cells were directly seeded on the top of the PLA scaffolds inserted in the PDMS holders of the bioreactor placed in a 6-well cell culture plate by using cell-releasing 0.5% collagen at a defined density of 3x106 cells and a defined volume of 200 µL, as described in Section 2.3.2. The samples were cultured for 21 days either in BM or osteogenic medium (OM) (low-glucose DMEM supplemented with 10% FBS, 1% antibiotics, 20 mM β-glycerophosphate, 50 µM ascorbic acid-2-phosphate, and 10-7 M dexamethasone). Samples in BM and OM were cultured in three different culture conditions: static culture, in which the samples were kept in the cell culture plate, and BM or OM was changed every 3-4 days; direct perfusion, in which samples were placed in the automated bioreactor under unidirectional, direct perfusion at 0.3 mL/min with 50 mL of BM or OM pumped from the reservoir, and the media were changed every 7 days; and direct perfusion with PEMF stimulation, in which samples were placed in the automated bioreactor under unidirectional, direct perfusion at 0.3 mL/min with 50 mL of BM or OM pumped from the reservoir, and media were changed every 7 days, accompanied by PEMF stimulation (1.5 mT, 75 Hz) for 4 h per day (corresponding to a cumulative dose of around 75 h over 21 days). Samples were evaluated in triplicates (n = 3).

2.3.4.2 Gene expression analyses

To evaluate osteogenesis, reverse transcription-quantitative PCR (RT-qPCR) was performed. First, the total RNA was extracted using TRIzol™ Reagent (Invitrogen Life Technologies) according to the manufacturer's instructions, except for allowing cell lysing for 10 minutes instead of 5 minutes, and the RNA yield and quality were assessed using a NanoDrop spectrophotometer (NanoDrop One, Thermo Fisher Scientific Inc.). Second, 1 µg of total RNA was treated with DNase I to remove genomic DNA contamination and was reverse transcribed using the iScriptTM gDNA Clear cDNA Synthesis Kit (Bio-Rad Laboratories) and a thermal cycler (Mastercycler X50s, Eppendorf). Third, the genes of interest and the reference gene were analyzed via qPCR which was performed on 1 ng/µL of cDNA using a master mix of SsoAdvanced™ Universal SYBR® Green Supermix (Bio-Rad Laboratories) and primers at a concentration of 2.5 µM, and the reactions were performed and monitored using a thermal cycler (CFX96TM Real-Time System, Bio-Rad Laboratories) according to the standard protocol. The cycle threshold for each gene of interest was normalized against the reference gene that is glyceraldehyde 3-phosphate dehydrogenase (GAPDH), and relative gene expression levels were determined using the Livak's method ($2^{-\Delta\Delta Cq}$) [25], [26] compared with the corresponding control group. This part of the gene expression analysis was aimed at helping in the selection of the culture medium, thus, we investigated the effects of PEMF stimulation in two different culture media: BM and OM. For this purpose, collagen type I alpha 1 chain (COL1A1), osteopontin (OPN), osteocalcin (OCN), and runt-related

transcription factor 2 (RUNX2) were used as markers of osteogenesis; whereas, collagen type II alpha 1 chain (COL2A1) was used as a marker of chondrogenesis. The primer pairs of the analyzed genes are listed in **Table 2.1**.

Table 2.1. Description of the designed primers

Gene	**Forward Primer**	**Reverse Primer**
Collagen type I alpha 1 chain (COL1A1)	5'- GGA TTC CAG TTC GAG TAT GG -3'	5'- CAG TGG TAG GTG ATG TTC TG -3'
Collagen type II alpha 1 chain (COL2A1)	5'- AGG ATG GGC AGA GGT ATA AT -3'	5'- CAG ATT ATG TCG TCG CAG AG -3'
Glyceraldehyde-3-phosphate dehydrogenase (GAPDH)	5'- GTA TGA CAA CAG CCT CAA GAT -3'	5'- GTC CTT CCA CGA TAC CAA AG -3'
Osteocalcin (OCN)	5'- AGG CGC TAC CTG TAT CAA -3'	5'- CTC CTG AAA GCC GAT GTG -3'
Osteopontin (OPN)	5'- CCC ATC TCA GAA GCA GAA TC -3'	5'- TGG CTT TCG TTG GAC TTA C -3'
Runt-related transcription factor 2 (RUNX2)	5'- GAA TGC CTC TGC TGT TAT GA -3'	5'- GAA GAC GGT TAT GGT CAA GG -3'

2.4 Results

2.4.1 3D trabecular, bone-like tissues

The first step in developing functional trabecular bone-like tissues involves efficient cell seeding, ensuring adequate cell density and distribution. After 21 days of cultivation under static conditions and bone-like mechanical stimulation, the interaction between BM-MSCs and the PLA scaffolds exhibited variations among the three different cell seeding methods. The live/dead cell assay showed no differences in cell viability (around 90%) among these methods, as indicated by abundant green fluorescence and the absence of red fluorescence. The absence of red fluorescence does not imply no cell loss occurred; instead, it may suggest that dead or detached cells were shed during the 21-day culture period. However, substantial differences in cell morphology, infiltration, and distribution were observed between the three cell seeding techniques, as demonstrated by both the live/dead assay and SEM analysis.

In detail, when cells were seeded via suspension, they exhibited a concentration bias toward one side of the PLA scaffold. Under static culture conditions, the cells tended to accumulate at the bottom side of the scaffold, since the gravity caused the downward flow of the cell suspension. Under dynamic culture conditions, where media flowed from the bottom to the top of the scaffold, cells were forced to concentrate on the top side of the scaffold **(Figure 2.2)**.

An alternative approach to increasing the efficiency of static seeding is the use of hydrogels, and in this case, the choice of the hydrogel is of utmost importance. Our findings revealed that cell-releasing 2% alginate led to nonuniform distribution and infiltration of cells throughout the scaffolds since they tended to cluster in specific regions. Moreover, cells were confined within the hydrogel matrix, maintaining their round morphology and having limited direct interaction with the scaffold **(Figure 2.3)**.

The second hydrogel evaluated in our study was a cell-releasing 0.5% collagen. This hydrogel exhibited optimal cell distribution and infiltration throughout the scaffold both under static and dynamic culture conditions. As shown in **Figure 2.4A**, live/dead assay confirmed that cells were evenly distributed at both the top and bottom of the scaffolds. The SEM analysis supported these findings, revealing that cells were able to spread and attach throughout the entire scaffold, as depicted in **Figure 2.4B**.

Considering the critical role of cell density in bone tissue engineering, we selected a seeding density of $3x10^6$ cells per scaffold, consistent with previous studies that highlighted the advantages of higher cell seeding densities for bone formation and clinical applications in bone tissue engineering. Therefore, we chose biomimetic PLA scaffolds seeded with $3x10^6$ BM-MSCs using 0.5% collagen as our trabecular bone-like tissue model for subsequent experiments.

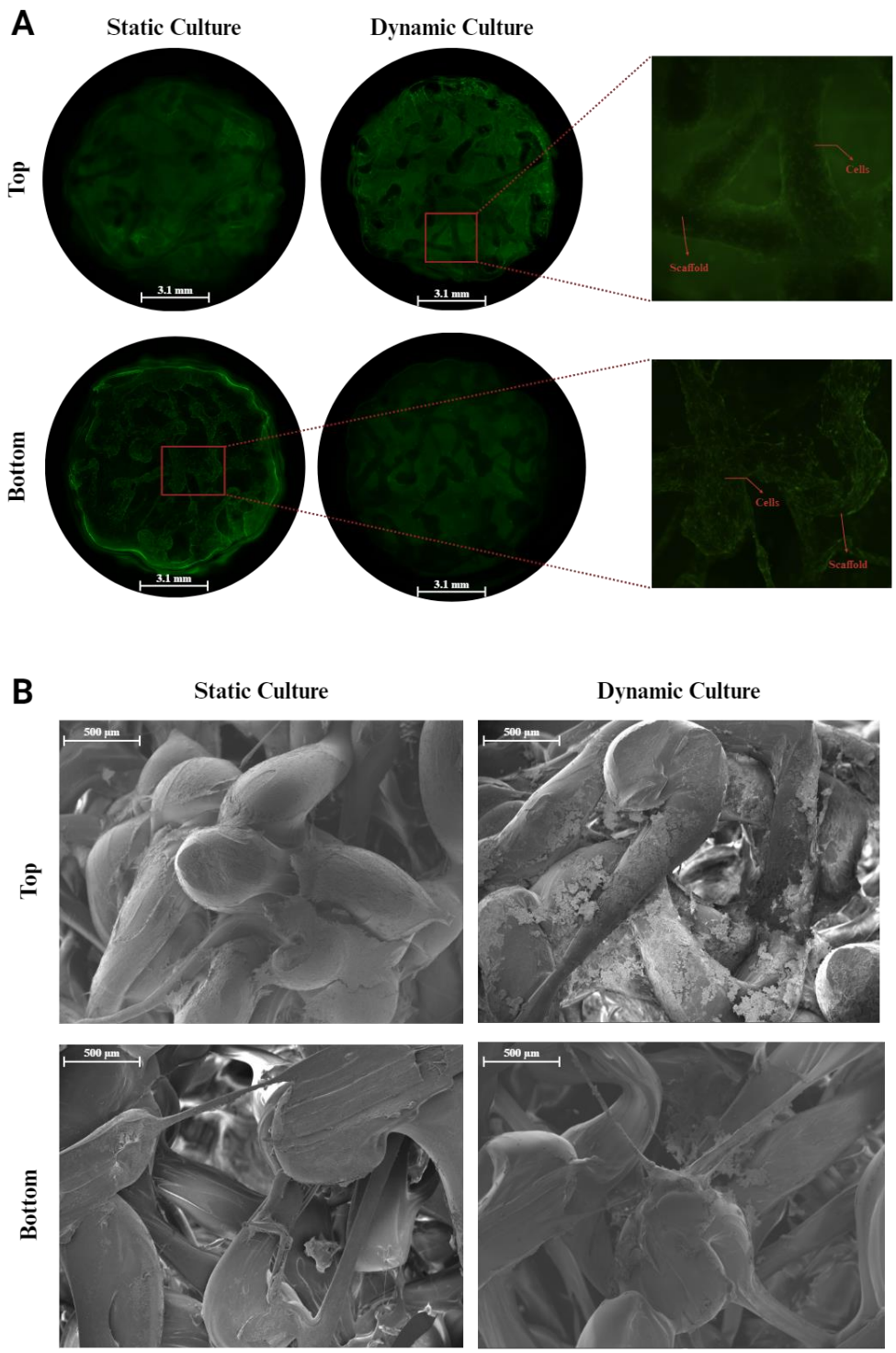

Figure 2.2. Live/dead cell assay and scanning electron microscope (SEM) analysis of biomimetic polylactic acid (PLA) scaffolds seeded with bone marrow-derived mesenchymal stem cells (BM-MSCs) via suspension seeding and cultured for 21 days under static culture conditions and in an automated perfusion bioreactor. **(A)** Representative calcein-AM/EthD-1 images of BM-MSCs. Images represent the upper and lower sides of the scaffold. Images were taken with 5x magnification; scale bars correspond to 3.1 mm. **(B)** SEM images of BM-MSCs. Images represent the upper and lower sides of the scaffold. Images were taken with 50x magnification; scale bars correspond to 500 µm.

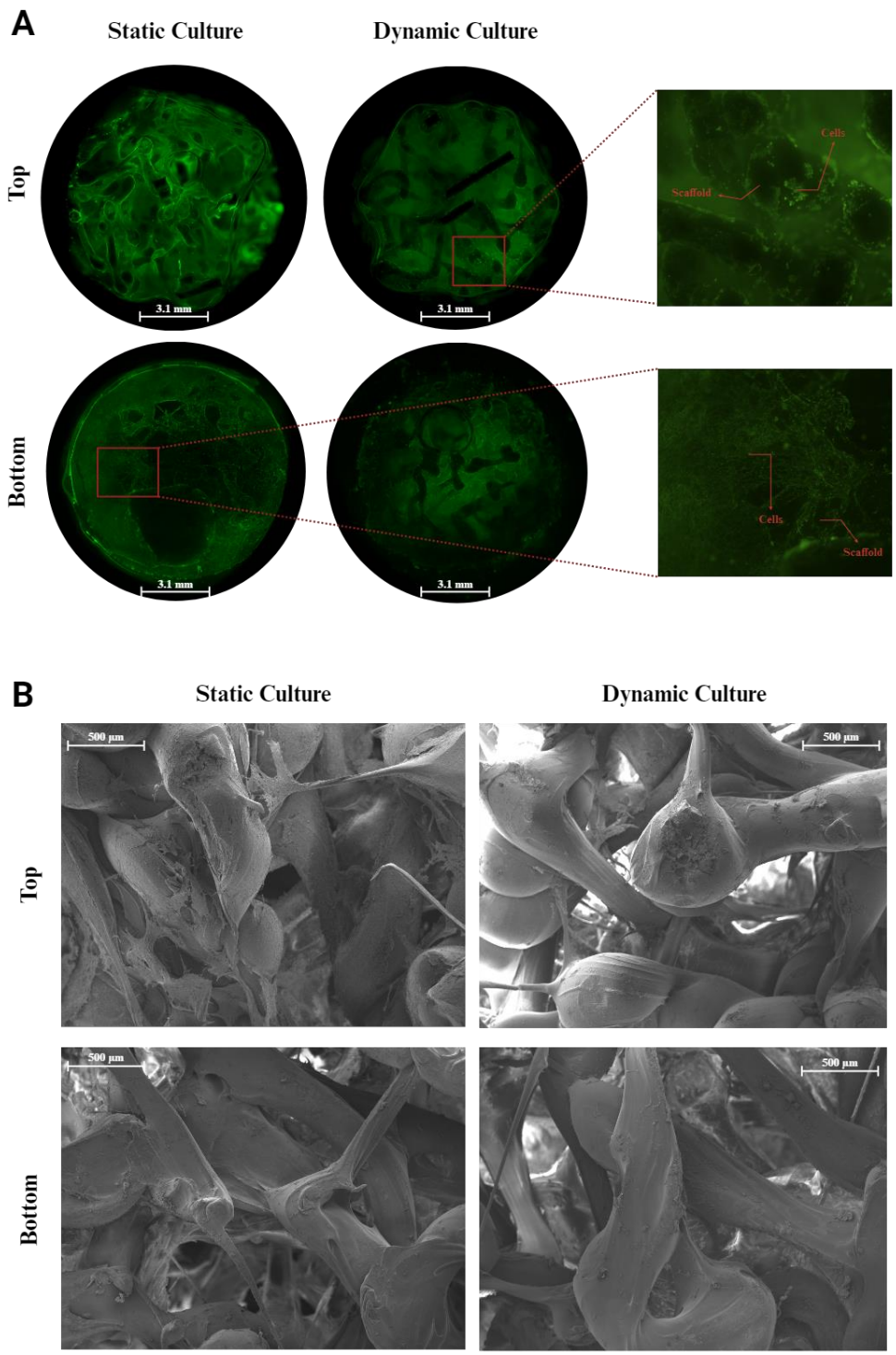

Figure 2.3. Live/dead cell assay and scanning electron microscope (SEM) analysis of biomimetic polylactic acid (PLA) scaffolds seeded with bone marrow-derived mesenchymal stem cells (BM-MSCs) via 2% alginate and cultured for 21 days under static culture conditions and in an automated perfusion bioreactor. **(A)** Representative calcein-AM/EthD-1 images of BM-MSCs. Images represent the upper and lower sides of the scaffold. Images were taken with 5x magnification; scale bars correspond to 3.1 mm. **(B)** SEM images of BM-MSCs. Images represent the upper and lower sides of the scaffold. Images were taken with 50x magnification; scale bars correspond to 500 µm.

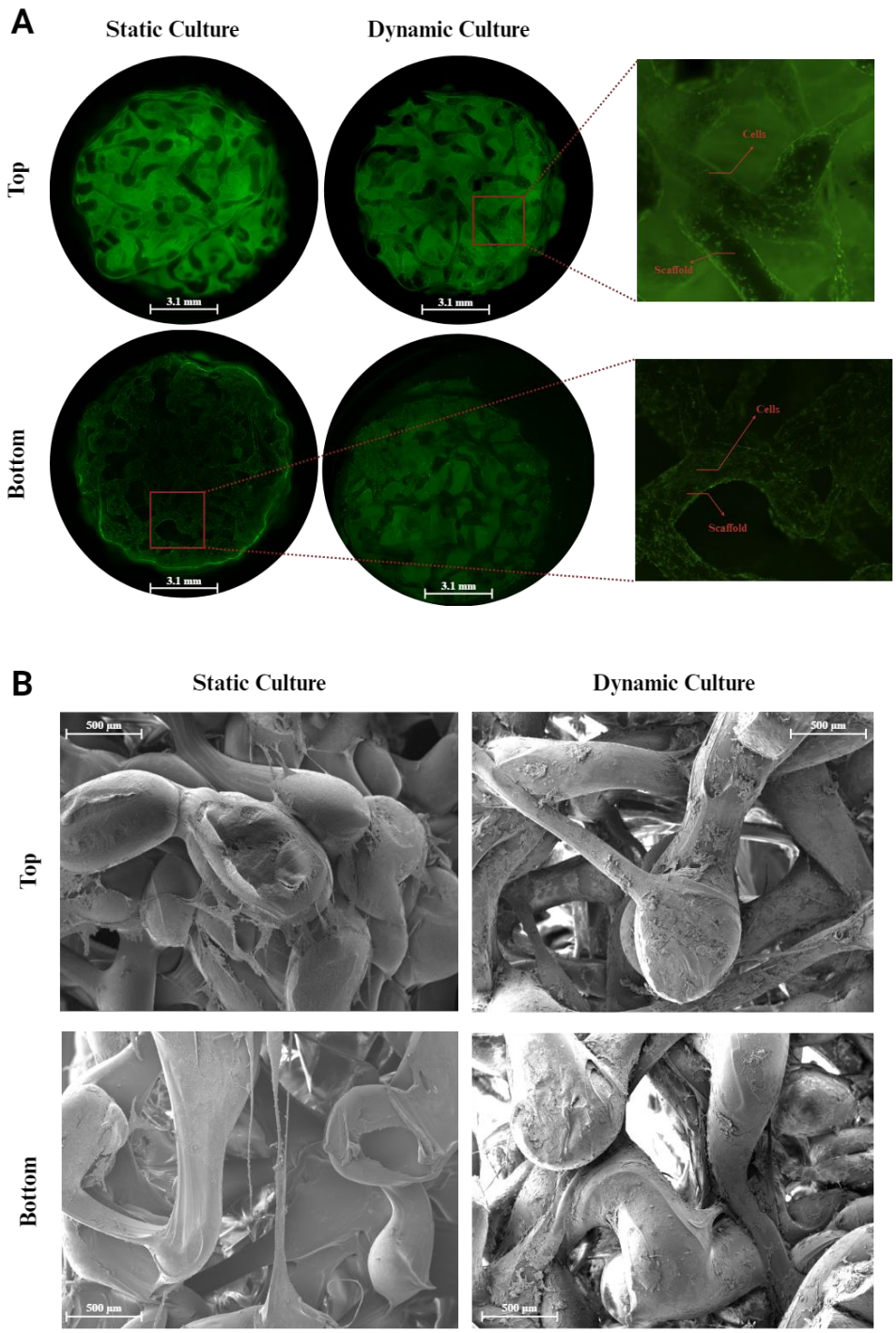

Figure 2.4. Live/dead cell assay and scanning electron microscope (SEM) analysis of biomimetic polylactic acid (PLA) scaffolds seeded with bone marrow-derived mesenchymal stem cells (BM-MSCs) via 0.5% collagen and cultured for 21 days under static culture conditions and in an automated perfusion bioreactor. **(A)** Representative calcein-AM/EthD-1 images of BM-MSCs. Images represent the upper and lower sides of the scaffold. Images were taken with 5x magnification; scale bars correspond to 3.1 mm. **(B)** SEM images of BM-MSCs. Images represent the upper and lower sides of the scaffold. Images were taken with 50x magnification; scale bars correspond to 500 µm.

2.4.2 The set-up of cell culture conditions

Following the selection of the cell seeding method, the trabecular bone-like tissues were cultured for 21 days in OM or BM under different conditions: static culture (control), direct, unidirectional perfusion without PEMF stimulation, and direct, unidirectional perfusion with PEMF stimulation. Our goal was to identify the optimal cell culture medium that enables the detection of the response of BM-MSCs to the biophysical stimulation provided by PEMF. Therefore, the expression levels of COL1A1, OPN, OCN, and RUNX2 as the osteogenic marker genes and COL2A1 as the chondrogenic marker gene were relatively quantified by RT-qPCR.

For cells cultured in OM, the results demonstrated that direct, unidirectional perfusion without and with PEMF stimulation induced only a slight upregulation in COL1A1 (~ 0.7 and 1.2-fold change, respectively), OCN (~ 1.5-fold change for both conditions), RUNX (~ 0.8 and 1.0-fold change, respectively), and COL2A1 (~ 1.7-fold change for both conditions) but not in OPN (~ 0.07 and 0.1-fold change, respectively), compared to static culture **(Figure 2.5A)**. The ratio of COL1A1 to COL2A1 (COL1A1/COL2A1), defined as an index of osteogenic differentiation, was slightly higher with PEMF stimulation in OM (**Figure 2.5C**). For cells cultured in BM and also in comparison to static culture, the results showed that direct, unidirectional perfusion without PEMF stimulation induced only a slight upregulation in COL1A1 (~ 1.2-fold change), OCN (~ 1.0-fold change), RUNX2 (~ 1.4-fold change) and COL2A1 (~ 0.3-fold change), but not in OPN (~ 0.09-fold change). However, direct, unidirectional perfusion with PEMF stimulation induced a notable upregulation in COL1A1 (~ 5.2-fold change) and OPN (~ 12.0-fold change) and a slight upregulation in OCN (~ 1.6-fold change), RUNX2 (~ 2.5-fold change), and COL2A1 (~ 0.7-fold change), compared to static culture (**Figure 2.5B**). The ratios of COL1A1 to COL2A1 (COL1A1/COL2A1) were higher in BM in comparison to those in OM. Moreover, in BM, the ratio of COL1A1 to COL2A1 (COL1A1/COL2A1) was considerably higher in the presence of PEMF stimulation in comparison to the absence of PEMF stimulation **(Figure 2.5C)**.

Based on the RT-qPCR results, we may propose that PEMF stimulation notably enhances the osteogenic commitment of BM-MSCs only when there are no biochemical stimuli provided by the OM. This observation suggests that the presence of biochemical stimuli in the OM might mask the specific effects of PEMF stimulation on osteogenic differentiation. Consequently, we opted to use BM rather than OM in subsequent experiments.

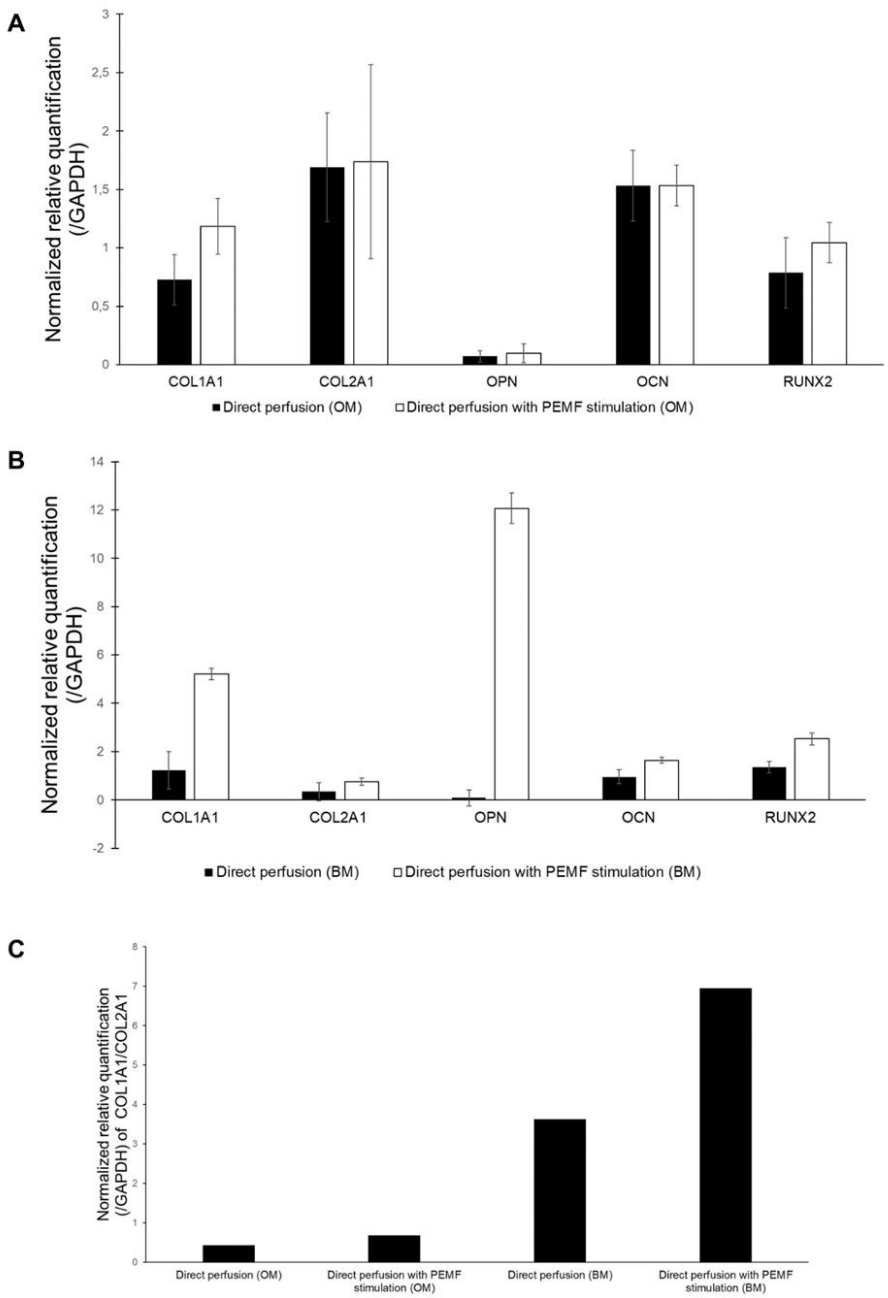

Figure 2.5. Gene expression analyses of bone marrow-derived mesenchymal stem cells (BM-MSCs) in the trabecular bone-like tissues after 21 days of culture. The osteogenic and chondrogenic mRNA expression in BM-MSCs cultured under direct, unidirectional perfusion without and with pulsed electromagnetic field (PEMF) stimulation in comparison with static culture in **(A)** osteogenic medium (OM) and **(B)** basal medium (BM). The relative expressions of collagen type I alpha 1 chain (COL1A1), osteopontin (OPN), osteocalcin (OCN), runt-related transcription factor 2 (RUNX2), and collagen type II alpha 1 chain (COL2A1) mRNAs were analyzed by reverse transcription-quantitative PCR (RT-qPCR) and were calculated by $2^{-\Delta\Delta CT}$ method with normalization to the levels of GAPDH. Bars represent the mean fold change of three biological replicates +/− standard error of the mean (SEM). **(C)** The ratio of COL1A1 to COL2A1 (COL1A1/COL2A1) of BM-MSCs cultured in OM and BM.

2.5 Discussion

Creating an *in vitro* platform that closely mimics bone tissue's architectural and mechanical properties is essential for bone biology research. To achieve this, we started our investigation by evaluating three cell seeding methods: suspension seeding, cell-releasing 2% alginate, and cell-releasing 0.5% collagen. This is a critical step in tissue engineering as it depicts cell density and distribution. Our findings indicate that employing 0.5% cell-releasing collagen is the best cell-seeding method, and they align with prior research. Cámara-Torres et al. (2020) explored variations in the viscosity and density of the culture medium using dextran and Ficoll, respectively. Their results demonstrated that increasing viscosity and density not only facilitated the homogeneous infiltration of BM-MSCs into the 3D scaffolds prepared from the copolymer poly(ethylene oxide terephthalate)/poly(butylene terephthalate) (PEOT/PBT), but also enhanced osteogenesis [36]. Moreover, collagen has been extensively evaluated in various studies for cell seeding. For instance, Fahimipour et al. (2019), developed a bone ECM-mimetic matrix composed of heparin-functionalized collagen and immobilized bone morphogenetic protein 2 (BMP2) to seed dental pulp MSCs into β-tricalcium phosphate (β-TCP) scaffolds. Their findings revealed that the collagen-heparin matrix maintained the bioactivity of BMP2, enhanced the cell seeding efficiency, and supported osteogenesis [37]. Our choice to adhere to high-density seeding is supported by the findings of several studies including those of Hsieh et al. (2019) [38]and Wu et al. (2015) [39]who verified the superiority of high cell seeding density.

The second step in developing an *in vitro* platform, specifically designed to assess the effects of PEMF on BM-MSCs within a bone-like mechanical environment involves carefully selecting the optimal cell culture conditions. Our research aimed to compare BM and OM in terms of cellular and molecular changes induced by mechanical and biophysical stimulation. Notably, we observed a subtle association between fluid flow-induced shear stress and the osteogenic differentiation of BM-MSCs in BM but not in OM. This was evidenced by a slight increase in the COL1A1 to COL2A1 ratio (COL1A1/COL2A1), suggesting a trend toward osteogenic differentiation. However, no significant differences in the gene expression levels of RUNX2, OPN, and OCN were observed between cells exposed to fluid flow-induced shear stress and those cultured statically in BM. In contrast, in OM, only OCN expression was slightly upregulated in cells exposed to fluid flow-induced shear stress compared to those cultured statically.

It is worth noting that other researchers have successfully highlighted the positive impact of mechanical stimuli on osteogenesis. In their study, Lim et al. (2019) successfully engineered a fully automated bioreactor system (fABS). This system induced the proliferation, osteogenesis, and chondrogenesis of human BM-MSCs within a water-jacketed culture chamber (WJCC) via a shear stress of 1.018×10^{-6} Pa even in the presence of the biochemical stimuli [40]. Expanding the scope to more intricate bioreactor applications, Vetsch et al. (2017) focused on a perfusion bioreactor that specifically emulates the mechanical environment during early fracture healing or bone remodeling, corresponding to flow rates of 0.001 m/s and 0.061 m/s, respectively. In their investigation, human BM-MSCs were cultured

alongside 3D silk fibroin scaffolds and an osteogenic medium under two distinct flow rates. Their results showed that the cell fate was steered toward either proliferation or osteogenic differentiation by applying one of the two distinct flow rates [41]. In an earlier study, Bjerre et al. (2008) also employed a 3D cell culture of human BM-MSCs cultivated on silicate-substituted tricalcium phosphate (Si-TCP) scaffolds in a perfusion bioreactor using media supplemented with 10^{-8} M 1,25-$(OH)_2$-vitamin D_3. Notably, at a flow rate of 0.1 mL/min, the authors observed enhanced proliferation, osteogenic differentiation, and cell/matrix deposition [42]. The divergent outcomes observed in bioreactor studies for bone tissue engineering can be attributed to variations in experimental conditions related to the bioreactor systems. These differences arise from unique experimental configurations, scaffold materials, scaffold properties, cell types, culture durations, and environmental factors. To facilitate meaningful comparisons, it is essential to employ identical, standardized bioreactor systems under consistent experimental and environmental conditions, as previously emphasized by Zhao et al. (2018) [43] and other researchers.

Our investigation successfully demonstrated the osteogenic potential of PEMF stimulation using our *in vitro* bioreactor-based platform with BM rather than OM. This was evidenced by the relatively high value of the COL1A1 to COL2A1 ratio (COL1A1/COL2A1) and the significantly increased expression of OPN in cells cultured dynamically with PEMF stimulation to those cultured dynamically in the absence of PEMF stimulation. Prior *in vitro* studies have also substantiated the role of PEMF stimulation in bone regeneration. Starting from experiments on 2D cell cultures, Ongaro et al. (2014) revealed that both human BM-MSCs and adipose-derived mesenchymal stem cells (AD-MSCs), when exposed to continuous PEMF stimulation (1.5 mT, 75 Hz) for 28 days in osteogenic medium (in the absence or presence of BMP2), promoted osteogenic differentiation [44]. Similarly, Kang et al. (2013) demonstrated comparable outcomes using PEMF stimulation (30/45 Hz, 1 mT) for 8 h per day over a 20-day period [45]. On a similar note, previous studies by Jansen et al. (2010) [46], Sun et al. (2010) [47], and Tsai et al. (2009) [48] reported enhanced osteogenesis owing to PEMF stimulation. Conversely, other studies on PEMF stimulation using 2D cell cultures, such as the ones performed by Kaivosoja et al. (2012) [49] and Yan et al. (2010) [50] were incapable of verifying the osteoinductive properties of PEMF. Yet, the response of cells to external stimuli varies significantly between 2D and 3D cell cultures, and the latter was amply shown by the study performed by Schwartz et al. (2009) [51]; thus, the evaluation of PEMF's biological outcomes should be compulsory done on 3D cell cultures [52]. The few studies on PEMF stimulation and 3D cell cultures involve titanium, calcium phosphate scaffolds, and polymers, as described previously by Galli et al. [53]. One of the most recent works on titanium by Bloise et al. (2018) involved nanostructured TiO_2, where human BM-MSCs were seeded on the scaffolds, cultured in osteogenic medium, and exposed to PEMF stimulation (2 mT, 75 Hz) for 10 min per day for a total of 28 days. The authors showed that PEMF can have a significant osteoinductive potential that involves selective calcium-related osteogenic pathways [54]. One of the latest studies employing calcium phosphate scaffolds, which was performed by Schwartz et al. (2008), did not achieve comparable results as the authors were unable to demonstrate that PEMF stimulation enhances the osteogenic effects of BMP2 on human BM-MSCs cultured in osteogenic medium [55]. Ultimately, among the

recent work on polymers, poly(caprolactone) (PCL) nanofibrous scaffolds and human AD-MSCs were cultured in basal medium or osteogenic medium for up to 21 days by Arjmand et al. (2017), who were able to show that PEMF stimulation alone has an osteoinductive potential similar to that of osteogenic medium [56]. By this stage, the osteoinductive potential of perfusion bioreactors and PEMF was examined separately, and as previously described, mimicking in vitro the bone tissue-specific environment is a central factor in bone biology research. Thus far, only a limited number of studies examined PEMF as part of an in vitro bone tissue experimental model encompassing 3D cell cultures and perfusion bioreactors. The latest work by Wang et al. (2019) evaluated EMF (15 Hz, 1 mT) exposure for 4 h per day in vitro using hydroxyapatite/collagen type I (HAC) scaffolds and rabbit BM-MSCs in basal and osteogenic media, as well as in vivo by implanting the obtained cell-laden constructs in a rabbit femur condyle defect model, and the obtained results showed that EMF ameliorated bone regeneration and bone integration [57]. The desirable outcomes of PEMF on bone cells using 3D cell cultures and perfusion bioreactors were also highlighted by Tsai et al. (2007) via poly(DL-lactic-co-glycolic acid) (PLGA) scaffolds and rat osteoblasts [58]. Although none of these platforms entirely replicate the bone tissue-specific environment, they represent a more legitimate tool for bone biology research.

2.6 Conclusions

In this study, we aimed to develop an advanced *in vitro* bioreactor-based platform that closely mimics the architectural and mechanical properties of trabecular bone tissue to investigate the effects of PEMF stimulation on BM-MSCs. We found that seeding BM-MSCs into the 3D-printed PLA scaffolds that mimic the architecture of trabecular bone using 0.5% collagen cell-releasing yielded high cell density and distribution. Fluid flow-induced shear stress had a subtle influence on the osteogenic differentiation of BM-MSCs due to the absence of significant differences in gene expression levels of key osteogenic markers between cells exposed to shear stress and those cultured statically. However, the addition of PEMF stimulation significantly enhanced the osteogenic differentiation of BM-MSCs cultured within the bioreactor-based platform, particularly in BM, as it promoted the expression of osteogenic markers. This suggests that the presence of biochemical stimuli from the OM can mask the effects of mechanical and physical stimuli on BM-MSCs. Although our bioreactor-based platform could successfully house trabecular bone tissue-like constructs for extended periods, future refinements are necessary to more accurately replicate the complex *in vivo* bone microenvironment. Incorporating factors, such as hydrostatic pressure, compression, and cell-cell co-culture could provide a more realistic model for studying bone regeneration. Despite these limitations, our findings highlight the potential of PEMF stimulation to enhance bone tissue regeneration. By further investigating the molecular pathways underlying PEMF-induced osteogenesis, we can unlock valuable insights into the therapeutic potential of PEMF for bone tissue regeneration and healing.

This chapter was published as part of a “research article” in the scientific journal *Bone* from *Elsevier*:

Daou, F., Masante, B., Gabetti, S., Mochi, F., Putame, G., Zenobi, E., Scatena, E., Dell'Atti, F., Favero, F., Leigheb, M., Del Gaudio, C., Bignardi, C., Massai, D., Cochis, A., & Rimondini, L. **(2024)**. Unraveling the transcriptome profile of pulsed electromagnetic field stimulation in bone regeneration using a bioreactor-based investigation platform. *Bone*, 182, 117065. https://doi.org/10.1016/j.bone.2024.117065

2.7 Fundings

This study was carried out within the BIGMECH project – funded by the European Union – Next Generation EU within the PRIN 2022 program (D.D. 104 - 02/02/2022 Ministero dell’Università e della Ricerca). This manuscript reflects only the authors’ views and opinions and the Ministry cannot be considered responsible for them.

2.8 Acknowledgments

I would like to thank Dr. Eleonora Zenobi and Dr. Elisa Scateno for kindly providing the 3D-printed PLA scaffolds, as well as Prof. Diana Massai, Dr. Stefano Gabetti, and Dr. Beatrice Masante for kindly providing the perfusion bioreactor. I would also like to thank Prof. Lia Rimondini and Prof. Andrea Cochis for their supervision, and Dr. Federica Dell’Atti for her help with performing the experiments.

2.9 References

1. Clarke, B. (2008) Normal Bone Anatomy and Physiology. *Clin J Am Soc Nephrol*, 3 (Suppl 3), S131.
2. Naji, A., Eitoku, M., Favier, B., Deschaseaux, F., Rouas-Freiss, N., and Suganuma, N. (2019) Biological functions of mesenchymal stem cells and clinical implications. *Cellular and Molecular Life Sciences 2019 76:17*, 76 (17), 3323–3348.
3. Feng, X. (2009) Chemical and Biochemical Basis of Cell-Bone Matrix Interaction in Health and Disease. *Curr Chem Biol*, 3 (2), 189.
4. Šromová, V., Sobola, D., and Kaspar, P. (2023) A Brief Review of Bone Cell Function and Importance. *Cells*, 12 (21), 2576.
5. Morgan, E.F., Unnikrisnan, G.U., and Hussein, A.I. (2018) Bone Mechanical Properties in Healthy and Diseased States. *Annu Rev Biomed Eng*, 20, 119.

6. Rho, J.Y., Kuhn-Spearing, L., and Zioupos, P. (1998) Mechanical properties and the hierarchical structure of bone. *Med Eng Phys*, 20 (2), 92–102.
7. Ma, C., Du, T., Niu, X., and Fan, Y. (2022) Biomechanics and mechanobiology of the bone matrix. *Bone Res*, 10 (1), 59.
8. Moysidou, C.M., Barberio, C., and Owens, R.M. (2021) Advances in Engineering Human Tissue Models. *Front Bioeng Biotechnol*, 8, 620962.
9. Amini, A.R., Laurencin, C.T., and Nukavarapu, S.P. (2012) Bone Tissue Engineering: Recent Advances and Challenges. *Crit Rev Biomed Eng*, 40 (5), 363.
10. Hollister, S.J., and Murphy, W.L. (2011) Scaffold Translation: Barriers Between Concept and Clinic. *Tissue Eng Part B Rev*, 17 (6), 459.
11. de Wildt, B.W.M., Ansari, S., Sommerdijk, N.A.J.M., Ito, K., Akiva, A., and Hofmann, S. (2019) From bone regeneration to three-dimensional in vitro models: tissue engineering of organized bone extracellular matrix. *Curr Opin Biomed Eng*, 10, 107–115.
12. Jensen, C., and Teng, Y. (2020) Is It Time to Start Transitioning From 2D to 3D Cell Culture? *Front Mol Biosci*, 7, 513823.
13. Karageorgiou, V., and Kaplan, D. (2005) Porosity of 3D biomaterial scaffolds and osteogenesis. *Biomaterials*, 26 (27), 5474–5491.
14. Langhans, S.A. (2018) Three-dimensional in vitro cell culture models in drug discovery and drug repositioning. *Front Pharmacol*, 9 (JAN), 334617.
15. Biju, T.S., Priya, V.V., and Francis, A.P. (2023) Role of three-dimensional cell culture in therapeutics and diagnostics: an updated review. *Drug Deliv Transl Res*, 13 (9), 2239–2253.
16. Carragher, N., Piccinini, F., Tesei, A., Trask, O.J., Bickle, M., and Horvath, P. (2018) Concerns, challenges and promises of high-content analysis of 3D cellular models. *Nature Reviews Drug Discovery 2018 17:8*, 17 (8), 606–606.
17. Fontoura, J.C., Viezzer, C., dos Santos, F.G., Ligabue, R.A., Weinlich, R., Puga, R.D., Antonow, D., Severino, P., and Bonorino, C. (2020) Comparison of 2D and 3D cell culture models for cell growth, gene expression and drug resistance. *Materials Science and Engineering: C*, 107, 110264.
18. Cortesi, M., Liu, D., Yee, C., Marsh, D.J., and Ford, C.E. (2023) A comparative analysis of 2D and 3D experimental data for the identification of the parameters of computational models. *Scientific Reports 2023 13:1*, 13 (1), 1–16.
19. Kim, Y.E., Jeon, H.J., Kim, D., Lee, S.Y., Kim, K.Y., Hong, J., Maeng, P.J., Kim, K.R., and Kang, D. (2018) Quantitative Proteomic Analysis of 2D and 3D Cultured Colorectal Cancer Cells: Profiling of Tankyrase Inhibitor XAV939-Induced Proteome. *Scientific Reports 2018 8:1*, 8 (1), 1–12.
20. Botchwey, E.A., Dupree, M.A., Pollack, S.R., Levine, E.M., and Laurencin, C.T. (2003) Tissue engineered bone: Measurement of nutrient transport in three-dimensional matrices. *J Biomed Mater Res A*, 67A (1), 357–367.
21. Ahmed, S., Chauhan, V.M., Ghaemmaghami, A.M., and Aylott, J.W. (2018) New generation of bioreactors that advance extracellular matrix modelling and tissue engineering. *Biotechnology Letters 2018 41:1*, 41 (1), 1–25.
22. Yamada, S., Ockermann, P.N., Schwarz, T., Mustafa, K., and Hansmann, J. (2023) Translation of biophysical environment in bone into dynamic cell culture under flow for bone tissue engineering. *Comput Struct Biotechnol J*, 21, 4395–4407.

23. Petzold, J., and Gentleman, E. (2021) Intrinsic Mechanical Cues and Their Impact on Stem Cells and Embryogenesis. *Front Cell Dev Biol*, 9, 761871.
24. Ambattu, L.A., and Yeo, L.Y. (2023) Sonomechanobiology: Vibrational stimulation of cells and its therapeutic implications. *Biophys Rev*, 4 (2).
25. Directive - 2010/63 - EN - EUR-Lex.
26. Funk, R.H.W., Monsees, T., and Özkucur, N. (2009) Electromagnetic effects – From cell biology to medicine. *Prog Histochem Cytochem*, 43 (4), 177–264.
27. Carter, A., Popowski, K., Cheng, K., Greenbaum, A., Ligler, F.S., and Moatti, A. (2021) Enhancement of Bone Regeneration Through the Converse Piezoelectric Effect, A Novel Approach for Applying Mechanical Stimulation. *Bioelectricity*, 3 (4), 255.
28. Joseph, T.M., Kallingal, A., Suresh, A.M., Mahapatra, D.K., Hasanin, M.S., Haponiuk, J., and Thomas, S. (2023) 3D printing of polylactic acid: recent advances and opportunities. *The International Journal of Advanced Manufacturing Technology 2023 125:3*, 125 (3), 1015–1035.
29. Tandon, B., Blaker, J.J., and Cartmell, S.H. (2018) Piezoelectric materials as stimulatory biomedical materials and scaffolds for bone repair. *Acta Biomater*, 73, 1–20.
30. Pecci, R., Baiguera, S., Ioppolo, P., Bedini, R., and Del Gaudio, C. (2020) 3D printed scaffolds with random microarchitecture for bone tissue engineering applications: Manufacturing and characterization. *J Mech Behav Biomed Mater*, 103, 103583.
31. Ledda, M., Merco, M., Sciortino, A., Scatena, E., Convertino, A., Lisi, A., and Del Gaudio, C. (2022) Biological Response to Bioinspired Microporous 3D-Printed Scaffolds for Bone Tissue Engineering. *International Journal of Molecular Sciences 2022, Vol. 23, Page 5383*, 23 (10), 5383.
32. Gabetti, S., Masante, B., Schiavi, A., Scatena, E., Zenobi, E., Israel, S., Sanginario, A., Del Gaudio, C., Audenino, A., Morbiducci, U., and Massai, D. (2024) Adaptable test bench for ASTM-compliant permeability measurement of porous scaffolds for tissue engineering. *Scientific Reports 2024 14:1*, 14 (1), 1–13.
33. Bancroft, G.N., Sikavitsas, V.I., Van Den Dolder, J., Sheffield, T.L., Ambrose, C.G., Jansen, J.A., and Mikos, A.G. (2002) Fluid flow increases mineralized matrix deposition in 3D perfusion culture of marrow stromal osteoblasts in a dose-dependent manner. *Proc Natl Acad Sci U S A*, 99 (20), 12600–12605.
34. Wittkowske, C., Reilly, G.C., Lacroix, D., and Perrault, C.M. (2016) In Vitro Bone Cell Models: Impact of Fluid Shear Stress on Bone Formation. *Front Bioeng Biotechnol*, 4 (NOV), 229085.
35. James, S., Fox, J., Afsari, F., Lee, J., Clough, S., Knight, C., Ashmore, J., Ashton, P., Preham, O., Hoogduijn, M., Ponzoni, R.D.A.R., Hancock, Y., Coles, M., and Genever, P. (2015) Multiparameter Analysis of Human Bone Marrow Stromal Cells Identifies Distinct Immunomodulatory and Differentiation-Competent Subtypes. *Stem Cell Reports*, 4 (6), 1004–1015.
36. Cámara-Torres, M., Sinha, R., Mota, C., and Moroni, L. (2020) Improving cell distribution on 3D additive manufactured scaffolds through engineered seeding media density and viscosity. *Acta Biomater*, 101, 183–195.
37. Fahimipour, F., Dashtimoghadam, E., Mahdi Hasani-Sadrabadi, M., Vargas, J., Vashaee, D., Lobner, D.C., Jafarzadeh Kashi, T.S., Ghasemzadeh, B., and Tayebi, L. (2019) Enhancing

cell seeding and osteogenesis of MSCs on 3D printed scaffolds through injectable BMP2 immobilized ECM-Mimetic gel. *Dental Materials*, 35 (7), 990–1006.

38. Hsieh, M.K., Wu, C.J., Su, X.C., Chen, Y.C., Tsai, T.T., Niu, C.C., Lai, P.L., and Wu, S.C. (2019) Bone regeneration in Ds-Red pig calvarial defect using allogenic transplantation of EGFP-pMSCs – A comparison of host cells and seeding cells in the scaffold. *PLoS One*, 14 (7), e0215499.
39. Wu, H., Kang, N., Wang, Q., Dong, P., Lv, X., Cao, Y., and Xiao, R. (2015) The dose–effect relationship between the seeding quantity of human marrow mesenchymal stem cells and in vivo tissue-engineered bone yield. *Cell Transplant*, 24 (10), 1957–1968.
40. Lim, K.T., Patel, D.K., Seonwoo, H., Kim, J., and Chung, J.H. (2019) A fully automated bioreactor system for precise control of stem cell proliferation and differentiation. *Biochem Eng J*, 150, 107258.
41. Vetsch, J.R., Betts, D.C., Müller, R., and Hofmann, S. (2017) Flow velocity-driven differentiation of human mesenchymal stromal cells in silk fibroin scaffolds: A combined experimental and computational approach. *PLoS One*, 12 (7), e0180781.
42. Bjerre, L., Bünger, C.E., Kassem, M., and Mygind, T. (2008) Flow perfusion culture of human mesenchymal stem cells on silicate-substituted tricalcium phosphate scaffolds. *Biomaterials*, 29 (17), 2616–2627.
43. Zhao, F., van Rietbergen, B., Ito, K., and Hofmann, S. (2018) Flow rates in perfusion bioreactors to maximise mineralisation in bone tissue engineering in vitro. *J Biomech*, 79, 232–237.
44. Ongaro, A., Pellati, A., Bagheri, L., Fortini, C., Setti, S., and De Mattei, M. (2014) Pulsed electromagnetic fields stimulate osteogenic differentiation in human bone marrow and adipose tissue derived mesenchymal stem cells. *Bioelectromagnetics*, 35 (6), 426–436.
45. Kang, K.S., Hong, J.M., Kang, J.A., Rhie, J.W., Jeong, Y.H., and Cho, D.W. (2013) Regulation of osteogenic differentiation of human adipose-derived stem cells by controlling electromagnetic field conditions. *Experimental & Molecular Medicine 2013 45:1*, 45 (1), e6–e6.
46. Jansen, J.H.W., Van Der Jagt, O.P., Punt, B.J., Verhaar, J.A.N., Van Leeuwen, J.P.T.M., Weinans, H., and Jahr, H. (2010) Stimulation of osteogenic differentiation in human osteoprogenitor cells by pulsed electromagnetic fields: An in vitro study. *BMC Musculoskelet Disord*, 11 (1), 1–11.
47. Sun, L.Y., Hsieh, D.K., Lin, P.C., Chiu, H.T., and Chiou, T.W. (2010) Pulsed electromagnetic fields accelerate proliferation and osteogenic gene expression in human bone marrow mesenchymal stem cells during osteogenic differentiation. *Bioelectromagnetics*, 31 (3), 209–219.
48. Tsai, M.T., Li, W.J., Tuan, R.S., and Chang, W.H. (2009) Modulation of osteogenesis in human mesenchymal stem cells by specific pulsed electromagnetic field stimulation. *Journal of Orthopaedic Research*, 27 (9), 1169–1174.
49. Kaivosoja, E., Sariola, V., Chen, Y., and Konttinen, Y.T. (2015) The effect of pulsed electromagnetic fields and dehydroepiandrosterone on viability and osteo-induction of human mesenchymal stem cells. *J Tissue Eng Regen Med*, 9 (1), 31–40.

50. Yan, J., Dong, L., Zhang, B., and Qi, N. (2010) Effects of Extremely Low-Frequency Magnetic Field on Growth and Differentiation of Human Mesenchymal Stem Cells. *Electromagn Biol Med*, 29 (4), 165–176.
51. Schwartz, Z., Fisher, M., Lohmann, C.H., Simon, B.J., and Boyan, B.D. (2009) Osteoprotegerin (OPG) production by cells in the osteoblast lineage is regulated by pulsed electromagnetic fields in cultures grown on calcium phosphate substrates. *Ann Biomed Eng*, 37 (3), 437–444.
52. Ehnert, S., Schröter, S., Aspera-Werz, R.H., Eisler, W., Falldorf, K., Ronniger, M., and Nussler, A.K. (2019) Translational Insights into Extremely Low Frequency Pulsed Electromagnetic Fields (ELF-PEMFs) for Bone Regeneration after Trauma and Orthopedic Surgery. *Journal of Clinical Medicine 2019, Vol. 8, Page 2028*, 8 (12), 2028.
53. Galli, C., Pedrazzi, G., Mattioli-Belmonte, M., and Guizzardi, S. (2018) The Use of Pulsed Electromagnetic Fields to Promote Bone Responses to Biomaterials In Vitro and In Vivo. *Int J Biomater*, 2018 (1), 8935750.
54. Bloise, N., Petecchia, L., Ceccarelli, G., Fassina, L., Usai, C., Bertoglio, F., Balli, M., Vassalli, M., De Angelis, M.G.C., Gavazzo, P., Imbriani, M., and Visai, L. (2018) The effect of pulsed electromagnetic field exposure on osteoinduction of human mesenchymal stem cells cultured on nano-TiO2 surfaces. *PLoS One*, 13 (6), e0199046.
55. Schwartz, Z., Simon, B.J., Duran, M.A., Barabino, G., Chaudhri, R., and Boyan, B.D. (2008) Pulsed electromagnetic fields enhance BMP-2 dependent osteoblastic differentiation of human mesenchymal stem cells. *Journal of Orthopaedic Research*, 26 (9), 1250–1255.
56. Arjmand, M., Ardeshirylajimi, A., Maghsoudi, H., and Azadian, E. (2018) Osteogenic differentiation potential of mesenchymal stem cells cultured on nanofibrous scaffold improved in the presence of pulsed electromagnetic field. *J Cell Physiol*, 233 (2), 1061–1070.
57. Wang, H., Tang, X., Li, W., Chen, J., Li, H., Yan, J., Yuan, X., Wu, H., and Liu, C. (2019) Enhanced osteogenesis of bone marrow stem cells cultured on hydroxyapatite/collagen I scaffold in the presence of low-frequency magnetic field. *J Mater Sci Mater Med*, 30 (8), 1–12.
58. Tsai, M.T., Chang, W.H.S., Chang, K., Hou, R.J., and Wu, T.W. (2007) Pulsed electromagnetic fields affect osteoblast proliferation and differentiation in bone tissue engineering. *Bioelectromagnetics*, 28 (7), 519–528.

Chapter 3

Unraveling the Transcriptome Profile of Pulsed Electromagnetic Field Stimulation in Bone Regeneration Using a Bioreactor-Based Investigation Platform

3.1 Abstract

Human mesenchymal stem cells (hMSCs) sense and respond to biomechanical and biophysical stimuli, yet the involved signaling pathways are not fully identified. The clinical application of biophysical stimulation including pulsed electromagnetic field (PEMF) has gained momentum in musculoskeletal disorders and bone tissue engineering. We herein aim to explore the role of PEMF stimulation in bone regeneration by culturing trabecular bone-like tissues under bone-like mechanical stimulation in an automated perfusion bioreactor combined with a custom-made PEMF stimulator. After selecting the optimal cell seeding and culture conditions for inspecting the effects of PEMF on hMSCs, as described in Chapter 2, transcriptomic studies were performed on cells cultured under direct perfusion with and without PEMF stimulation. We were able to identify a set of signaling pathways and upstream regulators associated with PEMF stimulation and to distinguish those linked to bone regeneration. Our findings suggest that PEMF induces the immune potential of hMSCs by activating and inhibiting various immune-related pathways, such as macrophage classical activation and MSP-RON signaling in macrophages, respectively, while promoting angiogenesis and osteogenesis, which mimics the dynamic interplay of biological processes during bone healing. Overall, the adopted bioreactor-based investigation platform can be used to investigate the impact of PEMF stimulation on bone regeneration.

3.2 Introduction

Bone tissue is highly responsive to biophysical stimuli, which means that it can convert these stimuli to biochemical cues that directly regulate bone remodeling [1]. Bone remodeling is further influenced by the tissue's piezoelectric properties, which enable the conversion of mechanical forces into electrical potentials, creating a physiological electrical microenvironment that plays a significant role in bone regeneration [2]. The piezoelectric properties of dried bone and wet bone were previously described by Fukada and Yasuda (1957) [3]and Reibish and Nowick (1975) [4], respectively. Given these findings, researchers suggest that mechanotransduction alone cannot fully capture the complexity of the native

bone environment. The term “biophysical transduction” was proposed to encompass both mechanotransduction and electrical coupling to represent the process of sensing, transmission, and regulation of biophysical stimuli promoting osteogenesis [5].

The anatomist and surgeon Julius Wolff proposed in 1892 that bone remodeling is influenced not only by biological factors but also by mechanical loading. Harold Frost, an orthopedic surgeon, expanded on Wolff's theory in 1987. He showed that the quality and frequency of the mechanical stimulus alter bone formation. Frost also postulated that different biomechanical loading ranges can either lead to bone formation or bone resorption, a concept he termed the "mechanostat theory" [6]. Other researchers also supported Frost’s theory. It is now well known now that bone cells, including osteoblasts, osteoclasts, osteocytes, bone lining cells, and mesenchymal stem cells (MSCs), sense and respond to a variety in endogenous and exogenous biophysical stimuli [7]. This biomechanical environment is also crucial during fracture healing and the underlying mechanism was described in Pauwels’ theory of “causal histogenesis” in 1960 [8], which was further detailed by the studies by Claes et al. on mesenchymal stem cells (MSCs) [9,10].

The biophysical stimuli to which bone cells are responsive can be categorized into: internal structural stimuli, such as matrix stiffness and topography; external stimuli including compression, tension, fluid flow-induced shear stress, hydrostatic pressure, and acoustic stimuli; and electromagnetic stimuli comprising electric current, electric field, magnetic field, and electromagnetic field [5]. This understanding has led to the implementation of exogenous physical stimuli in clinical settings to manipulate bone healing. A key advantage of translating biophysical stimuli to clinical settings is their non-invasive nature [11]. Moreover, biophysical stimuli are being recognized as a fourth pillar, alongside scaffolds, cells, and bioactive molecules, in bone tissue engineering [12].

In clinical settings, electrical stimulation has been applied to various conditions, including acute fractures, delayed unions, nonunions, and joint arthrodesis. It can be delivered through three primary methods: direct electrical current, capacitive coupling, and induction coupling. Direct electrical current techniques are invasive, requiring the implantation of one or more cathodes into the bone. In contrast, capacitive coupling and induction coupling are non-invasive. Capacitive coupling involves placing two electrodes on the skin overlying the fracture site, creating an electrical field across the affected area. Induction coupling utilizes a pulsed electromagnetic field (PEMF) device, which is placed on the skin over the fracture site to induce an electrical current within the tissues [13].

Ultrasound stimulation has also been used in clinical practice, more specifically, low-intensity pulsed ultrasound (LIPUS), which has been commercially available since the Food and Drug Administration (FDA) approved it in 1994 as an adjunct therapy for healing primary fractures and in 2000 for the treatment of non-union fractures [14].The accumulation of data on the efficacy of LIPUS in the treatment of delayed unions and nonunions led the UK National Institute for Health and Care Excellence (NICE) to issue a statement in 2010 supporting the use of LIPUS to reduce fracture healing time and to provide clinical benefit,

particularly in circumstances of delayed healing and non-union [15]. The most widely employed LIPUS stimulation parameters comprised an ultrasound frequency of 1.5 MHz, a burst waveform with a 200 μs on and 800 μs off, a 1 kHz repetition rate, a spatial average-temporal average intensity (I_{SATA}) of 30 mW/cm^2, and a dosage of 20 minutes per day [16]. However, additional research is necessary to delve deeper into the underlying mechanisms of LIPUS-enhanced fracture healing. While previous studies have indicated that ultrasound stimulation can positively influence multiple stages of bone repair, it remains unclear at which phase of the healing process stimulation yields the greatest benefit [17].

Static magnetic fields (SMFs) that are characterized by having constant intensity and orientation, due to their potential effects on bone metabolism. They have been used in the prevention and treatment of various bone-related diseases, such as osteoporosis and osteoarthritis, as well as for the promotion of fracture healing and bone defect repair [18]. Preclinical studies tested various magnetic flux densities, magnetic field directions, and exposure times with different cell types. The outcomes were highly dependent on the experimental conditions in in vitro studies. Yet, all animal studies in the literature demonstrated beneficial effects on bone regeneration [19]. Despite multiple beneficial effects reported *in vitro* and *in vivo*, SMFs remain unapproved by the FDA, and their underlying mechanisms remain unclear.

Other therapeutic strategies based on exogenous physical stimulation include the employment of photobiomodulation (PBM) at different wavelengths [20]. Low-level laser therapy (LLLT), the most commonly used type of PBM, has been used to treat bone fractures and have been shown to improve pain and physical function [21]. It has also been applied to accelerating orthodontic tooth movement [22] and preserving alveolar socket after tooth extraction [23]. While potential mechanisms have been identified, there are still gaps in our understanding. Moreover, optimal treatment settings for different conditions remain unclear, and more clinical research is needed to confirm the safety and efficacy of PBM for various bone repair applications [20]. Whole-body vibration (WBV) training [24] and shockwaves (sonic pulses) [25] are exogenous physical stimuli that, while employed in clinical settings for bone healing, are less frequently utilized than the others.

The clinical translation of bone growth stimulators involved also those based on pulsed electromagnetic field (PEMF). The accumulation of data on the safety and efficacy of PEMF stimulation led the FDA to reclassify them from Class III to Class II devices in 2020 [26]. The most established clinical application of PEMF are the treatment of delayed union or nonunion fractures, osteoarthritis, osteoporosis, osteonecrosis, and tendon disorders [27], in addition to musculoskeletal chronic pain including low back pain [28]. Moreover, following this reclassification, PEMF therapy has garnered increased attention and has been explored in various clinical settings.

One recent study demonstrated the efficacy of combining PEMF with platelet-rich plasma (PRP) for early-stage knee osteoarthritis, offering superior pain relief and functional improvement compared to either treatment alone. A PEMF device operating at 30 Hz and 1.5

mT was used for 20 minutes per session, 5 times per week, over 3 consecutive treatment courses each consisting of 15 sessions [29]. Furthermore, PEMF therapy has been explored for fracture healing. A clinical study examined the use of a Fracture Healing Patch (FHP) device, emitting pulsed electromagnetic fields at 20 kHz with a 10 Hz cycle frequency and an intensity of 0.05-0.5 mT, to accelerate the healing of acute distal radius fractures treated with open reduction and internal fixation (ORIF) [30]. In addition to fracture healing, PEMF therapy has shown promise in musculoskeletal conditions. A study demonstrated that a combination of PEMF therapy (1 mT at 50 Hz for 10 minutes per session, 16 sessions) and home-based exercise can significantly improve knee muscle strength and reduce pain in individuals with end-stage knee osteoarthritis, especially in females and older adults [31]. Another study investigated the use of PEMF therapy (via SpinalStim, designed specifically for patient use in the home setting) in conjunction with standard surgical care for lumbar spinal fusion. The results indicated that PEMF therapy can significantly improve fusion rates and patient-reported outcomes, such as pain, function, and quality of life, in patients with risk factors for pseudarthrosis [32]. In the field of dentistry, PEMF therapy has been investigated for pain management following tooth extraction. A randomized controlled trial utilizing the AlgoCare Maxillofacial device (TSS Medical, Turin, Italy) for 13 hours per day over 7 days was found to reduce post-operative pain after third molar removal [33]. As these studies highlight, PEMF therapy is being explored in a variety of clinical applications, with varying device specifications and treatment protocols. Further research is needed to optimize the use of PEMF therapy and to establish clear guidelines for its clinical application.

Researchers have been exploring broader indications of PEMF therapy, such as postoperative pain and edema after plastic surgery [34], treatment-resistant depression [35], and oncology [36]. Subsequently, scientists combined PEMF stimulation with biomaterials for bone tissue engineering to ameliorate the clinical outcomes of its applications [37]. ClinicalTrials.gov (accessed November 2024) lists around 30 ongoing clinical trials investigating PEMF as an intervention, while approximately 60 completed trials have results available for only 20 of them, with pain management being the most common focus [38]. A search of the EU Clinical Trials (https://euclinicaltrials.eu/) did not reveal any ongoing clinical studies on PEMF, suggesting that its evaluation by clinical trials is less prevalent in Europe compared to the US [39]. However, a search of PubMed identified over 10 studies published on PEMF clinical trials just in the year 2024 alone [40].

Yet, challenges remain due to the diverse EMF stimuli (frequencies, intensities, waveforms, and durations of exposure) and biomaterial heterogeneity [41]. Researchers have uncovered various signaling pathways underlying PEMF's physiological effects, particularly related to osteogenesis, chondrogenesis, and anti-inflammation. However, a comprehensive understanding of these pathways is still lacking [42-44]. Additionally, the absence of standardized clinical guidelines for PEMF stimulation parameters poses a challenge for its widespread clinical use [45,46]. Furthermore, the potential health risks associated with PEMF exposure in routine clinical settings for both healthcare providers and patients need consideration [47,48].

With the purpose of tackling the knowledge gap in PEMF research, the objective of our study was to explore the effects of PEMF stimulation on stem cell behavior and osteogenic commitment. To achieve this, we utilized the in vitro bioreactor-based investigation platform, described in Chapter 2, that is based on an automated perfusion bioreactor that provides bone-tissue-like mechanical stimulation (i.e., fluid flow-induced shear stress) and can be equipped with a custom-made PEMF stimulator. First, we prepared trabecular bone-like tissues, consisting of 3D-printed biomimetic polylactic acid (PLA) scaffolds and human bone marrow-derived mesenchymal stem cells (BM-MSCs) seeded on the scaffolds using 0.5% cell-releasing collagen. Then, we investigated the impact of PEMF stimulation on BM-MSCs cultured under bone-like mechanical stimulation provided by the automated perfusion bioreactor via transcriptomic studies. The latter was performed since understanding the signaling pathways involved in the effects of PEMF stimulation is crucial for identifying the underlying cellular and molecular mechanisms related to bone regeneration and repair.

3.3 Materials and Methods

3.3.1 Trabecular bone-like tissue preparation using PLA600 scaffolds

Human telomerase reverse transcriptase (hTERT)-immortalized BM-MSCs of clonal line Y201 were directly seeded on the top of the PLA600 scaffolds inserted in the PDMS holders of the bioreactor placed in a 6-well cell culture plate by using cell-releasing 0.5% collagen at a defined density of $3x10^6$ cells and a defined volume of 200 µL, as described in Section 2.3.3 of this thesis.

3.3.2 Trabecular bone-like tissue culturing under three conditions

The samples were cultured for 21 days in basal medium (low-glucose DMEM supplemented with 15% FBS and 1% antibiotics) under three different culture conditions: static culture, in which the samples were kept in the cell culture plate and the medium was changed every 3-4 days; direct perfusion, in which samples were placed in the automated bioreactor and perfused unidirectionally at a flow rate of 0.3 mL/min with 50 mL of medium, and the medium was changed every 7 days; and direct perfusion with PEMF stimulation, in which the samples were cultured as in condition 2, but with additional PEMF stimulation (1.5 mT, 75 Hz) for 4 h per day (corresponding to a cumulative dose of around 75 h over a period of 21 days). Samples were evaluated in triplicates (n = 3). The samples were labeled as follows: “S” represents static culture, “D” represents direct, unidirectional perfusion, and “P” represents direct, unidirectional perfusion with PEMF stimulation.

3.3.3 Transcriptomic studies: RNA-Sequencing (RNA-Seq)

3.3.3.1 RNA purification and quality assessment

Total RNA was isolated using TRIzol™ Reagent (Invitrogen Life Technologies), as described in Section 2.3.4 of this thesis, and then purified with the Qiagen RNeasy Mini Kit (Qiagen, Hilden, Germany), according to the manufacturer’s instructions. RNA yield and quality were assessed using a NanoDrop spectrophotometer (NanoDrop One, Thermo Fisher Scientific Inc.). Total RNA concentration was measured using QubitTM RNA BR Assay Kit and QubitTM 4.0 Fluorometer (Invitrogen, Thermo Fisher Scientific Inc.). The RNA integrity was assessed using the Agilent 4200 TapeStation System (G2991AA) with the Agilent High Sensitivity RNA ScreenTape Assay (Agilent Technologies Inc., Santa Clara, CA, USA). All RNA samples had an RNA integrity number (RIN) ≥ 9 and were considered high-quality samples.

3.3.3.2 RNA-seq library construction

For RNA-seq library preparation, 300 ng of total RNA per sample were subjected to a ribosomal RNA depletion protocol using the IlluminaTM Stranded Total RNA Prep, Ligation

with Ribo-Zero™ Plus Kit (Illumina, San Diego, CA, USA). The concentrations of the final libraries were measured using Qubit TM 1X dsDNA HS Assay Kit and QubitTM 4.0 Fluorometer (Invitrogen, Thermo Fisher Scientific Inc.), and their quality was assessed with Agilent 4200 TapeStation System and Agilent High Sensitivity D1000 ScreenTape Assay (Agilent Technologies Inc.). Libraries were then sequenced on the Illumina NextSeq™ 550 platform (Illumina Inc.) using a NextSeq 500/550 High Output Kit v2.5 (150 cycles, 2 × 75 bp read length, paired-end) (Illumina Inc.) to achieve sufficient read depth for the analysis.

3.3.3.3 RNA-Seq bioinformatics

FastQC [49] and MultiQC [50] softwares were used to verify the quality of RNA-Seq data. RSEM computational pipeline [51] was used to quantify the expression of each human gene annotated to Ensembl v100 database [52] and on hg38 reference genome. STAR aligner [53] was used in the alignment step of RSEM pipeline. To filter out the quantified genes that are not expressed in our model, only genes with a TPM ≥ 1 in at least one sample underwent further analysis, considered to be expressed. Principal component analysis (PCA) plotting was performed using the “prcomp” package of R on the matrix of expression data. DESeq2 [54] was used to define differentially expressed gene (DEGs) with the following thresholds |log2FC| > 1 and p.adj < 0.01. Heatmaps showing unsupervised hierarchical clustering of genes were produced using the “pheatmap” function in package of R. Functional analysis of DEGs was performed using Metascape [55] with default parameters and also using QIAGEN IPA software (QIAGEN Inc., https://www.qiagen.com/us products/discovery- and-translational-research/next-generation-sequencing/ informatics-and data/interpretation-content-databases/ ingenuity-pathway-analysis/). Selected IPA pathways were filtered using -log(p-value) > 3. Moreover, to find Gene Ontology (GO) terms associated with the upstream regulators detected by the IPA analysis in the comparison of “P” versus “D”, the list of upstream regulators was filtered to select only the "transcription regulator" molecules, with a p-value < 0.001 and associated target molecules in dataset ≥ 5. The resulting list of genes was then annotated with ToppGene Suite [56] with default parameters, and the resulting GO terms were filtered using a p-value adjusted with Bonferroni Correction < 0.001. Semantic Plot was produced using Revigo [57] with “Homo Sapiens” as species.

3.3.3.4 Data availability

The RNA-Seq data are available in the NCBI GEO with the following ID: GSE231791.

3.3.4 Gene expression analyses

Gene expression analyses were performed following the transcriptomic studies to validate the raw expression signals of 11 genes that are commonly investigated in the literature, and the differential expression of 3 genes that served as a validation of the RNA-Seq, as described in Section 2.3.4 of this thesis. The raw expression signals of the following genes were evaluated: the adenosine receptors A2A adenosine receptor (A2AAR), A2B adenosine

receptor (A2BAR), and A3 adenosine receptor (A3AR); the member of the Wnt/β-catenin signaling pathway that is Wnt family member 1 (WNT1); the epigenetic factor that is microRNA 26a-1 (miR26A1); the markers of osteogenesis that are osteocalcin (OCN) and Runt-related transcription factor 2 (RUNX2); and finally, the markers of angiogenesis that are intercellular adhesion molecule 1 (ICAM1) and kinase insert domain receptor (KDR). The differential expression of the following genes was evaluated: the marker of osteogenesis, osteopontin (OPN); the marker of chondrogenesis, SRY-Box transcription factor 9 (SOX9); and the marker of angiogenesis, platelet, and endothelial cell adhesion molecule 1 (PECAM1). The primer pairs of the analyzed genes are listed in **Table 3.1.**

Table 3.1. Description of the designed primers

Gene	**Forward Primer**	**Reverse Primer**
A_{2A} adenosine receptor (A_{2A}AR)	5'- CCA TGC TAG GTT GGA ACA A -3'	5'- GAC CAC ATC CTC AAA GAG AC -3'
A_{2B} adenosine receptor (A_{2B}AR)	5'- CCC AAG TGG GCA ATG AAT A -3'	5'- CTG CTT GGC AGA GAA GAT AC -3'
A3 adenosine receptor (A3AR)	5'- ATG ACT TGC CTA CTG CTT ATC -3'	5'- TGG TGA CCC TCT TGT ATC T -3'
Glyceraldehyde-3-phosphate dehydrogenase (GAPDH)	5'- GTA TGA CAA CAG CCT CAA GAT -3'	5'- GTC CTT CCA CGA TAC CAA AG -3'
Intercellular adhesion molecule 1 (ICAM1)	5'- GTC ATC ATC ACT GTG GTA GC -3'	5'- GGC CTG TTG TAG TCT GTA TTT -3'
Kinase insert domain receptor (KDR)	5'- CCT CAC CTG TTT CCT GTA TG -3'	5'- GCT CTT TCG CTT ACT GTT CT -3'
microRNA 26a-1 (miR26A1)	5'- GTG GCC TCG TTC AAG TAA TC -3'	5'- CCG TGC AAG TAA CCA AGA A -3'
Osteocalcin (OCN)	5'- AGG CGC TAC CTG TAT CAA -3'	5'- CTC CTG AAA GCC GAT GTG -3'
Osteopontin (OPN)	5'- CCC ATC TCA GAA GCA GAA TC -3'	5'- TGG CTT TCG TTG GAC TTA C -3'
Platelet and endothelial cell adhesion molecule 1 (PECAM1)	5'- CTA CAC CCA AGT TCC ACA TC -3'	5'- CGC CTT GTC CTT CTG AAT TA -3'
Runt-related transcription factor 2 (RUNX2)	5'- GAA TGC CTC TGC TGT TAT GA -3'	5'- GAA GAC GGT TAT GGT CAA GG -3'
SRY-Box transcription factor 9 (SOX9)	5'- TCT GAA CGA GAG CGA GAA -3'	5'- GCG GCT GGT ACT TGT AAT -3'
Wnt family member 1 (WNT1)	5'- CTT CGG CAA GAT CGT CAA C -3'	5'- GGA TTC GAT GGA ACC TTC TG -3'

3.4 Results

3.4.1 Read processing and alignment

The high throughput screening (HTS) quality control (QC) is summarized in **Figure 3.1**. **Figure 3.1A** shows that all samples had a read depth of 29 million paired-end reads on average. **Figure 3.1B** shows that the average of the Phred-scaled quality score of each nucleotide in all the reads was >34 in all the samples. Also, no adapter sequences were found in the raw reads, so trimming was not necessary. The reads were subsequently aligned against the human reference genome hg38 and a quantification of every expressed gene was obtained, where expressed gene were defined as those with transcripts per million (TPM) > 1 in at least one sample, as described in Section 3.3.3 of this thesis.

Furthermore, the inter-group and intra-group variabilities of the expressed genes were assessed by clustering the samples via the principal component analysis (PCA). The results that are presented in **Figure 3.1C** revealed the transcriptomes of the three distinct groups, which are “S”, “D”, and “P”, formed separate clusters, whereas the transcriptomes of the biological replicates of each group cluster tightly. These two observations indicate that the replicates are more highly correlated within samples than between samples.

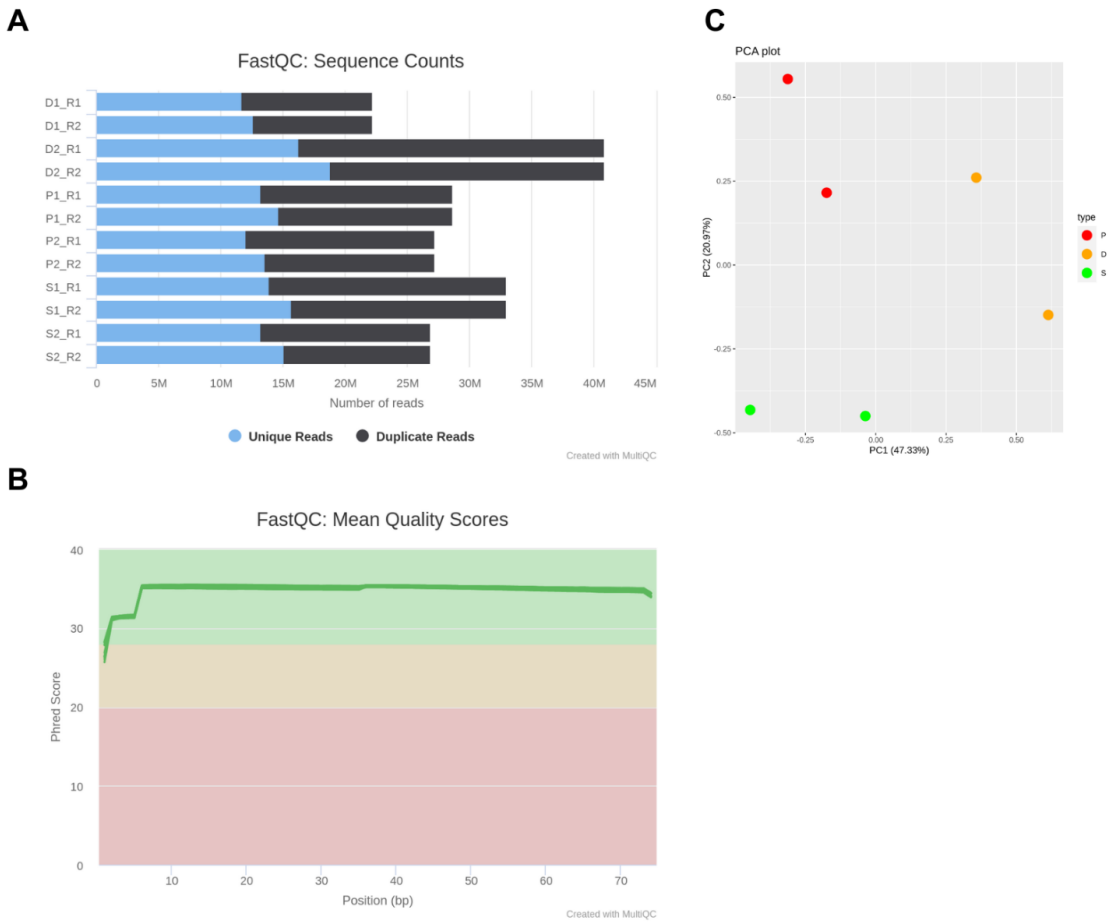

Figure 3.1. Read processing and alignment of RNA-Sequencing RNA-Seq) data. **(A)** Barplots representing the read depths for every sample of the RNA-Seq for both R1 and R2 FastQC files. The gray portion of the bars report the number of the duplicate reads and the blue ones report the number of the unique reads. The plot was generated using FastQC [49] and MultiQC [50] softwares. **(B)** Plot representing the average of the Phred-scaled quality score among the bp position of the reads for every sample of the RNA-Seq. The plot was generated using FastQC [49] and MultiQC [50] softwares. **(C)** Principal component analysis (PCA) plot of the samples of the RNA-Seq, in which "S" represents static culture, "D" represents direct, unidirectional perfusion, and "P" represents direct, unidirectional perfusion with PEMF stimulation.

3.4.2 Differential expression analysis

The differential expression analysis of the three comparisons ("D" versus "S", "P" versus "S", and "P" versus "D") detected changes in the expression levels of 368 genes in "D" versus "S", 654 genes in "P" versus "S", and 224 genes in "P" versus "D" **(Figure 3.2B)**, which summed up to a total of 956 unique DEGs **(Figure 3.2A)**. These DEGs were defined using $|\log2FC| > 1$ and $p.adj < 0.01$ as statistical cut-offs, as described in Section 3.3.3 of this thesis. The complete tables reporting log2FC and adjusted p-value of the DEGs in each comparison are provided as a supplementary file 1. Moreover, the upstream regulators were filtered to select only the "transcription regulator" molecules with a p-value < 0.001 and associated target molecules in the dataset ≥ 5.

To gain biological insights from these lists of DEGs, further analyses were performed. For the sake of explicating the results obtained by the transcriptomic studies in a concise and explicit manner, we focused our attention on the changes in the expression levels of genes and upstream regulators related to bone regeneration on one hand, and to some of the previously reported biological effects of PEMF stimulation on the other. The latter was done using QIAGEN IPA, as described in Section 3.3.3 of this thesis. The identified DEGs were first used to identify the signaling pathways that are affected by PEMF stimulation, and second, to identify the upstream regulators that are affected by PEMF stimulation. The identified upstream regulators then underwent pathway enrichment analysis to identify the pathways that are regulated by the identified upstream regulators and the genes that are involved in the pathways. Furthermore, we only included the results obtained for the comparison of "P" versus "D" since the principal objective of our study was to track down the signaling pathways targeted by PEMF stimulation in an in vitro environment resembling as closely as possible the physiological environment of bone tissue.

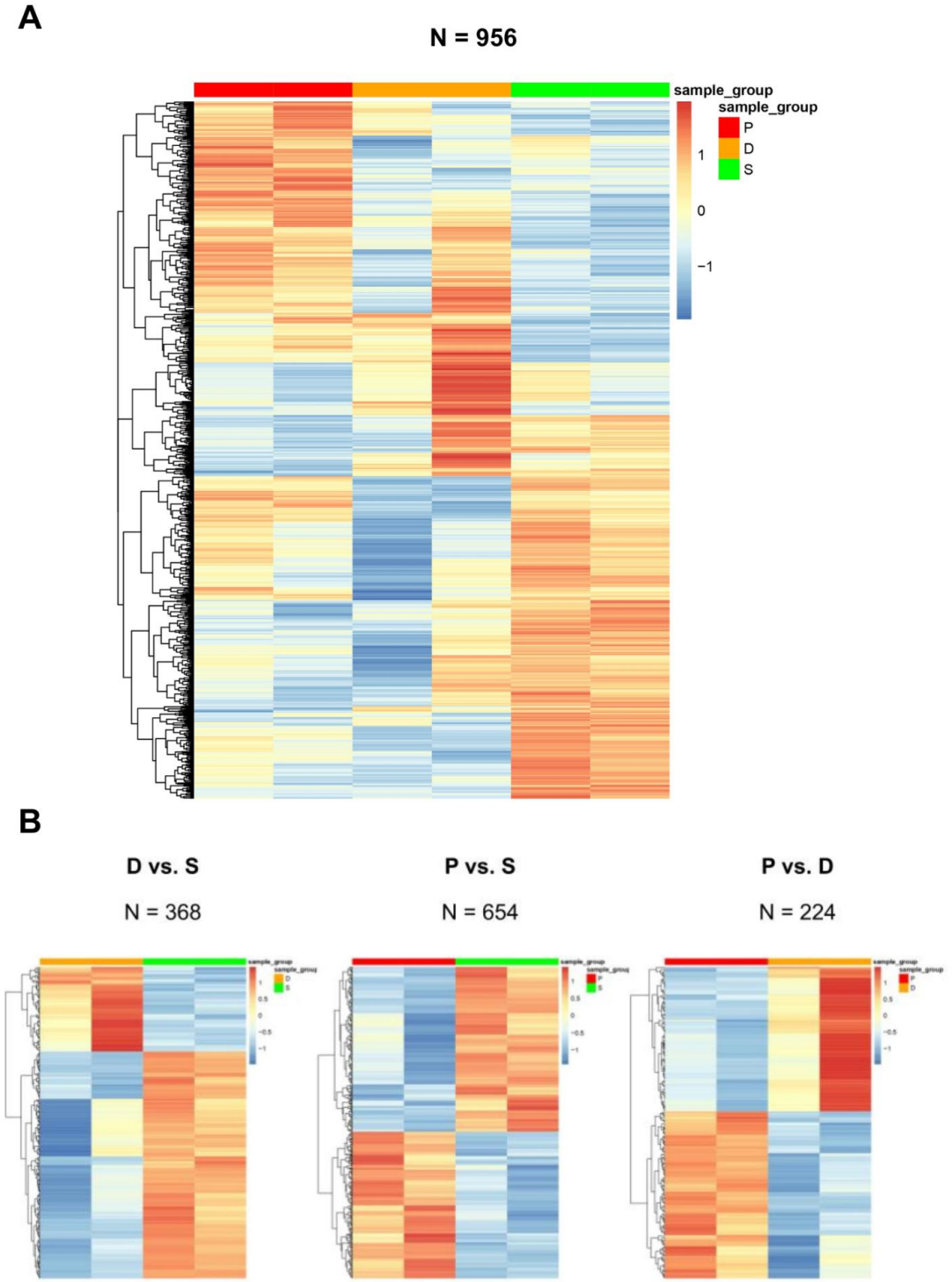

Figure 3.2. Heatmaps of differentially expressed genes (DEGs) of bone marrow-derived mesenchymal stem cells (BM-MSCs) cultured in basal medium for 21 days. **(A)** Heatmap of all DEGs in each of the three groups ("S", "D", and "P"). **(B)** Heatmaps of DEGs in the three comparisons ("D" versus "S", "P" versus "S", and "P" versus "D"). "S" represents static culture, "D" represents direct, unidirectional perfusion, and "P" represents direct, unidirectional perfusion with PEMF stimulation.

3.4.3 Immune potential of PEMF stimulation

Bone healing involves multiple phases that overlap, and these are the inflammatory phase, fibrovascular phase, bone formation phase, and bone remodeling phase. The acute inflammatory phase is known to facilitate normal bone healing, and as such, inhibition of inflammation and chronic inflammation are associated with delays and impairments in bone healing, respectively [58].

The GO enrichment analysis of the DEGs in the comparison of “P” versus “D” using Metascape **(Figure 3.3A)** showed that the signaling pathways evoked by PEMF stimulation and implicated in the first phase of bone healing are: GO:0006954 (inflammatory response), R-HSA-1280215 (cytokine signaling in immune system), GO:0001819 (positive regulation of cytokine production), WP5055 (burn wound healing), GO:0002697 (regulation of immune effector process), and R-HSA-6798695 (neutrophil degranulation). The analysis of DEGs in the comparison of “P” versus “D” using QIAGEN IPA **(Figure 3.4)** revealed additional signaling pathways, which are: mammalian target of rapamycin (mTOR) signaling (enriched only), macrophage classical activation signaling pathway (activated), antigen presentation pathway (enriched only), pathogen-induced cytokine storm signaling pathway (activated), Th1 pathway (activated), Th2 pathway (enriched only), MSP-RON signaling in macrophages pathway (deactivated), Th1 and Th2 activation pathway (enriched only), IL-12 signaling and production in macrophages (deactivated), wound healing signaling pathway (activated), macrophage alternative activation pathway (activated), and neuroinflammation signaling pathway (activated). The pathway enrichment analysis of the upstream regulators highlighted positive regulation of immune system process, response to wounding, and positive regulation of cytokine production **(Figure 3.5B)**.

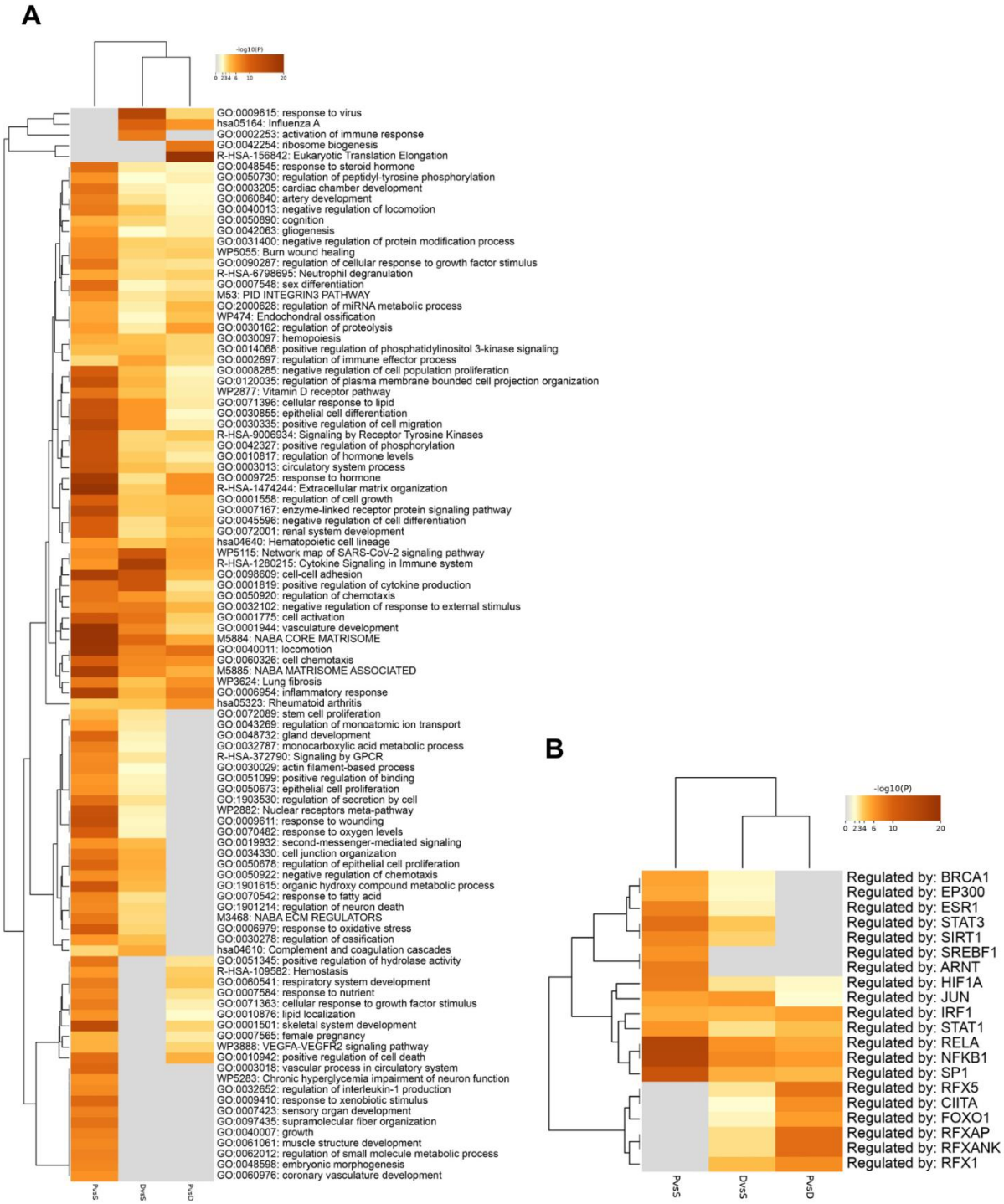

Figure 3.3. Functional analysis of the differentially expressed genes (DEGs) of bone marrow-derived mesenchymal stem cells (BM-MSCs) cultured in BM in the comparison of "P" versus "D" using Metascape. **(A)** Heatmap of the GO terms. **(B)** Heatmap of transcription factors (TFs). "S" represents static culture, "D" represents direct, unidirectional perfusion, and "P" represents direct, unidirectional perfusion with PEMF stimulation.

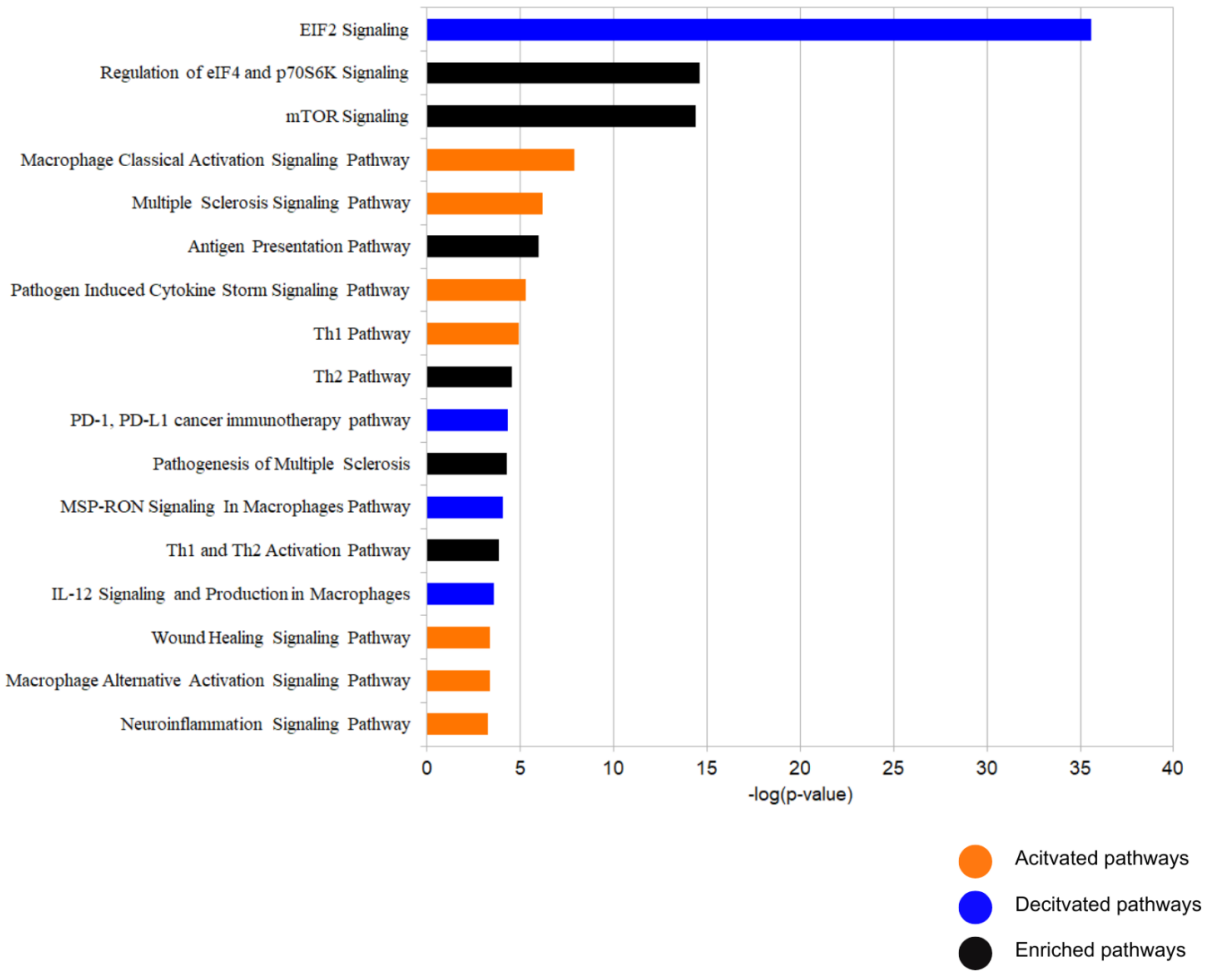

Figure 3.4. Bar plot representing selected enriched pathways from QIAGEN Ingenuity Pathway Analysis (IPA) of differentially expressed genes (DEGs) in the comparison of "P" versus "D", where "D" represents direct, unidirectional perfusion and "P" represents direct, unidirectional perfusion with PEMF stimulation. Orange bars represent activated pathways in "P" in comparison with "D"; Blue bars represent deactivated pathways in "P" in comparison with "D"; Black bars represent pathways that were only enriched in "P" in comparison with "D".

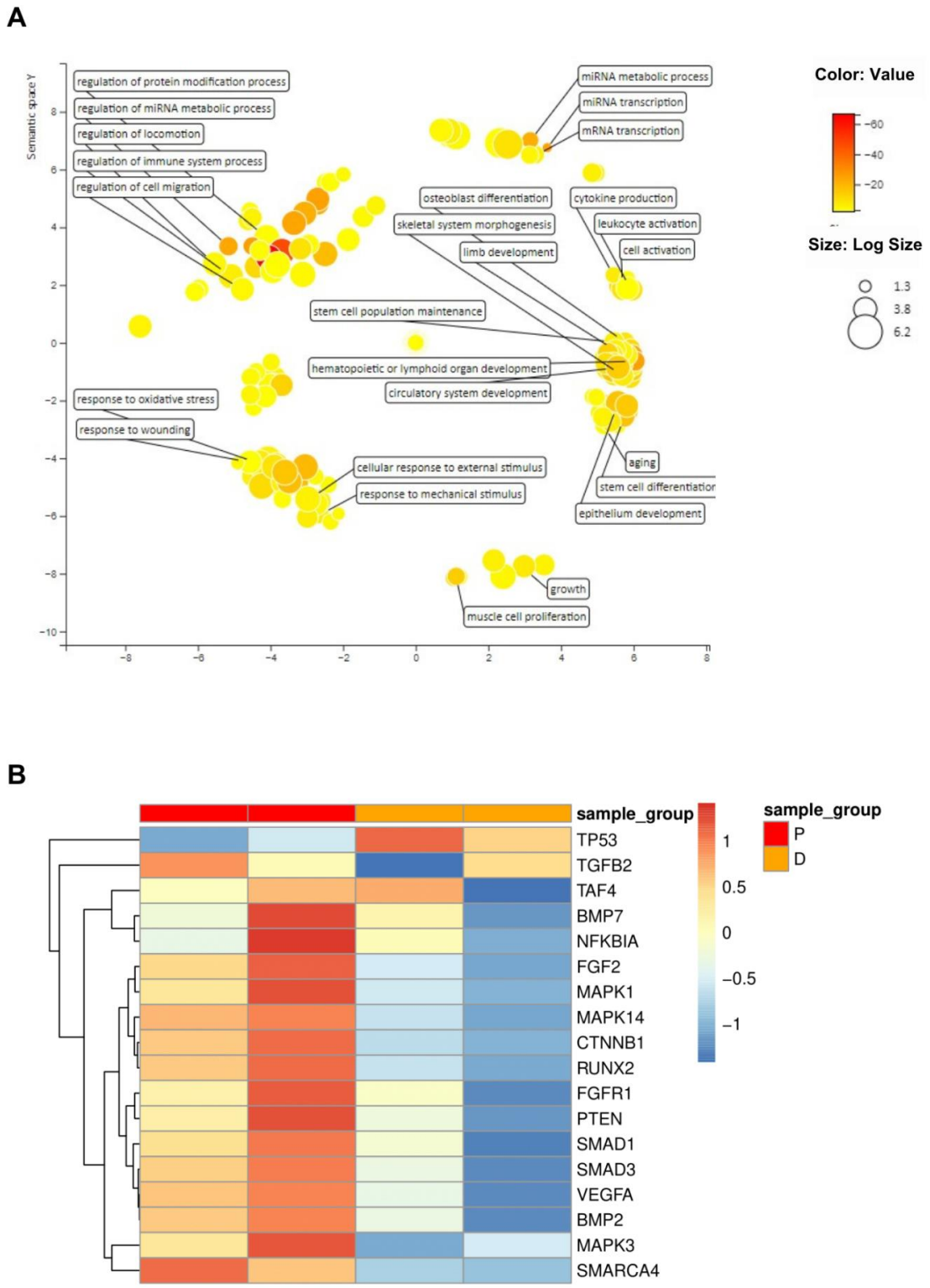

Figure 3.5. Upstream regulators detected on QIAGEN Ingenuity Pathway Analysis (IPA) of the comparison of "P" versus "D", where "D" represents direct, unidirectional perfusion and "P" represents direct, unidirectional perfusion with PEMF stimulation. (A) Heatmap of the upstream regulators that were differentially expressed. (B) Pathway enrichment analysis of the upstream regulators using Revigo.

3.4.4 Angiogenic potential of PEMF stimulation

With regards to the second stage of bone healing, the fibrovascular phase [58], the GO enrichment analysis in the comparison of "P" versus "D" using Metascape **(Figure 3.3)** highlighted GO:0001944 (vasculature development), GO:0003013 (circulatory system process), GO:0060840 (artery development), and WP3888 (vascular endothelial growth factor A-vascular endothelial growth factor receptor 2 (VEGFA-VEGFR2) signaling) as signaling pathways promoted by PEMF. The analysis of DEGs in the comparison of "P" versus "D" using QIAGEN IPA **(Figure 3.4)** did not identify signaling pathways associated with angiogenesis. However, the identified upstream regulators included VEGFA, transforming growth factor beta 2 (TGFB2), fibroblast growth factor 2 (FGF2), fibroblast growth factor receptor 1 (FGFR1), and some members of the mitogen-activated protein kinase (MAPK) signaling pathway, which are MAPK1, MAPK3, and MAPK14 **(Figure 3.5A)**. The pathway enrichment analysis of the upstream regulators highlighted the regulation of vasculature development **(Figure 3.5B)**.

3.4.5 Osteoinductive potential of PEMF stimulation

The final phases of bone healing are the bone formation and bone remodeling phases [58]. Since the preliminary gene expression analyses revealed that only when bone-like mechanical stimulation was coupled with PEMF the upregulation in the osteogenic marker COL1A1 became significant, the transcriptomic studies served the purpose of clarifying the osteoinductive potential of PEMF stimulation. The GO enrichment analysis of the DEGs in the comparison of "P" versus "D" using Metascape showed that PEMF stimulation evoked GO:0001501 (skeletal system development) with the main TFs involved being β-catenin 1 (CTNNB1) and nuclear factor kappa B (NF-κB) inhibitor alpha (NFKBIA) **(Figure 3.3)**. By contrast, the analysis of DEGs in the comparison of "P" versus "D" using QIAGEN IPA **(Figure 3.4)** did not identify signaling pathways associated with osteogenesis, but as in the case of angiogenesis, the related upstream regulators should be acknowledged, and these are: members of the canonical Smad-dependent signaling pathway of the transforming growth factor (TGF)-β/bone morphogenetic protein (BMP) signaling, which are BMP2, BMP7, SMAD1, and SMAD3; members of the non-canonical-Smad-independent signaling pathway of the TGF-β/BMP signaling (that is, p38 mitogen-activated protein kinase/p38 MAPK) including P38 MAPK; members of the WNT/β-catenin signaling pathway including CTNNB1 and WNT3A (predicted by IPA, but not actually expressed in our samples); the member of the NF-κB signaling pathway that is NFKBIA; as well as the runt-related transcription factors (RUNX) including RUNX2 **(Figure 3.5A)**. The pathway enrichment analysis of the upstream regulators highlighted regulation of osteoblast differentiation, ossification, and regulation of WNT signaling pathway **(Figure 3.5B)**.

3.4.6 Secondary pathways altered by PEMF stimulation

As the present work aimed to explore the biological effects of PEMF stimulation using an innovative bioreactor-based investigation platform, the results obtained by the transcriptomic studies were thoroughly examined. Not surprisingly, the biological effects of PEMF have gone beyond bone healing and in this section, we presented a few of the biological effects of PEMF stimulation that were investigated by previous studies.

To start with, the possible role of PEMF stimulation in initiating epigenetic alterations was checked, especially that this role called attention recently. Cited as an example, the work by De Mattei et al. (2020) presented that PEMF stimulation can modulate miRNAs involved in osteogenesis and angiogenesis, mainly miR26a and miR29b [59]. In the current study, the pathway enrichment analysis of the upstream regulators highlighted miRNA transcription and miRNA metabolic process **(Figure 3.5B)**. Therefore, a deeper insight into the biological significance of these epigenetic alterations can present a great topic for future research.

Moreover, the first signaling pathway that was primarily underlined by the analysis of DEGs in the comparison of "P" versus "D" using IPA, that is the eukaryotic Initiation Factor 2 (eIF2) (deactivated), refocused the attention on the possible modifications in gene expression of human BM-MSCs that can be triggered by exposure to PEMF. eIF2 is known to play a central role in the integrated stress response (ISR), an adaptive signaling pathway required for the maintenance of cellular homeostasis by reducing protein synthesis, while allowing the translation of a set of mRNAs encoding transcription factors and other proteins [60]. The modified signaling pathways and downstream events involved in gene expression were searched for, and included the regulation of eIF4 and p70S6K signaling (enriched only) **(Figure 3.4)**, and the upstream regulators comprised SWI/SNF related, matrix associated, actin dependent regulator of chromatin, subfamily a, member 4 (SMARCA4) and TATA-box binding protein associated factor 4 (TAF4), among others **(Figure 3.5A)**. The pathway enrichment analysis of the upstream regulators highlighted positive regulation of gene expression **(Figure 3.5B)**. These data can support the hypothesis that PEMF perpetrated its functions by directly altering gene expression, from transcription and translation to epigenetics.

Another utility of PEMF stimulation that was previously described by various studies is its potential use in certain pathological conditions with the intention of ameliorating the pathogenesis of these conditions. The pathological conditions that were detected in the present study include multiple sclerosis (MS) and tumor. For MS, the analysis of DEGs in the comparison of "P" versus "D" using QIAGEN IPA **(Figure 3.4)** highlighted MS signaling pathway (activated) and pathogenesis of MS (enriched only), and this desirable outcome of PEMF was detected by various studies that explored the effects of PEMF on spasticity [61]. Besides MS, biophysically stimulated BM-MSCs exhibited tumor suppression properties, and the analysis of DEGs in the comparison of "P" versus "D" using QIAGEN IPA **(Figure 3.4)** included PD-1, PD-L1 cancer immunotherapy pathway (deactivated), in addition to the

expression of the upstream regulators TP53 and phosphatase and tensin homolog (PTEN) that are known tumor suppressors **(Figure 3.5A)**.

3.4.3 Validation of raw expression signals and differential gene expression

To further investigate the signaling pathways that were reported by previous studies as potential pathways targeted by PEMF and to validate the results obtained by the transcriptomic studies, gene expression analyses were performed. Accordingly, the changes in the relative expression levels of certain mRNAs from all three groups ("S", "D", and "P") were tracked down for the validation of the raw expression signals **(Figure 3.6)** and for the validation of the DEGs **(Figure 3.7)**.

Here we present the outcomes of the gene expression analyses obtained for the comparison of "P" versus "D" in order to compare them with the outcomes of the transcriptomic studies **(Figure 3.6C)**. Starting with signaling pathways, the relative expression levels of $A_{2A}AR$, $A_{2B}AR$, and A_3AR mRNAs were detected to examine adenosine signaling as it is extensively reported in the literature, but was not highlighted by the transcriptomic studies of our study. While $A_{2A}AR$ and $A_{2B}AR$ were slightly upregulated (~1.0 and 0.6-fold change, respectively) due to PEMF stimulation, $A_{3A}R$ was not. Another signaling pathway that is highly noted by previous works is the Wnt/β-catenin signaling pathway with WNT1 being the mainly reported member. The relative expression level of WNT1 mRNA showed that WNT1 was not expressed by BM-MSCs, even after PEMF stimulation. This finding is in line with the results of the transcriptomic studies, since CTNNB1 and WNT3A (predicted by QIAGEN IPA, but not actually expressed in our samples), and not WNT1, were the identified members of the WNT/β-catenin signaling pathway. To get additional information on the epigenetic alterations caused by PEMF, the relative expression level of the most commonly reported epigenetic modulator in the literature, that is miR26A1, was evaluated, and results showed that PEMF caused a slight elevation in the expression of miR26A1 (~1.0-fold change), and this was also verified by transcriptomic studies that highlighted other miRNAs, and not miR26A1, as major epigenetic players.

To corroborate the biological effects of PEMF on the cellular level, the relative expression levels of the osteogenic markers, angiogenic markers, and chondrogenic markers were traced. The outcomes showed higher expression of RUNX2, OCN, and OPN mRNAs with PEMF stimulation in comparison with perfusion alone (~1.9, 1.7, and 147.7-fold change, respectively), and similar tendencies were seen with the mRNAs of the angiogenic markers ICAM1, PECAM1, and KDR (~1.9, 13.7, and 1.1-fold change, respectively) and the mRNA of the chondrogenic marker SOX9 (~2.5-fold change). Based on the results, we can hypothesize that PEMF stimulation tends to preserve the ability of BM-MSCs to differentiate into various cell types. This is because both osteogenic and angiogenic markers were upregulated. This property is a key characteristic of stem cells, which are known for their ability to differentiate into different cell types.

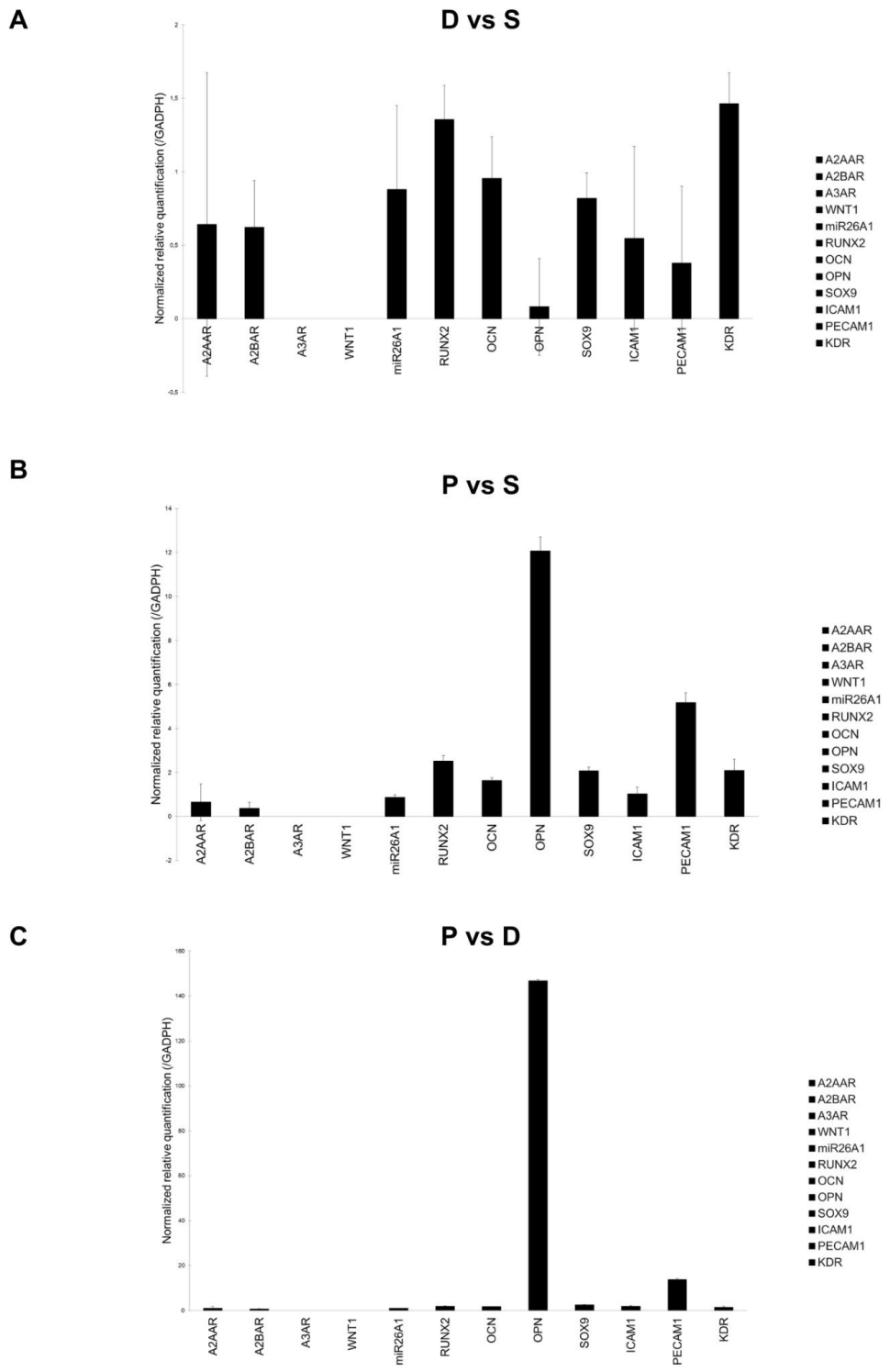

Figure 3.6. Gene expression analyses of bone marrow-derived mesenchymal stem cells (BM-MSCs) cultured in basal medium. The relative expressions of various mRNAs in the three comparisons **(A)** "D" versus "S"; **(B)** "P" versus "S"; and **(C)** "P" versus "D", in which "S" represents static culture, "D" represents direct, unidirectional perfusion, and "P" represents direct, unidirectional perfusion with PEMF stimulation. The relative expressions of the mRNAs were analyzed by reverse transcription-quantitative PCR (RT-qPCR) and were

calculated by $2^{-\Delta\Delta CT}$ method with normalization to the levels of GAPDH. Bars represent the mean fold change of three biological replicates +/− standard error of the mean (SEM).

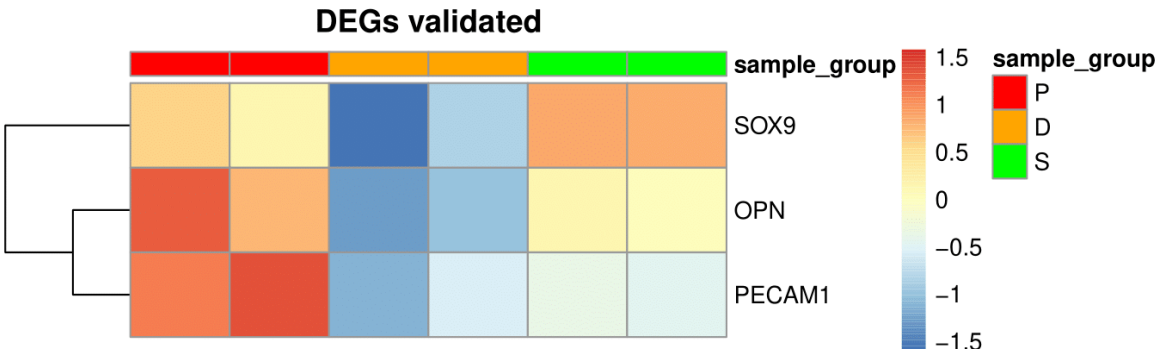

Figure 3.7. Heatmap of validated differentially expressed genes (DEGs) of bone marrow-derived mesenchymal stem cells (BM-MSCs) cultured in basal medium. The genes are SRY-Box transcription factor 9 (SOX9), osteopontin (OPN), and platelet and endothelial cell adhesion molecule 1 (PECAM1). "S" represents static culture, "D" represents direct, unidirectional perfusion, and "P" represents direct, unidirectional perfusion with PEMF stimulation.

3.5 Discussion

Understanding how cells respond to external physical stimuli is crucial for unraveling complex signaling pathways involved in disease treatment. In our study, transcriptomic analysis was employed to elucidate the molecular and cellular alterations induced by PEMF stimulation. The DEGs identified by transcriptomic studies were analyzed to identify the signaling pathways and upstream regulators altered by PEMF stimulation by comparing the culture conditions "P" and "D". Moreover, the identified upstream regulators underwent pathway enrichment analysis. Starting with the first phase of bone healing, our results showed that in the absence of a pathological state, such as bone fracture, PEMF has an immune potential as it stimulates the immune properties of human BM-MSCs and can therefore modulate the immune system. This outcome is consistent with the findings of previous studies that presented the anti-inflammatory properties of PEMF. However, it is worth noting that most *in vitro* studies performed to date were done on 2D cell cultures and in the presence of an inflammatory state, and only a few of them investigated MSCs. For instance, synovial fibroblasts from OA patients were exposed to PEMF by Ongaro et al. (2011), who showed that EMF predisposed an anti-inflammatory state via the activation and upregulation of the adenosine receptors A_{2A} and A_3, the inhibited release of prostaglandin E_2 (PGE_2) and other proinflammatory cytokines, and finally, the elevated release of anti-inflammatory cytokines [62]. For the immune potential of PEMF stimulation, several studies

suggested the involvement of ARs, and proposed A2AAR and A3AR as the major players in various cell lines including human neutrophils, synoviocytes, chondrocytes, and osteoblasts [63]. The transcriptomic studies of the present work did not highlight signaling pathways involving ARs; yet, these transmembrane receptors are not the only ones that can be linked to the immune potential of PEMF stimulation. This point was demonstrated by other studies, such as the work done by Ferroni et al. (2018), who studied mTOR signaling pathway in particular, and revealed that human AD-MSCs exposed to PEMF showed increased cell proliferation, cell adhesion, and osteogenic commitment even in inflammatory conditions via mTOR signaling pathway [64]. The involvement of the mTOR signaling pathway was also demonstrated in the transcriptomic studies of the present study, as mentioned above.

The second phase of bone healing, the fibrovascular phase, is also targeted by PEMF stimulation, according to our results. This capacity of PEMF stimulation has been reported by previous in vitro studies too, yet, they were mainly performed on 2D cultures. One example is the recent study by Gerdesmeyer et al. (2022), who used primary human BM-MSCs cultured in osteogenic medium and exposed them to high-intensive PEMF (80–150 mT, 1–3 Hz) for up to 14 days. The authors showed that only at day 7 of culture PEMF with a magnetic field strength of 80 mT caused an increase in the released proangiogenic factor VEGF, while it did not upregulate the expression of VEGF and pro-osteogenic factors genes [65]. In previous work in vitro and in vivo, Tepper et al. (2004) also depicted a major role of FGF2 in the angiogenic potential of PEMF [66]. Regardless of the heterogeneity among the examined angiogenic markers, there is substantial evidence of the involvement of the MAPK signaling pathway, with a concrete role of FGF2 in the angiogenic potential of PEMF stimulation. This was also observed in the present study using BM-MSCs, since the transcriptomic studies underlined upstream regulators that are tightly linked to the activation of MAPK signaling pathway and to the regulation of angiogenesis.

Finally, the last phases of bone healing, which are the bone formation phase and bone remodeling phase, are also altered by PEMF stimulation relative to our findings. However, it is noteworthy that regardless of the firm bond between PEMF stimulation and bone healing, the complete mechanisms participating in this action are slightly recognized, and adding to this, the findings of studies are not well defined. In 2D cultures, for instance, Gerdesmeyer et al. (2022) did not observe a significant upregulation in the expression of COL1, ALP, OCN, and BMP2 by human BM-MSCs exposed to PEMF after 7 and 14 days of culture in comparison with cells cultured in the absence of PEMF [65]. Conversely, Wu et al. (2018), using mouse embryonic stem cells exposed to PEMF (0.1–10 mT, 30 Hz), revealed that PEMF induced osteoblastogenesis through increased intracellular Ca^{2+} and the Wnt-Ca^{2+}/Wnt-β-catenin signaling pathway [67] The effect of PEMF stimulation on bone healing was also tested in 3D cultures. Using calcium phosphate (CaP) surfaces and three different cell lines (human BM-MSCs, human osteoblast-like osteosarcoma MG63 and SaOS-2 cells, and normal human osteoblasts), Schwartz et al. (2009) showed that PEMF stimulation elevated the expression of the TNF receptor superfamily member 11b (TNFRSF11B), but did not alter that of RANKL, suggesting that PEMF stimulation acts via a signaling pathway other than those that mediate RANKL expression or secretion [68]. The signaling pathways

involved in bone metabolism that are mainly correlated with the osteogenic potential of PEMF include TGF-β/BMP signaling [69], WNT/β-catenin signaling [70], and NF-κB signaling [71]. In the present study, members of all three pathways were detected to be upregulated by PEMF stimulation. Alongside this, the single most startling finding is the remarkable upregulation of the expression of OPN caused by PEMF stimulation in comparison with perfusion alone. The latter is worth further investigation, especially that OPN possesses multiple functions and plays roles in inflammation, cardiovascular diseases, cellular viability, cancer, diabetes, and renal stone disease [72].

3.6 Conclusions

In spite of the advancements in uncovering the biological effects of biophysical stimulation, including PEMF, a comprehensive understanding of the altered signaling pathways is yet to be realized. There is no doubt that *in vitro* experiments omitting the complexity and peculiarity of tissue types are henceforward deficient, and in parallel, legislations aiming to stop the use of animals for scientific purposes make *in vivo* experiments an unfeasible alternative. As such, the most propitious substitute is the application of advanced *in vitro* investigation tools that attempt to replicate the parameters of specific physiological environments as closely as possible. Human mesenchymal stem cells (hMSCs) are sensitive to biomechanical and biophysical stimuli, which means that it is enormously substantial to track down the signaling pathways involved in the stimulus-response transformations resulting from biomechanical and biophysical stimulation.

Based on evidence from the current study, human BM-MSCs cultivated in an *in vitro* investigation platform replicating the microarchitecture of trabecular bone and the physiological environment of bone tissue can respond to PEMF stimulation by inducing bone healing via the expression of immune, angiogenic, and osteogenic potential. The study also successfully mapped the gene transcripts of human BM-MSCs that are sensitive to biomechanical and biophysical stimulation. Another observation to emerge from this study is the ability of PEMF stimulation to initiate new features in the human BM-MSCs including the aptitude to interfere in certain pathological states. Thus, based on evidence from the present study, the proposed *in vitro* investigation platform represents a suitable tool for investigating the biological effects of PEMF stimulation.

The current work is a call for other researchers to avail themselves of the opportunity to access the transcriptome profile of human BM-MSCs to direct their future research. It should be emphasized that a lot remains obscured, and more work is needed to discover how different cell types respond to PEMF stimulation, how mechanical stimuli resembling the bone physiological environment affect the biological effects of PEMF, and how the modification of PEMF parameters (amplitude, frequency, pulse shape, and duration of exposure) modify the biological outcome.

This chapter was published as part of a “research article” in the scientific journal *Bone* from *Elsevier*:

Daou, F., Masante, B., Gabetti, S., Mochi, F., Putame, G., Zenobi, E., Scatena, E., Dell'Atti, F., Favero, F., Leigheb, M., Del Gaudio, C., Bignardi, C., Massai, D., Cochis, A., & Rimondini, L. **(2024)**. Unraveling the transcriptome profile of pulsed electromagnetic field stimulation in bone regeneration using a bioreactor-based investigation platform. *Bone*, 182, 117065. https://doi.org/10.1016/j.bone.2024.117065

3.7. Fundings

This study was carried out within the BIGMECH project – funded by the European Union – Next Generation EU within the PRIN 2022 program (D.D. 104 - 02/02/2022 Ministero dell’Università e della Ricerca). This manuscript reflects only the authors’ views and opinions and the Ministry cannot be considered responsible for them.

3.8 Acknowledgments

I would like to thank Dr. Eleonora Zenobi and Dr. Elisa Scateno for kindly providing the 3D-printed PLA scaffolds, as well as Prof. Diana Massai, Dr. Stefano Gabetti, and Dr. Beatrice Masante for kindly providing the perfusion bioreactor. I would also like to thank Prof. Lia Rimondini and Prof. Andrea Cochis for their supervision. A sincere thank you goes to Mrs. Marta Mellai for her help with performing the transcriptomic analysis and to Dr. Francesco Favero for his help with the bioinformatic analysis of the transcriptomic data.

3.9 References

1. Yamada, S., Ockermann, P.N., Schwarz, T., Mustafa, K., and Hansmann, J. (2023) Translation of biophysical environment in bone into dynamic cell culture under flow for bone tissue engineering. *Comput Struct Biotechnol J*, 21, 4395–4407.
2. Tandon, B., Blaker, J.J., and Cartmell, S.H. (2018) Piezoelectric materials as stimulatory biomedical materials and scaffolds for bone repair. *Acta Biomater*, 73, 1–20.
3. Fukada, E., and Yasuda, I. (2013) On the Piezoelectric Effect of Bone. *https://doi.org/10.1143/JPSJ.12.1158*, 12 (10), 1158–1162.
4. Reinish, G.B., and Nowick, A.S. (1975) Piezoelectric properties of bone as functions of moisture content. *Nature 1975 253:5493*, 253 (5493), 626–627.
5. Hao, Z., Xu, Z., Wang, X., Wang, Y., Li, H., Chen, T., Hu, Y., Chen, R., Huang, K., Chen, C., and Li, J. (2021) Biophysical Stimuli as the Fourth Pillar of Bone Tissue Engineering. *Front Cell Dev Biol*, 9, 790050.

6. Haffner-Luntzer, M., Liedert, A., and Ignatius, A. (2020) Mechanobiology of bone remodeling and fracture healing in the aged organism. *Innov Surg Sci*, 1 (2), 57–63.
7. Stewart, S., Darwood, A., Masouros, S., Higgins, C., and Ramasamy, A. (2020) Mechanotransduction in osteogenesis. *Bone Joint Res*, 9 (1), 1.
8. Haffner-Luntzer, M., Liedert, A., and Ignatius, A. (2016) Mechanobiology of bone remodeling and fracture healing in the aged organism. *Innov Surg Sci*, 1 (2), 57.
9. Claes, L.E., and Heigele, C.A. (1999) Magnitudes of local stress and strain along bony surfaces predict the course and type of fracture healing. *J Biomech*, 32 (3), 255–266.
10. Claes, L., Veeser, A., Göckelmann, M., Simon, U., and Ignatius, A. (2009) A novel model to study metaphyseal bone healing under defined biomechanical conditions. *Arch Orthop Trauma Surg*, 129 (7), 923–928.
11. Bai, Y., Li, X., Wu, K., Heng, B.C., Zhang, X., and Deng, X. (2024) Biophysical stimuli for promoting bone repair and regeneration. *Medical Review*.
12. Lopes, D., Martins-Cruz, C., Oliveira, M.B., and Mano, J.F. (2018) Bone physiology as inspiration for tissue regenerative therapies. *Biomaterials*, 185, 240–275.
13. Kuzyk, P.R.T., and Schemitsch, E.H. (2009) The science of electrical stimulation therapy for fracture healing. *Indian J Orthop*, 43 (2), 127.
14. Palanisamy, P., Alam, M., Li, S., Chow, S.K.H., and Zheng, Y.P. (2021) Low-Intensity Pulsed Ultrasound Stimulation for Bone Fractures Healing: A Review. *Journal of Ultrasound in Medicine*, 41 (3), 547.
15. Higgins, A., Glover, M., Yang, Y., Bayliss, S., Meads, C., and Lord, J. (2014) EXOGEN Ultrasound Bone Healing System for Long Bone Fractures with Non-Union or Delayed Healing: A NICE Medical Technology Guidance. *Appl Health Econ Health Policy*, 12 (5), 477–484.
16. Jiang, X., Savchenko, O., Li, Y., Qi, S., Yang, T., Zhang, W., and Chen, J. (2019) A Review of Low-Intensity Pulsed Ultrasound for Therapeutic Applications. *IEEE Trans Biomed Eng*, 66 (10), 2704–2718.
17. Palanisamy, P., Alam, M., Li, S., Chow, S.K.H., and Zheng, Y.P. (2022) Low-Intensity Pulsed Ultrasound Stimulation for Bone Fractures Healing. *Journal of Ultrasound in Medicine*, 41 (3), 547–563.
18. Yang, J., Feng, Y., Li, Q., and Zeng, Y. (2023) Evidence of the static magnetic field effects on bone-related diseases and bone cells. *Prog Biophys Mol Biol*, 177, 168–180.
19. Xie, W., Song, C., Guo, R., and Zhang, X. (2024) Static magnetic fields in regenerative medicine. *APL Bioeng*, 8 (1), 011503.
20. Lu, P., Peng, J., Liu, J., and Chen, L. (2024) The role of photobiomodulation in accelerating bone repair. *Prog Biophys Mol Biol*, 188, 55–67.
21. Neto, F.C.J., Martimbianco, A.L.C., de Andrade, R.P., Bussadori, S.K., Mesquita-Ferrari, R.A., and Fernandes, K.P.S. (2020) Effects of photobiomodulation in the treatment of fractures: a systematic review and meta-analysis of randomized clinical trials. *Lasers Med Sci*, 35 (3), 513–522.
22. Zheng, J., and Yang, K. (2021) Clinical research: low-level laser therapy in accelerating orthodontic tooth movement. *BMC Oral Health*, 21 (1), 1–7.
23. Rosero, K.A.V., Sampaio, R.M.F., Deboni, M.C.Z., Corrêa, L., Marques, M.M., Ferraz, E.P., and da Graça Naclério-Homem, M. (2020) Photobiomodulation as an adjunctive therapy for

alveolar socket preservation: a preliminary study in humans. *Lasers Med Sci*, 35 (8), 1711–1720.
24. Marín-Cascales, E., Alcaraz, P.E., Ramos-Campo, D.J., Martinez-Rodriguez, A., Chung, L.H., and Rubio-Arias, J. (2018) Whole-body vibration training and bone health in postmenopausal women: A systematic review and meta-analysis. *Medicine*, 97 (34), e11918.
25. Zelle, B.A., Gollwitzer, H., Zlowodzki, M., and Bühren, V. (2010) Extracorporeal shock wave therapy: Current evidence. *J Orthop Trauma*, 24 (SUPPL. 1).
26. Food and Drug Administration (FDA) ORDP - Bone Growth Stimulators Executive Summary-08.07.20-FINAL_Redacted fda.
27. Hu, H., Yang, W., Zeng, Q., Chen, W., Zhu, Y. Bin, Liu, W., Wang, S., Wang, B., Shao, Z., and Zhang, Y. (2020) Promising application of Pulsed Electromagnetic Fields (PEMFs) in musculoskeletal disorders. *Biomedicine and Pharmacotherapy*, 131.
28. Andrade, R., Duarte, H., Pereira, R., Lopes, I., Pereira, H., Rocha, R., and Espregueira-Mendes, J. (2016) Pulsed electromagnetic field therapy effectiveness in low back pain: A systematic review of randomized controlled trials. *Porto Biomed J*, 1 (5), 156–163.
29. Xu, R. Da, Li, J.H., Zhang, H., Liang, H.R., Duan, S.Y., Sun, M., Wen, H., Zhou, X.T., Liu, H.F., and Cai, Z.C. (2024) The combined application of pulsed electromagnetic fields and platelet-rich plasma in the treatment of early-stage knee osteoarthritis: A randomized clinical trial. *Medicine*, 103 (35), e39369.
30. Factor, S., Druckmann, I., Kazum, E., Atlan, F., Tordjman, D., Rosenblatt, Y., Eisenberg, G., and Pritsch, T. (2024) A novel pulsed electromagnetic field device as an adjunct therapy to surgical treatment of distal radius fractures: a prospective, double-blind, sham-controlled, randomized pilot study. *Arch Orthop Trauma Surg*, 144 (1), 543–550.
31. Wang, Q.W., Ong, M.T. yun, Man, G.C. wai, Franco-Obregón, A., Choi, B.C. yin, Lui, P.P. yee, Fong, D.T.P., Qiu, J.H., He, X., Ng, J.P., and Yung, P.S. hang (2024) The effects of pulsed electromagnetic field therapy on muscle strength and pain in patients with end-stage knee osteoarthritis: a randomized controlled trial. *Front Med (Lausanne)*, 11, 1435277.
32. Weinstein, M.A., Beaumont, A., Campbell, P., Hassanzadeh, H., Patel, V., Vokshoor, A., Wind, J., Radcliff, K., Aleem, I., and Coric, D. (2023) Pulsed Electromagnetic Field Stimulation in Lumbar Spine Fusion for Patients With Risk Factors for Pseudarthrosis. *Int J Spine Surg*, 17 (6), 816.
33. Ferragina, F., Caruso, D., Barca, I., Kallaverja, E., Arrotta, A., and Cristofaro, M.G. (2024) Efficacy of Pulsed Electromagnetic Field Therapy for Pain Management After Impacted Mandibular Third Molar Surgery. A Randomized Clinical Trial. *Journal of Oral and Maxillofacial Surgery*, 82 (6), 692–698.
34. Strauch, B., Herman, C., Dabb, R., Ignarro, L.J., and Pilla, A.A. (2009) Evidence-Based Use of Pulsed Electromagnetic Field Therapy in Clinical Plastic Surgery. *Aesthet Surg J*, 29 (2), 135–143.
35. Larsen, E.R., Licht, R.W., Nielsen, R.E., Lolk, A., Borck, B., Sørensen, C., Christensen, E.M., Bizik, G., Ravn, J., Martiny, K., Vinberg, M., Jankuviené, O., Jørgensen, P.B., Videbech, P., and Bech, P. (2020) Transcranial pulsed electromagnetic fields for treatment-resistant depression: A multicenter 8-week single-arm cohort study: The eighth trial of the Danish University Antidepressant Group. *European Psychiatry*, 63 (1), e18.

36. Vadalà, M., Morales-Medina, J.C., Vallelunga, A., Palmieri, B., Laurino, C., and Iannitti, T. (2016) Mechanisms and therapeutic effectiveness of pulsed electromagnetic field therapy in oncology. *Cancer Med*, 5 (11), 3128–3139.
37. Kazimierczak, P., and Przekora, A. (2022) Bioengineered Living Bone Grafts—A Concise Review on Bioreactors and Production Techniques In Vitro. *International Journal of Molecular Sciences 2022, Vol. 23, Page 1765*, 23 (3), 1765.
38. Search for: Pulsed electromagnetic field therapy | Card Results | ClinicalTrials.gov.
39. Search for clinical trials - EMA.
40. pulsed electromagnetic field - Search Results - PubMed.
41. Galli, C., Pedrazzi, G., Mattioli-Belmonte, M., and Guizzardi, S. (2018) The Use of Pulsed Electromagnetic Fields to Promote Bone Responses to Biomaterials in Vitro and in Vivo. *Int J Biomater*, 2018.
42. Varani, K., Vincenzi, F., Pasquini, S., Blo, I., Salati, S., Cadossi, M., and De Mattei, M. (2021) Pulsed electromagnetic field stimulation in osteogenesis and chondrogenesis: Signaling pathways and therapeutic implications. *Int J Mol Sci*, 22 (2), 1–17.
43. Caliogna, L., Medetti, M., Bina, V., Brancato, A.M., Castelli, A., Jannelli, E., Ivone, A., Gastaldi, G., Annunziata, S., Mosconi, M., and Pasta, G. (2021) Pulsed Electromagnetic Fields in Bone Healing: Molecular Pathways and Clinical Applications. *Int J Mol Sci*, 22 (14), 7403.
44. Cadossi, R., Massari, L., Racine-Avila, J., and Aaron, R.K. (2020) Pulsed Electromagnetic Field Stimulation of Bone Healing and Joint Preservation: Cellular Mechanisms of Skeletal Response. *J Am Acad Orthop Surg Glob Res Rev*, 4 (5).
45. Peng, L., Fu, C., Xiong, F., Zhang, Q., Liang, Z., Chen, L., He, C., and Wei, Q. (2020) Effectiveness of Pulsed Electromagnetic Fields on Bone Healing: A Systematic Review and Meta-Analysis of Randomized Controlled Trials. *Bioelectromagnetics*, 41 (5), 323–337.
46. Ehnert, S., Schröter, S., Aspera-Werz, R.H., Eisler, W., Falldorf, K., Ronniger, M., and Nussler, A.K. (2019) Translational Insights into Extremely Low Frequency Pulsed Electromagnetic Fields (ELF-PEMFs) for Bone Regeneration after Trauma and Orthopedic Surgery. *Journal of Clinical Medicine 2019, Vol. 8, Page 2028*, 8 (12), 2028.
47. Panagopoulos, D.J. (2019) Comparing DNA damage induced by mobile telephony and other types of man-made electromagnetic fields. *Mutation Research/Reviews in Mutation Research*, 781, 53–62.
48. Bailey, W.H. (2002) Health effects relevant to the setting of EMF exposure limits. *Health Phys*, 83 (3), 376–386.
49. Babraham Bioinformatics - FastQC A Quality Control tool for High Throughput Sequence Data.
50. Ewels, P., Magnusson, M., Lundin, S., and Käller, M. (2016) MultiQC: summarize analysis results for multiple tools and samples in a single report. *Bioinformatics*, 32 (19), 3047–3048.
51. Li, B., and Dewey, C.N. (2011) RSEM: Accurate transcript quantification from RNA-Seq data with or without a reference genome. *BMC Bioinformatics*, 12 (1), 1–16.
52. Cunningham, F., Allen, J.E., Allen, J., Alvarez-Jarreta, J., Amode, M.R., Armean, I.M., Austine-Orimoloye, O., Azov, A.G., Barnes, I., Bennett, R., Berry, A., Bhai, J., Bignell, A., Billis, K., Boddu, S., Brooks, L., Charkhchi, M., Cummins, C., Da Rin Fioretto, L., Davidson, C., Dodiya, K., Donaldson, S., El Houdaigui, B., El Naboulsi, T., Fatima, R.,

Giron, C.G., Genez, T., Martinez, J.G., Guijarro-Clarke, C., Gymer, A., Hardy, M., Hollis, Z., Hourlier, T., Hunt, T., Juettemann, T., Kaikala, V., Kay, M., Lavidas, I., Le, T., Lemos, D., Marugán, J.C., Mohanan, S., Mushtaq, A., Naven, M., Ogeh, D.N., Parker, A., Parton, A., Perry, M., Pilizota, I., Prosovetskaia, I., Sakthivel, M.P., Salam, A.I.A., Schmitt, B.M., Schuilenburg, H., Sheppard, D., Perez-Silva, J.G., Stark, W., Steed, E., Sutinen, K., Sukumaran, R., Sumathipala, D., Suner, M.M., Szpak, M., Thormann, A., Tricomi, F.F., Urbina-Gómez, D., Veidenberg, A., Walsh, T.A., Walts, B., Willhoft, N., Winterbottom, A., Wass, E., Chakiachvili, M., Flint, B., Frankish, A., Giorgetti, S., Haggerty, L., Hunt, S.E., Iisley, G.R., Loveland, J.E., Martin, F.J., Moore, B., Mudge, J.M., Muffato, M., Perry, E., Ruffier, M., Tate, J., Thybert, D., Trevanion, S.J., Dyer, S., Harrison, P.W., Howe, K.L., Yates, A.D., Zerbino, D.R., and Flicek, P. (2022) Ensembl 2022. *Nucleic Acids Res*, 50 (D1), D988–D995.

53. Dobin, A., Davis, C.A., Schlesinger, F., Drenkow, J., Zaleski, C., Jha, S., Batut, P., Chaisson, M., and Gingeras, T.R. (2013) STAR: ultrafast universal RNA-seq aligner. *Bioinformatics*, 29 (1), 15–21.
54. Love, M.I., Huber, W., and Anders, S. (2014) Moderated estimation of fold change and dispersion for RNA-seq data with DESeq2. *Genome Biol*, 15 (12), 1–21.
55. Zhou, Y., Zhou, B., Pache, L., Chang, M., Khodabakhshi, A.H., Tanaseichuk, O., Benner, C., and Chanda, S.K. (2019) Metascape provides a biologist-oriented resource for the analysis of systems-level datasets. *Nature Communications 2019 10:1*, 10 (1), 1–10.
56. Chen, J., Bardes, E.E., Aronow, B.J., and Jegga, A.G. (2009) ToppGene Suite for gene list enrichment analysis and candidate gene prioritization. *Nucleic Acids Res*, 37 (suppl_2), W305–W311.
57. Supek, F., Bošnjak, M., Škunca, N., and Šmuc, T. (2011) REVIGO Summarizes and Visualizes Long Lists of Gene Ontology Terms. *PLoS One*, 6 (7), e21800.
58. Bahney, C.S., Zondervan, R.L., Allison, P., Theologis, A., Ashley, J.W., Ahn, J., Miclau, T., Marcucio, R.S., and Hankenson, K.D. (2019) Cellular biology of fracture healing. *Journal of Orthopaedic Research®*, 37 (1), 35–50.
59. De Mattei, M., Grassilli, S., Pellati, A., Brugnoli, F., De Marchi, E., Contartese, D., and Bertagnolo, V. (2020) Pulsed Electromagnetic Fields Modulate miRNAs During Osteogenic Differentiation of Bone Mesenchymal Stem Cells: a Possible Role in the Osteogenic-angiogenic Coupling. *Stem Cell Rev Rep*, 16 (5), 1005–1012.
60. Marintchev, A., and Ito, T. (2020) EIF2B and the Integrated Stress Response: A Structural and Mechanistic View. *Biochemistry*, 59 (13), 1299–1308.
61. Vinolo-Gil, M.J., Rodríguez-Huguet, M., García-Muñoz, C., Gonzalez-Medina, G., Martin-Vega, F.J., and Martín-Valero, R. (2022) Effects of Peripheral Electromagnetic Fields on Spasticity: A Systematic Review. *Journal of Clinical Medicine 2022, Vol. 11, Page 3739*, 11 (13), 3739.
62. Ongaro, A., Varani, K., Masieri, F.F., Pellati, A., Massari, L., Cadossi, R., Vincenzi, F., Borea, P.A., Fini, M., Caruso, A., and De Mattei, M. (2012) Electromagnetic fields (EMFs) and adenosine receptors modulate prostaglandin E2 and cytokine release in human osteoarthritic synovial fibroblasts. *J Cell Physiol*, 227 (6), 2461–2469.
63. Varani, K., Vincenzi, F., Ravani, A., Pasquini, S., Merighi, S., Gessi, S., Setti, S., Cadossi, M., Borea, P.A., and Cadossi, R. (2017) Adenosine Receptors as a Biological Pathway for the

Anti-Inflammatory and Beneficial Effects of Low Frequency Low Energy Pulsed Electromagnetic Fields. *Mediators Inflamm*, 2017 (1), 2740963.

64. Ferroni, L., Gardin, C., Dolkart, O., Salai, M., Barak, S., Piattelli, A., Amir-Barak, H., and Zavan, B. (2018) Pulsed electromagnetic fields increase osteogenetic commitment of MSCs via the mTOR pathway in TNF-α mediated inflammatory conditions: an in-vitro study. *Scientific Reports 2018 8:1*, 8 (1), 1–13.
65. Gerdesmeyer, L., Zielhardt, P., Klüter, T., Gollwitzer, H., Gerdesmeyer, L., Hausdorf, J., Ringeisen, M., Knobloch, K., Saxena, A., and Krath, A. (2022) Stimulation of human bone marrow mesenchymal stem cells by electromagnetic transduction therapy - EMTT. *Electromagn Biol Med*, 41 (3), 304–314.
66. Tepper, O.M., Callaghan, M.J., Chang, E.I., Galiano, R.D., Bhatt, K.A., Baharestani, S., Gan, J., Simon, B., Hopper, R.A., Levine, J.P., and Gurtner, G.C. (2004) Electromagnetic fields increase in vitro and in vivo angiogenesis through endothelial release of FGF-2. *The FASEB Journal*, 18 (11), 1231–1233.
67. Wu, S., Yu, Q., Lai, A., and Tian, J. (2018) Pulsed electromagnetic field induces Ca2+-dependent osteoblastogenesis in C3H10T1/2 mesenchymal cells through the Wnt-Ca2+/Wnt-β-catenin signaling pathway. *Biochem Biophys Res Commun*, 503 (2), 715–721.
68. Schwartz, Z., Fisher, M., Lohmann, C.H., Simon, B.J., and Boyan, B.D. (2009) Osteoprotegerin (OPG) production by cells in the osteoblast lineage is regulated by pulsed electromagnetic fields in cultures grown on calcium phosphate substrates. *Ann Biomed Eng*, 37 (3), 437–444.
69. Wu, M., Chen, G., and Li, Y.P. (2016) TGF-β and BMP signaling in osteoblast, skeletal development, and bone formation, homeostasis and disease. *Bone Research 2016 4:1*, 4 (1), 1–21.
70. Maeda, K., Kobayashi, Y., Koide, M., Uehara, S., Okamoto, M., Ishihara, A., Kayama, T., Saito, M., and Marumo, K. (2019) The Regulation of Bone Metabolism and Disorders by Wnt Signaling. *International Journal of Molecular Sciences 2019, Vol. 20, Page 5525*, 20 (22), 5525.
71. Jimi, E., and Katagiri, T. (2022) Critical Roles of NF-κB Signaling Molecules in Bone Metabolism Revealed by Genetic Mutations in Osteopetrosis. *International Journal of Molecular Sciences 2022, Vol. 23, Page 7995*, 23 (14), 7995.
72. Icer, M.A., and Gezmen-Karadag, M. (2018) The multiple functions and mechanisms of osteopontin. *Clin Biochem*, 59, 17–24.

Chapter 4

Upgrading the Automated Perfusion Bioreactor with Hydrostatic Pressure to Better Mimic Bone's Mechanical Environment

4.1 Abstract

Bone is a dynamic tissue that experiences a complex mechanical environment. The intricate interplay between various mechanical stimuli and bone cells orchestrates processes such as bone remodeling, adaptation, and repair. In this work, we upgraded the previously described *in vitro* bioreactor-based platform. By incorporating pinch valves with adjustable settings (period and duty cycle), we can deliver hydrostatic pressure, simulating physiological loading or unloading. For this purpose, human bone marrow-derived mesenchymal stem cells (BM-MSCs) were seeded onto 3D-printed polylactic acid (PLA), as described in Chapter 2, and cultured under three different condition: static culture; within the perfusion bioreactor providing fluid flow-induced shear stress, as previously described in Chapter 1; and within the upgraded perfusion bioreactor providing both fluid flow-induced shear stress and intermittent hydrostatic pressure simulating physiological unloading to evaluate cell viability.

4.2 Introduction

The response of bone cells to physical forces plays a significant role not only during bone modeling and remodeling, but also during bone healing, bone regeneration, and implant osseointegration. Exercise intervention programs have shown to reduce bone loss or increase bone mass regardless of the gender, age, and initial bone health status. It is speculated that the maintenance of skeletal integrity relies on the interplay between cellular response to hormonal stimuli and mechanical load stimuli [1], although the mechanisms through which the mechanical microenvironment alters cellular behavior is still not well known. Several studies have shown that athletes have higher bone mineral density (BMD) and linked this improvement to the mechanical stimuli, since the greater the mechanical loading, the greater the BMD [2]. On the other hand, astronauts who participate on long-duration space missions and remain in a zero-gravity environment are known to experience substantial reduction in BMD and bone strength due to the absence of mechanical loading [3].

The mechanical microenvironment's significant influences on bone health is also evidenced by various clinical interventions. Distraction osteogenesis (DO), for instance, is a surgical technique employed to address conditions, such as leg length discrepancy, bone deformity, large bone defects, or bone resection. This technique involves creating a transverse bone section (osteotomy) and separating the bone segments rhythmically and gradually, applying specific tensile forces. This longitudinal mechanical strain triggers bone regeneration, which begins with the formation of immature bone, followed by mineralization, and ultimately, consolidation with the surrounding bone tissue [4]. Similar principles apply to bone fractures. Although personalized clinical guidelines for optimal mechanical strain parameters (frequency and magnitude) in fracture healing remain elusive, a consensus exists on the importance of a sequential approach: initial stability (immobilization and compression, non-load-bearing), followed by progressive loading (partial and full load-bearing) [5]. Mechanical forces also play a critical role in bone implant osseointegration. Consequently, implant design, particularly in terms of force transmission, is a crucial factor [6].

The underlying reason for all the aforementioned examples of how the presence or absence of mechanical cues alter bone health is rooted in the biomechanical and biophysical environment of bone tissue. These environments vary significantly at different anatomical levels (macroscopic, microscopic and nanoscopic). Bone adaptation is regulated by the complex interplay of biomechanical and biophysical factors, encompassing the commonly considered ones, which are matrix strain, fluid flow-induced shear stress, and hydrostatic pressure, as well as the piezoelectricity and streaming potential [7]. However, non-mechanical factors, such as hormones, immune responses, and angiogenesis, are equally important and interact with the biomechanical and biophysical cues to regulate bone regeneration [8]. To fully understand bone regeneration, advanced *in vitro* models capable of recapitulating multiple stimuli, including physical, mechanical, biological, and chemical factors, are necessary.

Interstitial fluid flow is a key player in bone health. Mechanical loading generates interstitial fluid flow through poroelastic flow within the lacunar-canalicular network and via intramedullary pressurization. While the former primarily generates flow within the bone matrix, the latter induces significant flow at both the endosteal surface and within the tissue [9]. This interstitial fluid flow generates various mechanical stimuli, particularly fluid flow-induced shear stress and hydrostatic pressure [10].

Weinbaum and colleagues (1994) developed a model of fluid flow within the bone matrix, considering the presence of proteoglycans. Their model predicted that the shear stress exerted by this fluid flow on bone cells ranges from 8 to 30 dyn/cm² [11]. However, different studies reported varying values of shear stress, depending on factors such as the type of loading (bending, axial loading, torsional loading, etc.), velocity, and other variables. Notably, the fluid shear stress experienced by human bone remains undetermined [7].

According to Zhang et al. (1998), when we walk, our bones experience a certain level of cyclic stress (0–18 MPa) and strain (1000 με). This stress and strain can lead to a buildup of pressure within the bone, particularly in the low-density regions. This pressure, estimated to be around 0.27 MPa, is significantly higher than the pressure in blood vessels [12]. While *in vitro* studies have shown that this pressure can stimulate bone growth, it is difficult to directly measure and study this effect in living organisms due to technological limitations. It is speculated that the unique structure of bones, with areas of concentrated stress, might amplify this pressure, potentially leading to even higher levels than the estimated 0.27 MPa [7].

To assess the role of mechanical cues in bone healing and regeneration, this study aimed to investigate the effects of hydrostatic pressure on stem cell behavior and osteogenic differentiation. To achieve this, we employed an upgraded bioreactor-based platform. This platform was designed based on the bioreactor-based platform described in Chapter 2. It incorporated pinch valves with adjustable settings (period and duty cycle) to deliver hydrostatic pressure simulating either physiological unloading or loading. The hydrostatic pressure characterization was performed using collagen-loaded PLA600 scaffolds. Moreover, bone marrow-derived mesenchymal stem cells (BMSCs) were seeded onto polylactic acid (PLA600) scaffolds (described in Chapter 2), and cultured under various bone-tissue-like mechanical stimulations. Cells were cultured statically, or exposed to fluid flow-induced shear stress without and with hydrostatic pressure simulating physiological unloading (5 kPa). Cell viability was assessed under these conditions on day 7.

4.3 Materials and Methods

4.3.1 Parallelized, automated perfusion bioreactor equipped with pinch valves

The automated perfusion bioreactor equipped that was previously described in Chapter 2 was equipped with solenoid-actuated pinch valve (Cole Parmer GmbH) **(Figure 4.1A)** placed downstream to provide intermittent hydrostatic pressure **(Figure 4.1C and 4.1D)**. The pinch valve settings, including period (0.25-30 s) and duty cycle (0-100%), can be modified via a fully automated Arduino-based control box. The pinch valves can be easily and quickly connected to perfusion system. Pressure measurements were performed using non-invasive pressure sensors (HJK Sensoren) **(Figure 4.1B)** using the PLA600 scaffolds (described in Chapter 2 of the thesis) loaded with collagen.

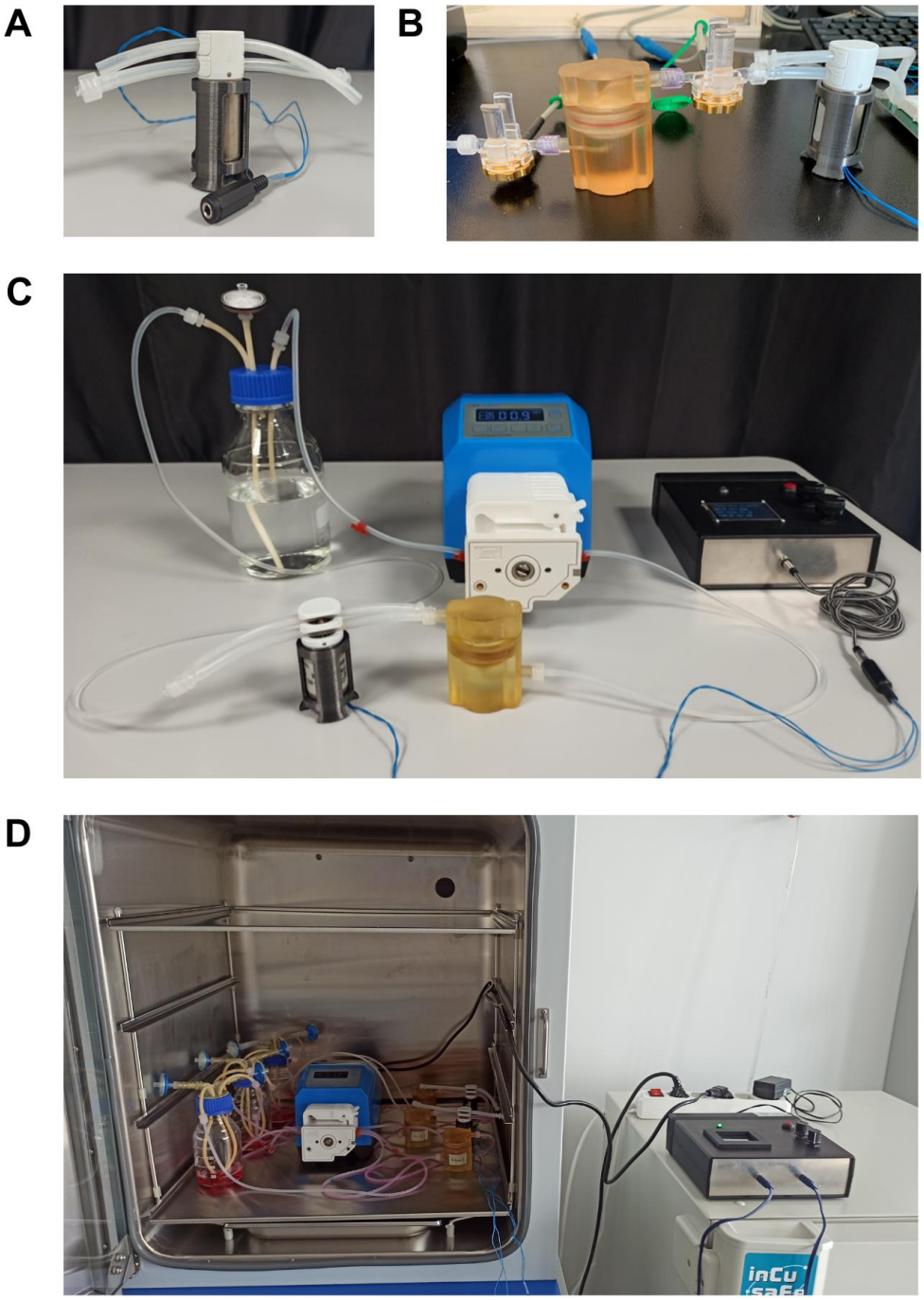

Figure 4.1. The upgraded bioreactor-based investigation platform. **(A)** The solenoid-actuated pinch valve (Cole Parmer GmbH). **(B)** The pressure sensors (HJK Sensoren). **(C)** The solenoid-actuated pinch valve placed downstream the culture chamber of the bioreactor. **(D)** The upgraded automated perfusion bioreactor set-up with two active solenoid-actuated pinch valves within the incubator.

4.3.2 PLA600 trabecular bone-like tissue culturing within the perfusion bioreactor equipped with pinch valves

4.3.2.1 Cell culture conditions

Human telomerase reverse transcriptase (hTERT)-immortalized BM-MSCs of clonal line Y201, which was generated by James et al. [13], were cultivated in basal medium that is low-glucose Dulbecco's modified Eagle's medium (DMEM, gibco, Thermo Fisher Scientific, Inc.) supplemented with 15% fetal bovine serum (FBS, gibco Thermo Fisher Scientific, Inc.) and 1% antibiotics (penicillin/streptomycin, gibco Thermo Fisher Scientific, Inc.) and incubated in a humidified atmosphere with 5% CO_2 at 37°C. The cells were passaged once they reached 80-90% confluency by enzymatic digestion using trypsin/ethylenediamine tetraacetic acid (trypsin/EDTA, gibco Thermo Fisher Scientific, Inc.) before each assay.

4.3.2.2 Cell seeding on PLA600 and culturing under three conditions

PLA600 scaffolds were inserted into PDMS holders placed in a 6-well cell culture plate. To reduce the hydrophobicity of the scaffolds prior to cell seeding, they were washed with PBS (1X). Subsequently, two drops of 5 mg/mL PureCol EZ Gel solution (Merck, Italy) were added to the scaffolds to remove residual PBS from the pores. The scaffolds were then incubated at 37°C to allow the polymerization of collagen, thereby minimizing cell loss. Cells were seeded directly onto the PLA600 scaffolds at a defined cell density of approximately $3x10^6$ cells and a defined volume of 200 µL, as described in Section 2.3.3 of the thesis. The samples were incubated for 4 h to facilitate cell infiltration and adhesion, then covered with BM and incubated overnight. After the overnight incubation, the samples were cultured for 7 days under three different culture conditions: static culture, in which the samples were kept in the cell culture plate and the medium was changed every 3-4 days; direct perfusion, in which samples were placed in the automated bioreactor and perfused unidirectionally at a flow rate of 0.3 mL/min with 50 mL of medium; and direct perfusion with hydrostatic pressure, in which the samples were cultured as in condition 2, but with additional intermittent hydrostatic pressure of around 5 kPa (period = 10 s, duty cycle = 50%) to simulate physiological unloading. Samples were evaluated in triplicates (n = 3). The samples were labeled as follows: "S" represents static culture, "D" represents direct, unidirectional perfusion, and "DHP" represents direct, unidirectional perfusion with hydrostatic pressure simulating physiological unloading.

4.3.2.3 Cell metabolic activity assay

The resazurin reduction assay was performed to assess cell metabolic activity of BM-MSCs. Resazurin sodium salt (powder, Merck, Darmstadt, Germany) was used to prepare 1% resazurin solution in 1X PBS, which was diluted in basal medium to a final concentration of 0.015% (v/v) to prepare the working solution prior to easy assay. On day 7 of culture, the scaffolds were removed from the CCs of the bioreactor and placed in a 12-well cell culture plate. 3 mL of resazurin working solution were added to each scaffold. Following a 3-h incubation period, 100 µL aliquots were used for fluorescence quantification at excitation and emission wavelengths of 530 and 590 nm, respectively, using a microplate reader (Tecan

GENios Microplate Reader, Spark, Tecan Trading AG, Männedorf, Switzerland). The results were averaged over three biological replicates (n = 3).

4.3.2.4 Cell viability assay

On day 7 of culture, the viability of BM-MSCs seeded on the biomimetic PLA600 scaffolds was evaluated via the live/dead cell assay (LIVE/DEAD™ Viability/Cytotoxicity Kit for mammalian cells, Invitrogen Life Technologies). Briefly, the scaffolds were removed from the CCs of the bioreactor, placed in a 24-well cell culture plate, washed with PBS (1X), and then incubated in a basal medium containing 2 µM calcein-AM and 2 µM ethidium homodimer-1 (EthD-1). After 15 min of incubation at 37°C and 5% CO_2 atmosphere, cells were imaged using a fluorescence microscope (THUNDER Imager 3D Cell Culture, Leica Microsystems) to visualize the green calcein AM that stains live cells and the red EthD-1 that stains dead cells.

4.3.2.5 Cell infiltration and distribution assessment

On day 7 of culture, the infiltration and distribution of BM-MSCs were examined using a scanning electron microscope (SEM) (JSM-IT500, JEOL, Italy). For SEM analysis, the scaffolds were removed from the CCs of the bioreactor, placed in a 24-well cell culture plate, and gently washed with PBS (1X). Then, cells were fixed with 2.5% glutaraldehyde at 4°C overnight, and after cell fixation, the 2.5% glutaraldehyde was dispensed, and samples were washed with PBS (1X), dehydrated in graded alcohol of 30%, 50%, 70%, 90%, and 100% (twice) for 30 min each, covered by hexamethyldisilazane (HMDS) for 30 min, and then air-dried in a chemical fume hood. Finally, samples were coated with gold using a sputter coating machine (DII-29030SCTR Smart Coater, JEOL, Italy).

4.4.3. Statistical analysis

All experiments were performed with three biological replicates. Data are presented as means ± standard deviation (SD). Statistical comparisons were performed using a one-way analysis of variance (ANOVA), followed by the Tukey post-hoc test. Statistical significance was defined as a p-value < 0.05. The analysis was conducted using R (R Core Team, 2020) [14], RStudio (Rstudio Team, 2020) [15], and the tidyverse package [16].

4.4 Results

4.4.1 Hydrostatic pressure characterization using collagen-loaded PLA600 scaffolds

As shown in **Figure 4.2**, adjustments to the solenoid-actuated pinch valve's settings, specifically period (s) and duty cycle (%), while maintaining a constant fluid flow rate of 0.3 mL/min, allow for the attainment of hydrostatic pressure values within the collagen-loaded PLA600 scaffold that fall within the physiological unloading and loading ranges. Several studies estimated the hydrostatic pressure values during physiological unloading and loading. These studies indicate that at rest, pressure values range between 30 and 60 mmHg (4-8 kPa), while physiological loading results in values greater than or equal to 80 mmHg (10 kPa) [17]. Therefore, the following settings were selected to evaluate cell viability within the upgraded automated perfusion bioreactor: 0.3 mL/min with a 10-second period and 50% duty cycle to simulate physiological unloading, achieving a pressure value of 5 kPa (approximately 37.5 mmHg) **(Figure 4.2)**.

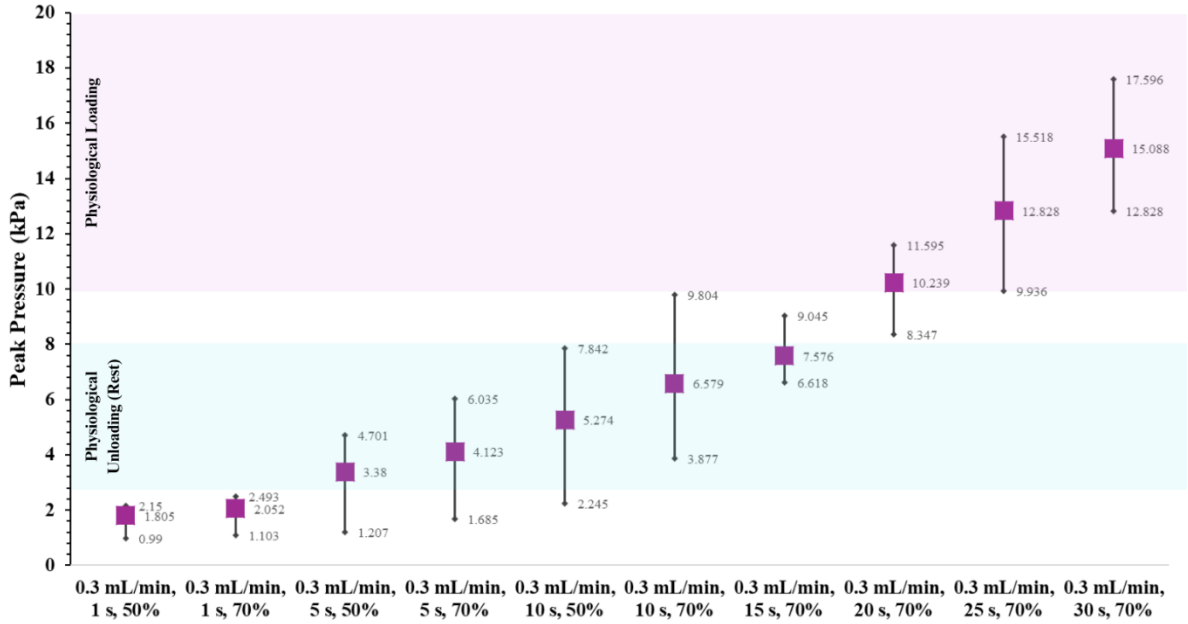

Figure 4.2. Peak pressure values (kPa) measured using pressure sensors (HJK Sensoren) for a solenoid-actuated pinch valve (Cole Parmer GmbH). The x-axis shows the settings of the upgraded automated perfusion bioreactor: flow rate (mL/min) for perfusion, in addition to period (s) and duty cycle (%) of the pinch valve. PLA600 scaffolds loaded with 200 µL PureCol EZ Gel solution (Merck) were used for characterization.

4.4.2 Cell viability and infiltration within the PLA600 scaffolds under three culture conditions

BM-MSCs seeded within PLA600 scaffolds using 0.5% cell-releasing collagen were cultured for 7 days under three different conditions: static “S”, perfusion only (fluid flow-induced shear stress) “D”, and perfusion with pinch valves added (fluid flow-induced shear stress and hydrostatic pressure simulating physiological rest) “DHP”. Resazurin reduction assay demonstrated that cell metabolic activity in the presence of hydrostatic pressure was comparable to that without hydrostatic pressure. Moreover, the metabolic activity was statistically significantly higher for cells cultured under fluid flow-induced shear stress in comparison to those cultured under static conditions ("D" vs. "S", p-value = 0.027). However, this was not the case for cells cultured under fluid flow-induced shear stress with hydrostatic pressure simulating physiological rest in comparison to those cultured under static conditions ("DHP" vs. "S", p-value = 0.054) **(Figure 4.3A)**. These results were further confirmed by live/dead assay **(Figure 4.3B)**. Additionally, SEM analysis revealed that the addition of hydrostatic pressure did not alter cell infiltration and distribution within the scaffolds **(Figure 4.4)**.

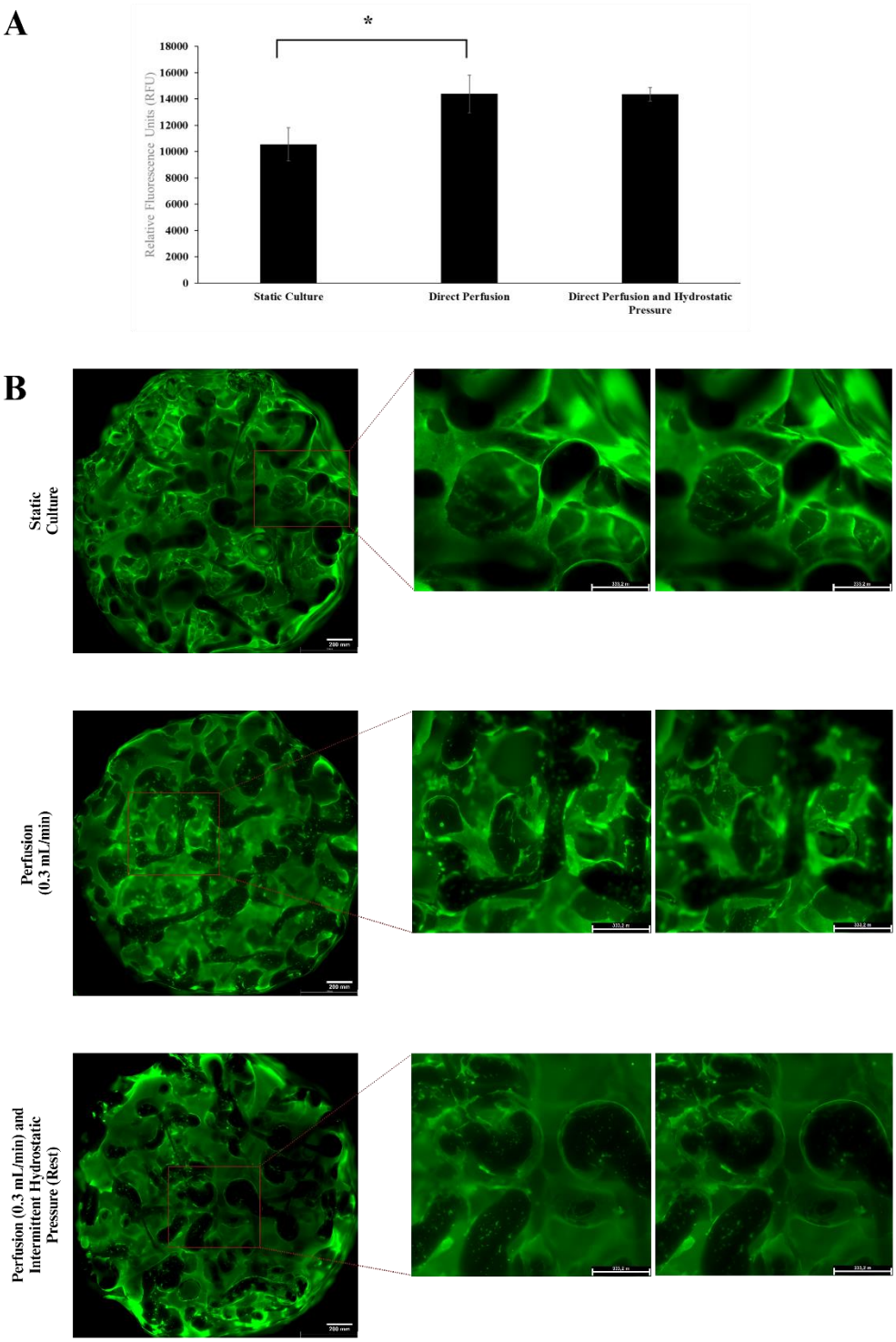

Figure 4.3. Viability of bone marrow-derived mesenchymal stem cells (BM-MSCs) within the PLA600 scaffolds under static, direct perfusion, and direct perfusion with hydrostatic pressure culture conditions for 7 days; (*$p < 0.05$). **(A)** Metabolic activity of BM-MSCs cultured within PLA600 scaffolds using Resazurin reduction assay. **(B)** Live/dead assay of BM-MSCs cultured within PLA600 scaffolds.

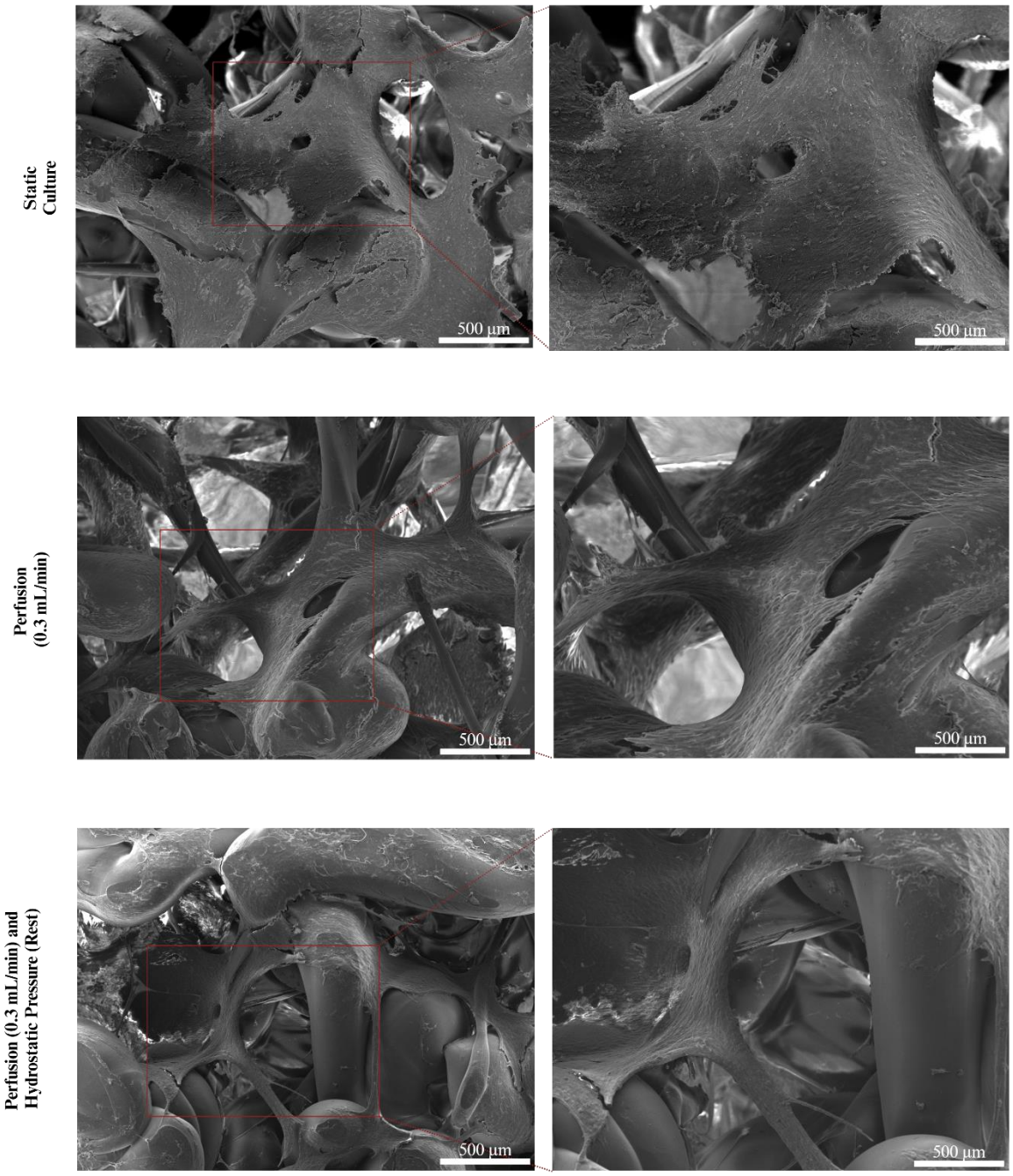

Figure 4.4. Infiltration of bone marrow-derived mesenchymal stem cells (BM-MSCs) within the PLA600 scaffolds under static, direct perfusion, and direct perfusion with intermittent hydrostatic pressure culture conditions for 7 days using scanning electron microscopy (SEM) analysis.

4.5 Discussion

The development of advanced technologies based on in vitro platforms that accurately simulate bone tissue's complex mechanical microenvironment is crucial for advancing bone tissue engineering research [18]. The current study presents a novel approach that incorporates both fluid flow-induced shear stress and hydrostatic pressure to mimic physiological conditions (i.e. physiological unloading and loading). The results demonstrated that the addition of hydrostatic pressure to the automated perfusion bioreactor did not adversely affect cell viability or infiltration within the scaffold. This suggests that the platform can provide a suitable environment for studying stem cell behavior under various mechanical stimuli.

There are currently four commonly used dynamic bioreactors used in bone tissue engineering, which are the rotating wall vessel bioreactor, spinner flask bioreactor, compression bioreactor, and perfusion bioreactor [19]. Currently, perfusion bioreactors are the most popular dynamic bioreactor [20]. However, the *in vivo* mechanical milieu of bone tissue is considerably more intricate, encompassing an array of stimuli. To faithfully recapitulate this complexity *in vitro*, a combinatorial approach is necessary, integrating multiple mechanical cues. Consequently, researchers have endeavored to develop bioreactors capable of synergistically delivering fluid flow-induced shear stress, induced by perfusion, with additional stimuli, such as compression and hydrostatic pressures.

In a state-of-the-art perfusion bioreactor, Rindt et al. (2024) combined perfusion (1.7 mL/min) with cyclic compressive loading (5 % strain and 1 Hz for 1 h) to evaluate the viability and differentiation of osteocytes cultured within various 3D microporous scaffolds. Their findings confirmed that they were to develop a 3D model to study bone cell behavior under realistic mechanical conditions [21]. Similar efforts were also reported by Lovecchio et al. (2019) [22] and Hoffmann et al. (2015) [23], among others. Yet, combining two mechanical stimuli is not enough. Sandino & Lacroix (2010) demonstrated the crucial role of recapitulating the dynamics of mechanical stimuli transmitted to cells during tissue differentiation. By combining computational models with 3D cell cultures exposed to compressive load and perfusion flow, they were able to capture the discontinuous nature of mechanical stimuli experienced by cells seeded within a scaffold over time [24].

Hydrostatic pressure has also been implemented in bioreactors systems, alone or in combination with other stimuli. Zvicer & Obradovic (2018) discussed the importance of biomimetic bioreactors for simulating hydrostatic pressure values similar to those found in human intervertebral discs [25]. Researchers have also combined hydrostatic pressure with other stimuli to promote tissue regeneration *de novo* [26]. Nazemour et al. (2017), have applied a biomimetic bioreactor based on perfusion and oscillating hydrostatic pressure to examine the effects of these stimuli on chondrogenesis [27]. Aw Yong et al. (2022) were able to culture osteocytes in a 3D environment mimicking bone tissue, while applying perfusion and adjustable hydrostatic pressure. They were able to show that the developed bioreactor

accurately simulates the mechanical response of osteocytes and provides a valuable tool for investigating the role of osteocytes in both healthy bone and cancer-related bone disease [28].

However, it is important to note that this study focused on simulating physiological rest conditions. Future studies should investigate the effects of dynamic mechanical loading on stem cell behavior within this platform. By incorporating various loading regimes, we can gain a deeper understanding of the mechanisms underlying bone formation and remodeling.

4.6 Conclusions

In conclusion, this study presents a promising *in vitro* platform for investigating bone biology under physiologically relevant conditions. The platform successfully simulates both fluid flow-induced shear stress and hydrostatic pressure, providing a more accurate representation of the *in vivo* microenvironment. Future research will focus on expanding the platform's capabilities to simulate dynamic mechanical loading, enabling the study of bone tissue response to various physiological and pathological stimuli. This advanced platform has the potential to accelerate the development of innovative therapies for bone regeneration and repair.

4.7. Fundings

This study was carried out within the BIGMECH project – funded by the European Union – Next Generation EU within the PRIN 2022 program (D.D. 104 - 02/02/2022 Ministero dell'Università e della Ricerca). This manuscript reflects only the authors' views and opinions and the Ministry cannot be considered responsible for them.

4.8 Acknowledgments

I would like to thank Dr. Eleonora Zenobi and Dr. Elisa Scateno for kindly providing the 3D-printed PLA scaffolds, as well as Prof. Diana Massai, Dr. Stefano Gabetti, and Dr. Beatrice Masante for kindly providing the upgraded perfusion bioreactor. I would also like to thank Prof. Lia Rimondini and Prof. Andrea Cochis for their supervision.

4.9 References

1. Smith, E.L., and Gilligan, C. (1991) Physical activity effects on bone metabolism. *Calcif Tissue Int*, **49** (1 Supplement), S50–S54.

2. Andreoli, A., Monteleone, M., Van Loan, M., Promenzio, L., Tarantino, U., and De Lorenzo, A. (2001) Effects of different sports on bone density and muscle mass in highly trained athletes. *Med Sci Sports Exerc*, **33** (4), 507–511.
3. Lang, T., LeBlanc, A., Evans, H., Lu, Y., Genant, H., and Yu, A. (2004) Cortical and Trabecular Bone Mineral Loss From the Spine and Hip in Long-Duration Spaceflight. *Journal of Bone and Mineral Research*, **19** (6), 1006–1012.
4. Sailhan, F. (2011) Bone lengthening (distraction osteogenesis): A literature review. *Osteoporosis International*, **22** (6), 2011–2015.
5. Mavčič, B., and Antolič, V. (2012) Optimal mechanical environment of the healing bone fracture/osteotomy. *Int Orthop*, **36** (4), 689–695.
6. Çehreli, M., Şahin, S., and Akça, K. (2004) Role of mechanical environment and implant design on bone tissue differentiation: current knowledge and future contexts. *J Dent*, **32** (2), 123–132.
7. Ren, L., Yang, P., Wang, Z., Zhang, J., Ding, C., and Shang, P. (2015) Biomechanical and biophysical environment of bone from the macroscopic to the pericellular and molecular level. *J Mech Behav Biomed Mater*, **50**, 104–122.
8. Bai, Y., Li, X., Wu, K., Heng, B.C., Zhang, X., and Deng, X. (2024) Biophysical stimuli for promoting bone repair and regeneration. *Medical Review*.
9. Kwon, R.Y., Meays, D.R., Meilan, A.S., Jones, J., Miramontes, R., Kardos, N., Yeh, J.C., and Frangos, J.A. (2012) Skeletal Adaptation to Intramedullary Pressure-Induced Interstitial Fluid Flow Is Enhanced in Mice Subjected to Targeted Osteocyte Ablation. *PLoS One*, **7** (3), e33336.
10. Wei, F., Flowerdew, K., Kinzel, M., Perotti, L.E., Asiatico, J., Omer, M., Hovell, C., Reumers, V., and Coathup, M.J. (2022) Changes in interstitial fluid flow, mass transport and the bone cell response in microgravity and normogravity. *Bone Research 2022 10:1*, **10** (1), 1–19.
11. Weinbaum, S., Cowin, S.C., and Zeng, Y. (1994) A model for the excitation of osteocytes by mechanical loading-induced bone fluid shear stresses. *J Biomech*, **27** (3), 339–360.
12. Zhang, D., Weinbaum, S., and Cowin, S.C. (1998) On the calculation of bone pore water pressure due to mechanical loading. *Int J Solids Struct*, **35** (34–35), 4981–4997.
13. James, S., Fox, J., Afsari, F., Lee, J., Clough, S., Knight, C., Ashmore, J., Ashton, P., Preham, O., Hoogduijn, M., Ponzoni, R.D.A.R., Hancock, Y., Coles, M., and Genever, P. (2015) Multiparameter Analysis of Human Bone Marrow Stromal Cells Identifies Distinct Immunomodulatory and Differentiation-Competent Subtypes. *Stem Cell Reports*, **4** (6), 1004–1015.
14. R: The R Project for Statistical Computing.
15. Posit | The Open-Source Data Science Company.
16. Wickham, H., Averick, M., Bryan, J., Chang, W., McGowan, L.D., François, R., Grolemund, G., Hayes, A., Henry, L., Hester, J., Kuhn, M., Pedersen, T.L., Miller, E., Bache, S.M., Müller, K., Ooms, J., Robinson, D., Seidel, D.P., Spinu, V., Takahashi, K., Vaughan, D., Wilke, C., Woo, K., and Yutani, H. (2019) Welcome to the Tidyverse. *J Open Source Softw*, **4** (43), 1686.
17. Gurkan, U.A., and Akkus, O. (2008) The mechanical environment of bone marrow: A review. *Ann Biomed Eng*, **36** (12), 1978–1991.

18. Hung, B.P., Hutton, D.L., and Grayson, W.L. (2013) Mechanical control of tissue-engineered bone. *Stem Cell Res Ther*, **4** (1), 1–7.
19. Vetsch, J.R., Müller, R., and Hofmann, S. (2015) The evolution of simulation techniques for dynamic bone tissue engineering in bioreactors. *J Tissue Eng Regen Med*, **9** (8), 903–917.
20. Gaspar, D.A., Gomide, V., and Monteiro, F.J. (2012) The role of perfusion bioreactors in bone tissue engineering. *Biomatter*, **2** (4), 167.
21. Rindt, W.D., Krug, M., Yamada, S., Sennefelder, F., Belz, L., Cheng, W.H., Azeem, M., Kuric, M., Evers, M., Leich, E., Hartmann, T.N., Pereira, A.R., Hermann, M., Hansmann, J., Mussoni, C., Stahlhut, P., Ahmad, T., Yassin, M.A., Mustafa, K., Ebert, R., and Jundt, F. (2024) A 3D bioreactor model to study osteocyte differentiation and mechanobiology under perfusion and compressive mechanical loading. *Acta Biomater*, **184**, 210–225.
22. Lovecchio, J., Gargiulo, P., Vargas Luna, J.L., Giordano, E., and Sigurjónsson, Ó.E. (2019) A standalone bioreactor system to deliver compressive load under perfusion flow to hBMSC-seeded 3D chitosan-graphene templates. *Scientific Reports 2019 9:1*, **9** (1), 1–11.
23. Hoffmann, W., Feliciano, S., Martin, I., de Wild, M., and Wendt, D. (2015) Novel Perfused Compression Bioreactor System as an in vitro Model to Investigate Fracture Healing. *Front Bioeng Biotechnol*, **3**, 10.
24. Sandino, C., and Lacroix, D. (2011) A dynamical study of the mechanical stimuli and tissue differentiation within a CaP scaffold based on micro-CT finite element models. *Biomech Model Mechanobiol*, **10** (4), 565–576.
25. Zvicer, J., and Obradovic, B. (2018) Bioreactors with hydrostatic pressures imitating physiological environments in intervertebral discs. *J Tissue Eng Regen Med*, **12** (2), 529–545.
26. Watanabe, S., Inagaki, S., Kinouchi, I., Takai, H., Masuda, Y., and Mizuno, S. (2005) Hydrostatic pressure/perfusion culture system designed and validated for engineering tissue. *J Biosci Bioeng*, **100** (1), 105–111.
27. Nazempour, A., Quisenberry, C.R., Abu-Lail, N.I., and Van Wie, B.J. (2017) Combined effects of oscillating hydrostatic pressure, perfusion and encapsulation in a novel bioreactor for enhancing extracellular matrix synthesis by bovine chondrocytes. *Cell Tissue Res*, **370** (1), 179–193.
28. Aw Yong, K.M., Horst, E., Neale, D., Royzenblat, S., Lahann, J., Greineder, C., Weivoda, M., Mehta, G., and Keller, E.T. (2022) A Bioreactor for 3D In Vitro Modeling of the Mechanical Stimulation of Osteocytes. *Front Bioeng Biotechnol*, **10**, 797542.

Chapter 5

Synergistic Effects of Various Mechanical Cues on Mesenchymal Stem Cell Behavior in Engineered 3D Microenvironments

5.1 Abstract

Bone is a dynamic tissue with physical and mechanical properties specific to each location. These properties can also vary within the same anatomical site and among individuals. As bone cells are sensitive to changes in their environment, such alterations influence cellular behavior. Here, we aimed to investigate cellular behavior within our advanced bioreactor-based system using trabecular bone tissue-like constructs mimicking the morphological features of bones, specifically the ulna, tibia, and femur. For this purpose, human bone marrow-derived mesenchymal stem cells (BM-MSCs) were seeded onto the novel 3D-printed polylactic acid (PLA), referred to as P3S3, using cell-releasing collagen (as described in Chapter 2), and cultured under two different condition: static culture and within the perfusion bioreactor providing fluid flow-induced shear stress (as described in Chapter 1) to evaluate cell viability. After confirming the cell viability within the P3S3 scaffolds and the bioreactor system, cell-seeded scaffolds were cultured within the upgraded perfusion bioreactor providing fluid flow-induced shear stress, either alone or with hydrostatic pressure, mimicking a 2-hour daily physiological loading, similar to an in-patient rehabilitation program, for 14 days. Cell viability and gene expression analyses were conducted. Our findings indicated that the viability of BM-MSCs within the 3D-printed scaffolds remained unaffected by the various dynamic culture conditions. While the simulated physiological loading program did not significantly impact gene expression related to mechanotransduction and osteogenesis, future studies will explore the effects of longer culture durations and higher pressure magnitudes to optimize the rehabilitation protocol.

5.2 Introduction

Trabecular bone is a mechanosensitive and metabolically active tissue. As such, its microarchitecture and composition vary between anatomical locations and with age [1]. The microarchitecture of trabecular bone can be described by several indices, such as bone volume/total volume (BV/TV), trabecular thickness (Tb.Th), trabecular separation (Tb.Sp), and trabecular number (Tb.N) values obtained commonly via microcomputed tomography (μCT) [2]. The composition of trabecular bone, measured mainly via Fourier transform

infrared (FTIR) microspectroscopy, provides data on mineral-to-matrix ratio, mineral maturity/crystallinity, and collagen maturity/crosslinks [3]. Both bone microarchitecture and composition, in addition to whole bone geometry, are determinants of bone strength and fragility [4]. Although the mechanical strength of bone stems from the interplay of a variety of factors, the effects of microarchitecture are most commonly studied. Studies have shown that microarchitecture plays a crucial role in bone fragility, independent of bone density [5].

Another important factor contributing to bone strength or fragility is mechanical stimulation. Thus, bone adapts its microarchitecture and composition in response to mechanical loading (e.g., weight-bearing exercise) [6] and its opposite, mechanical unloading (e.g., bed rest or spaceflight) [7]. This is called bone adaptation. According to Charles H. Turner (1998), it follows these three principles: (1) dynamic loading: Bone responds to movement and activity, not stillness; (2) quick response: Even brief periods of stress can trigger bone growth or repair; and (3) adaptation to routine: Bone adjusts to regular patterns of stress, becoming less sensitive to familiar loads [8].

During bone healing, the recruitment of circulating mesenchymal stem cells (MSCs) to the injury site is a natural biological process. While the mechanisms of MSC homing are not fully understood, studies have demonstrated that the biochemical and mechanical microenvironments synergistically induce and promote osteogenesis. The biochemical microenvironment, composed of cytokines and chemokines, and the mechanical microenvironment, characterized by mechanical cues, both play significant roles in this process [9]. The direct physical environment significantly influences MSC behavior, prompting the design of biomaterials for bone tissue engineering to incorporate physical, mechanical, and chemical factors whenever possible [10].

The optimal scaffold design must balance porosity and pore size to promote both cellular activity and vascularization, while also considering mechanical properties, to ultimately lead to successful bone regeneration. Future research should explore the use of gradient pore size scaffolds to develop intricate tissue structures that resemble the natural bone architecture [11]. Given the inherent heterogeneity in bone microarchitecture and composition at different anatomical locations and among different individuals, tailoring the bone material to specific repair needs is a key factor. Studies have shown that the minimum pore size should be 100 μm to allow for cellular activity and nutrient transport, but ideally over 300 μm to enhance bone formation and vascularization [10]. Physical factors include porosity, pore size, surface roughness, surface topography, surface free energy, wettability, crystallographic texture, and patterned surfaces [10].

Since the response of MSCs to mechanical stimuli within the bone tissue environment plays a crucial role in bone health and healing it is essential to consider it. Mechanical stimuli encompass the mechanical properties of the extracellular matrix and mechanical stimuli intrinsic to bone tissue include fluid flow-induced shear stress, hydrostatic pressure, compression, and tension [10]. The impacts of mechanical loading on fracture healing and bone regeneration have been reported by several *in vitro* studies examining various types of

mechanical loading (compressive pressure, tensile strain, and fluid shear stress) and *in vivo* ones examining various types of movement (interfragmentary, tensile, or shear). However, findings from *in vitro* models have not been fully validated in *in vivo* models, due to the significant differences among these models. Thus, identifying mechanical stimuli-responsive molecular targets and developing clinical therapies targeting these molecules requires future research to bridge this gap by standardizing mechanical parameters [12].

Consequently, understanding the architecture, composition, and mechanical environment of bone tissue at specific anatomical locations is essential for designing advanced *in vitro* technologies targeted for bone tissue. As such, bioreactors that can accurately mimic the *in vivo* bone environment and optimize MSC-mediated bone tissue regeneration are considered a great tool, especially when they can host 3D bone tissue-like constructs. While existing *in vitro* investigation platforms cannot satisfy all the requirements to fully replicate the native bone tissue environment, significant progress has been made in the design and application of bioreactors for enhancing artificial bone tissue grafts [13,14] and advancing bone biology research [15–17].

In line with the movement towards more representative 3D bone tissue-like constructs and bioreactors that better mimic the mechanical environment of bone tissue, the primary objective of our study was to test the performance of the prior and upgraded versions of the *in vitro* bioreactor-based investigation platform using new scaffolds, referred to as P3S3. These scaffolds are 3D-printed polylactic acid (PLA) scaffolds designed to mimic the human trabecular bone architecture in physiological conditions and to resemble the morphological features of bones, specifically the ulna [18], tibia, and femur [19]. Bone marrow-derived mesenchymal stem cells (BMSCs) were seeded onto the P3S3 scaffolds and cultured under various bone-tissue-like mechanical stimulations. In the first experimental condition, cells were cultured statically or exposed to fluid flow-induced shear stress. Cell viability was assessed under these conditions on day 21. In the second condition, cells were exposed to fluid flow-induced shear stress in the absence and presence of hydrostatic pressure simulating physiological loading (15 kPa) for 2 hours per day for 14 days, mimicking an in-patient rehabilitation program. Cell viability was assessed, and gene expression analysis was performed to evaluate the effects of hydrostatic pressure on osteogenic differentiation and mechanotransduction.

5.3 Materials and Methods

5.3.1 3D printing and characterization of the trabecular bone-like polylactic acid (PLA) scaffolds resembling the morphological features of bones, specifically the ulna, tibia, and femur (referred to as P3S3)

The design and fabrication of the 3D-printed, biomimetic P3S3 scaffolds have been carried out according to a previously reported procedure [20]. Briefly, a random 3D distribution of spheres, as virtual porogens with a diameter of 300 µm, was created by means of a custom-made script to be subtracted from a cylindrical volume (10 mm diameter, 5 mm height) to prepare the scaffold computer-aided design (CAD) models. The resulting files were imported to ideaMaker (Raise3D Inc., Irvine, CA, USA) and sliced in the Z direction at 0.25 mm. Scaffolds were then fabricated by processing a PLA filament (FormFutura BV, The Netherlands) using a Raise 3D N2 printer (Raise 3D Inc., Irvine, CA, USA), setting the nozzle temperature at 205 °C and the build plate temperature at 60 °C. The resulting scaffolds had a trabecular spacing of 284 µm, a trabecular thickness of 258 µm, and a total porosity of 44.7%. The scaffolds were submerged in phosphate-buffered saline (PBS, 1X) and agitated on an orbital shaker for 2 h to remove polymeric residues. Subsequently, they were sterilized by immersion in 70% ethanol for 4 h, followed by air drying.

5.3.2 Parallelized, automated perfusion bioreactor equipped with pinch valves

The upgraded automated perfusion bioreactor described in Section 4.3.1 of the thesis was used for the following experiments. Non-invasive pressure sensors (HJK Sensoren) were used to measure pressure in P3S3 scaffolds loaded with collagen.

5.3.3 P3S3 trabecular bone-like tissue preparation and evaluation within the perfusion bioreactor

5.3.3.1 Cell culture conditions

Human telomerase reverse transcriptase (hTERT)-immortalized BM-MSCs of clonal line Y201, which was generated by James et al. [21], were cultivated in basal medium that is low-glucose Dulbecco's modified Eagle's medium (DMEM, gibco, Thermo Fisher Scientific, Inc.) supplemented with 15% fetal bovine serum (FBS, gibco Thermo Fisher Scientific, Inc.) and 1% antibiotics (penicillin/streptomycin, gibco Thermo Fisher Scientific, Inc.) and incubated in a humidified atmosphere with 5% CO_2 at 37°C. The cells were passaged once they reached 80-90% confluency by enzymatic digestion using trypsin/ethylenediamine tetraacetic acid (trypsin/EDTA, gibco Thermo Fisher Scientific, Inc.) before each assay.

5.3.3.2 Cell seeding on P3S3 and culturing under two conditions

P3S3 scaffolds were inserted into PDMS holders placed in a 6-well cell culture plate. To reduce the hydrophobicity of the scaffolds prior to cell seeding, they were washed with PBS (1X). Subsequently, two drops of 5 mg/mL PureCol EZ Gel solution (Merck, Italy) were added to the scaffolds to remove residual PBS from the pores. The scaffolds were then incubated at 37°C to allow the polymerization of collagen, thereby minimizing cell loss. Cells were seeded directly onto the P3S3 scaffolds at a defined cell density of approximately $2x10^6$ cells and a total volume of 150 µL, composed of 40 µL of basal medium and 110 µL of 5 mg/mL PureCol EZ Gel solution (Merck, Italy). The samples were incubated for 4 h to facilitate cell infiltration and adhesion, then covered with basal medium and incubated overnight. After the overnight incubation, the samples were cultured in two different culture conditions for 21 days: static culture, in which the samples were kept in the cell culture plate and the medium was changed every 3-4 days; and direct perfusion, in which samples were placed in the automated bioreactor and perfused unidirectionally at a flow rate of 0.3 mL/min with 50 mL of medium, and the medium was changed every 7 days. Samples were evaluated in triplicates (n = 3).

5.3.3.3 Cell metabolic activity assay

The resazurin reduction assay was performed to assess cell metabolic activity of BM-MSCs. Resazurin sodium salt (powder, Merck, Darmstadt, Germany) was used to prepare 1% resazurin solution in 1X PBS, which was diluted in basal medium to a final concentration of 0.015% (v/v) to prepare the working solution prior to easy assay. On day 21 of culture, the scaffolds were removed from the CCs of the bioreactor and placed in a 12-well cell culture plate. 3 mL of resazurin working solution were added to each scaffold. Following a 3-h incubation period, 100 µL aliquots were used for fluorescence quantification at excitation and emission wavelengths of 530 and 590 nm, respectively, using a microplate reader (Tecan GENios Microplate Reader, Spark, Tecan Trading AG, Männedorf, Switzerland). The results were averaged over three biological replicates (n = 3).

5.3.3.4 Cell viability assay

On day 21 of culture, the viability of BM-MSCs seeded on the biomimetic PLA600 scaffolds was evaluated via the live/dead cell assay (LIVE/DEAD™ Viability/Cytotoxicity Kit for mammalian cells, Invitrogen Life Technologies). Briefly, the scaffolds were removed from the CCs of the bioreactor, placed in a 24-well cell culture plate, washed with PBS (1X), and then incubated in basal medium containing 2 µM calcein-AM and 2 µM ethidium homodimer-1 (EthD-1). After 15 min of incubation at 37°C and 5% CO_2 atmosphere, cells were imaged using a fluorescence microscope (THUNDER Imager 3D Cell Culture, Leica Microsystems) to visualize the green calcein AM that stains live cells and the red EthD-1 that stains dead cells.

5.3.3.4 Cell infiltration and distribution assessment

On day 21 of culture, the infiltration and distribution of BM-MSCs were examined using a scanning electron microscope (SEM) (JSM-IT500, JEOL, Italy). For SEM analysis, the

scaffolds were removed from the CCs of the bioreactor, placed in a 24-well cell culture plate, and gently washed with PBS (1X). Then, cells were fixed with 2.5% glutaraldehyde at 4°C overnight, and after cell fixation, the 2.5% glutaraldehyde was dispensed, and samples were washed with PBS (1X), dehydrated in graded alcohol of 70%, 90%, and 100% (twice) for 30 min each, covered by hexamethyldisilazane (HMDS) for 30 min, and then air-dried in a chemical fume hood. Finally, samples were coated with gold using a sputter coating machine (DII-29030SCTR Smart Coater, JEOL, Italy).

5.3.4 P3S3 trabecular bone-like tissue culturing within the perfusion bioreactor equipped with pinch valves under a simulated rehabilitation program

5.3.4.1 Cell seeding on P3S3 and culturing under two conditions

Cells were seeded onto the P3S3 scaffolds as previously described in Section 5.3.3. The samples were cultured for 14 days under two different culture conditions: direct perfusion, in which samples were placed in the automated bioreactor and perfused unidirectionally at a flow rate of 0.3 mL/min with 50 mL of medium; and direct perfusion with hydrostatic pressure, in which the samples were cultured as in condition 2, but with additional hydrostatic pressure of around 15 kPa (period = 10 s, duty cycle = 70%) to simulate physiological loading. Samples were evaluated in triplicates (n = 3). The samples were labeled as follows: “D” represents direct, unidirectional perfusion, and “RP1” represents direct, unidirectional perfusion with hydrostatic pressure simulating a rehabilitation program.

5.3.4.2 Cell metabolic activity assay

The resazurin reduction assay was performed to assess cell metabolic activity of BM-MSCs. Resazurin sodium salt (powder, Merck, Darmstadt, Germany) was used to prepare 1% resazurin solution in 1X PBS, which was diluted in basal medium to a final concentration of 0.015% (v/v) to prepare the working solution prior to easy assay. On day 14 of culture, the scaffolds were removed from the CCs of the bioreactor and placed in a 12-well cell culture plate. 3 mL of resazurin working solution were added to each scaffold. Following a 3-h incubation period, 100 µL aliquots were used for fluorescence quantification at excitation and emission wavelengths of 530 and 590 nm, respectively, using a microplate reader (Tecan GENios Microplate Reader, Spark, Tecan Trading AG, Männedorf, Switzerland). The results were averaged over three biological replicates (n = 3).

5.3.4.3 Gene expression analyses

Gene expression analyses were performed as described in Section 2.3.4 of this thesis. Briefly, total RNA was extracted using TRIzol™ Reagent (Invitrogen Life Technologies), 1 µg of total RNA was treated to remove genomic DNA contamination and to be reverse transcribed using Verso cDNA Synthesis Kit (Thermo Fisher, Italy), and qPCR was performed using the SYBR™ Select Master Mix (Applied Biosystems, thermo Fisher, Italy). The cycle threshold for each gene of interest was normalized against the reference gene that is tyrosine 3-

monooxygenase/tryptophan 5-monooxygenase (YWHAZ), and relative gene expression levels were determined using the Livak's method ($2^{-\Delta\Delta Cq}$) [22,23].

The evaluated genes include those involved in osteogenesis, which are Runt-related transcription factor 2 (RUNX2), alkaline phosphatase (ALP), osteopontin (OPN), osteocalcin (OCN), and matrix metalloproteinase 3 and 9 (MMP3 and MMP9); the cation channel piezo-type mechanosensitive ion channel component 1 (PIEZO1); the integrins alpha-v beta-3 (Integrin αVβ3) and alpha-5 beta1 (Integrin α5β1); the transcriptional coactivators yes-associated protein 1 (YAP1) and WW domain-containing transcription regulator protein 1 (WWTR1, also known as TAZ1); proteins of the ras homolog family member A (RhoA)/Rho-associated coiled-coil containing protein kinase (ROCK) signaling pathway, which are RhoA, ROCK1, and ROCK2; proteins of the transforming growth factor beta (TGFβ)/SMAD signaling pathway, which are TGFβ1, SMAD family member 2 (SMAD2), and SMAD family member 7 (SMAD7); the protein Janus Kinase 1 (JAK1) of the JAK/ Signal transducer and activator of transcription (STAT) signaling pathway that is also known as interleukin (IL)-6 signaling pathway; members of the Wingless-related integration site (WNT)/Catenin beta (β-catenin) signaling pathway, which are Wnt family member 5A (WNT5A) and catenin Beta 1 (CTNNB1); mitogen-activated protein kinase 1 (MAPK1) of extracellular signal-regulated kinases 1/2 (ERK1/2) signaling pathway; and finally, proteins involved in cell-cell connections, which are neurogenic locus notch homolog protein 3 (NOTCH3) and frizzled class receptor 8 (FZD8). The primer pairs of the analyzed genes are listed in **Table 5.1.**

Table 5.1. Description of the designed primers

Gene	**Forward Primer**	**Reverse Primer**
Runt-related transcription factor 2 (RUNX2)	5’- GAA TGC CTC TGC TGT TAT GA -3’	5’- GAA GAC GGT TAT GGT CAA GG -3’
Alkaline phosphatase (ALP)	5’- GAG TAT GAG AGT GAC GAG AAA G -3’	5’- GAA GTG GGA GTG CTT GTA TC -3’
Osteopontin (OPN)	5’- CCC ATC TCA GAA GCA GAA TC -3’	5’- TGG CTT TCG TTG GAC TTA C -3’
Osteocalcin (OCN)	5’- AGG CGC TAC CTG TAT CAA -3’	5’- CTC CTG AAA GCC GAT GTG -3’
Matrix metalloproteinase 3 (MMP3)		
Matrix metalloproteinase 9 (MMP9)		
Piezo-type mechanosensitive ion channel component 1 (PIEZO1)	5’- AAG GAG ATG ATG GAC AGA GA -3’	5’- CTG ACG TGC AGG TAG TAA TG -3’
Integrin alpha-v beta-3 (Integrin ITGAV)	5’- GCC AAG TTG GGA GAT TAG AC -3’	5’- GCA GAC GAC TTC AGA GAA TAG -3’
Integrin alpha-5 beta1 (ITGA5)	5’- GAA TCT CAA CAA CTC GCA AAG -3’	5’- CAG TCG CTT ACT GGG AAT AG -3’

Yes-associated protein 1 (YAP1)	5’- AGA ACC GTT TCC CAG ACT A -3’	5’- TCA GCT CCT CTC CTT CTA TG -3’
WW domain-containing transcription regulator protein 1 (TAZ1)	5’- AAA TCA CCA CAT GGC AAG A -3’	5’- GAG ATT TGG CTG GGA TAC TG -3’
Ras homolog family member A (RhoA)	5’- ACC TGA AGA AGG CAG AGA TA -3’	5’- CAG CTC TCG TAG CCA TTT C -3’
Rho-associated coiled-coil containing protein kinase 1 (ROCK1)	5’- GGC ATG GTA CGA TGT GAT AC -3’	5’- CCA CCA GTC ACA TTC TCT TC -3’
Rho-associated coiled-coil containing protein kinase 2 (ROCK2)	5’- CTG GTG GAG ACC TTG TAA AC -3’	5’- GGA GTG TAT TGC ATC CAG AG -3’
Transforming growth factor beta (TGFB)	5’- GAC AGC AGG GAT AAC ACA C -3’	5’- CCA TGA GAA GCA GGA AAG G -3’
SMAD family member 2 (SMAD2)	5’- GAA GAG GAG TGC GCT TAT AC -3’	5’- GCC AGC CAT ATC TCT GAT TAC -3’
SMAD family member 7 (SMAD7)	5’- CCA TCA AGG CTT TCG ACT AC -3’	5’- GCT GAT CTG CAC GGT AAA G -3’
Janus Kinase 1 (JAK1)	5’- TGG AAC CAA CGA CAA TGA G -3’	5’- GTC CCT GAG CAA ACA GAT AC -3’
Wingless-related integration site family member 5A (WNT5A)	5’- GGA CTT TCT CAA GGA CAG AAG -3’	5’- CCT TCG ATG TCG GAA TTG AT -3’
catenin Beta 1 (CTNNB1)	5’- AGG AAG AGG ATG TGG ATA CC -3’	5’- GAG CTC GAG TCA TTG CAT AC -3’
Mitogen-activated protein kinase 1 (MAPK1)	5’- GTA CAG GAC CTC ATG GAA AC -3’	5’- CTC TGA GGA TCT GGT AGA GAA -3’
Neurogenic locus notch homolog protein 3 (NOTCH3)	5’- GAG AGC TGC AGT CAG AAT ATC -3’	5’- GCA GGC ACA GTA GAA AGA A -3’
Frizzled class receptor 8 (FZD8)	5’- CTT CAC CGT CTT CTG GAT CG -3’	5’- GGC CGA GAG GAA GAT AAT GG -3’
Tyrosine 3-monooxygenase/tryptophan 5-monooxygenase (YWHAZ)	5’- GGA GGG TCG TCT CAA GTA T -3’	5’- ATC TCT TAG CTC CGT CTC AA -3’

5.3.4. Statistical analysis

All experiments were performed with three biological replicates. Data are presented as means ± standard deviation (SD). Continuous variables were compared using a two-tailed t-test. Statistical significance was defined as a p-value < 0.05. The analysis was conducted using R (R Core Team, 2020) [24], RStudio (Rstudio Team, 2020) [25], and the tidyverse package [26].

5.4 Results

5.4.1 Cell viability and infiltration within the P3S3 scaffolds under dynamic culture conditions

To create functional bone-like tissue, it is essential to efficiently seed cells onto 3D scaffolds. We used 0.5% cell-releasing collagen to seed BM-MSCs within the P3S3 scaffolds, as it demonstrated optimal results when used with PLA600 scaffolds (described in Chapters 2, 3, and 4 of the thesis). After 21 days of culture under specific conditions, we observed no significant differences in how BM-MSCs interacted with the P3S3 scaffolds, regardless of static or dynamic culture conditions. The applied cell seeding method maintained high cell viability, as confirmed by the resazurin reduction assay. Moreover, the metabolic activity of BM-MSCs within P3S3 cultured under perfusion was significantly higher than that of samples cultured under static culture (p-value = 0.021) **(Figure 5.1A)** and live/dead assay **(Figure 5.1B)**. Additionally, there were no significant variations in cell shape, penetration into the scaffold, and overall distribution, as evidenced by both live/dead staining and SEM images **(Figure 5.1B)**.

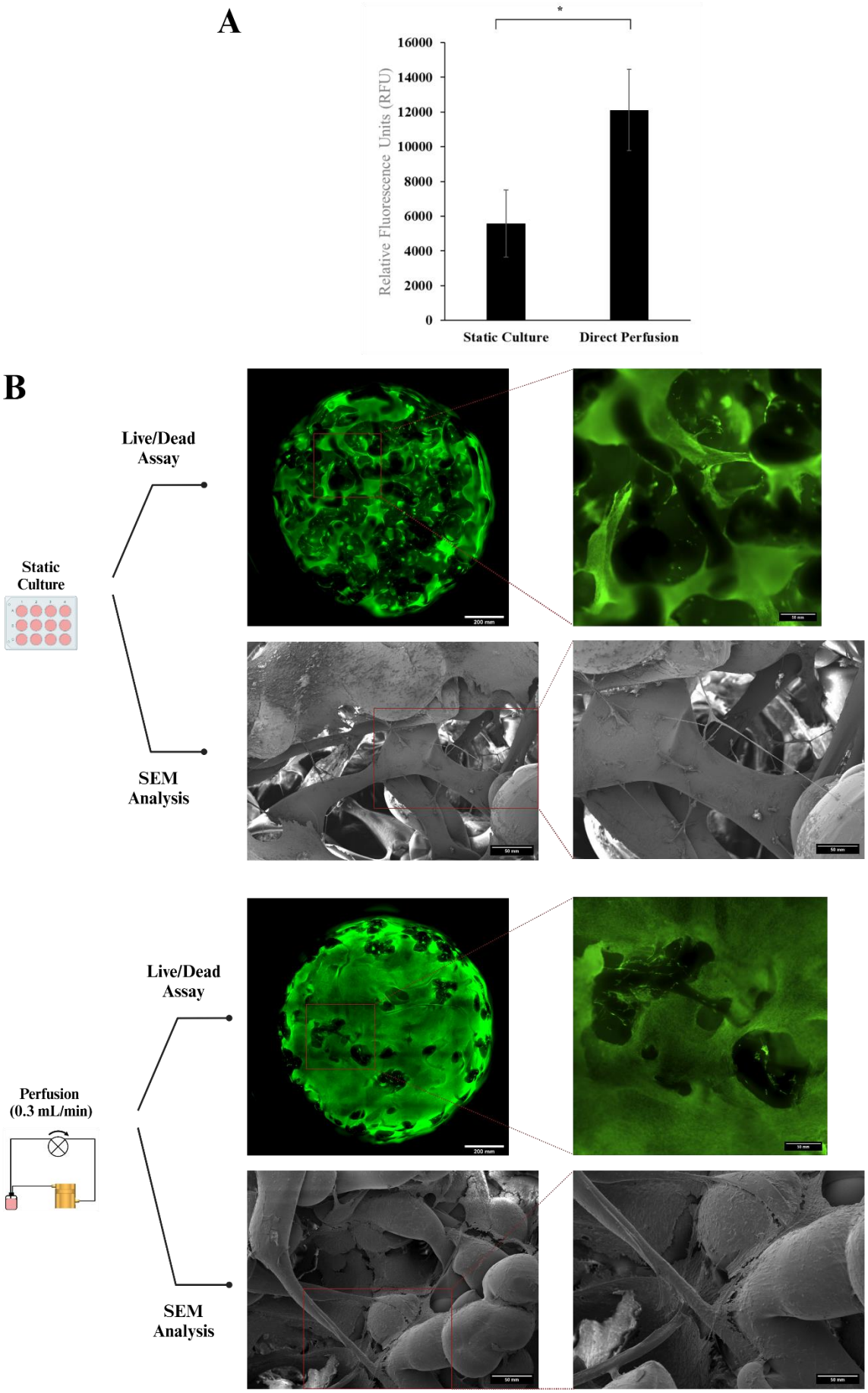
A
*
16000
14000
12000
10000
8000
6000
4000
2000
0
Relative Fluorescence Units (RFU)
Static Culture
Direct Perfusion
B
Live/Dead Assay
Static Culture
SEM Analysis
Live/Dead Assay
Perfusion (0.3 mL/min)
SEM Analysis

Figure 5.1. Viability and infiltration of bone marrow-derived mesenchymal stem cells (BM-MSCs) within the P3S3 scaffolds under static and direct perfusion culture conditions for 21 days. **(A)** Metabolic activity of BM-MSCs cultured within P3S3 scaffolds using resazurin reduction assay (* p-value < 0.05). **(B)** Live/dead assay and scanning electron microscopy (SEM) analysis of BM-MSCs cultured within P3S3 scaffolds.

5.4.2 Hydrostatic pressure characterization using collagen-loaded P3S3 scaffolds

As shown in **Figure 5.2**, changes in the settings of the solenoid-actuated pinch valve in terms of period (s) and duty cycle (%), while maintaining a constant fluid flow (0.3 mL/min) allows the achievement of hydrostatic pressure values within the collagen-loaded P3S3 scaffold falling within the physiological unloading (rest) and physiological loading ranges. Several studies estimated the hydrostatic pressure values during physiological unloading and loading. They showed that at rest, pressure values range between 30 and 60 mmHg (4-8 kPa), while physiological loading results in values greater than or equal to from 80 mmHg (10 kPa) [27]. For this reason, the following settings were chosen to evaluate cell viability within the upgraded automated perfusion bioreactor: 0.3 mL/min with 10s period and 50% duty cycle to simulate physiological loading achieving a pressure value of 15 kPa **(Figure 5.2)**.

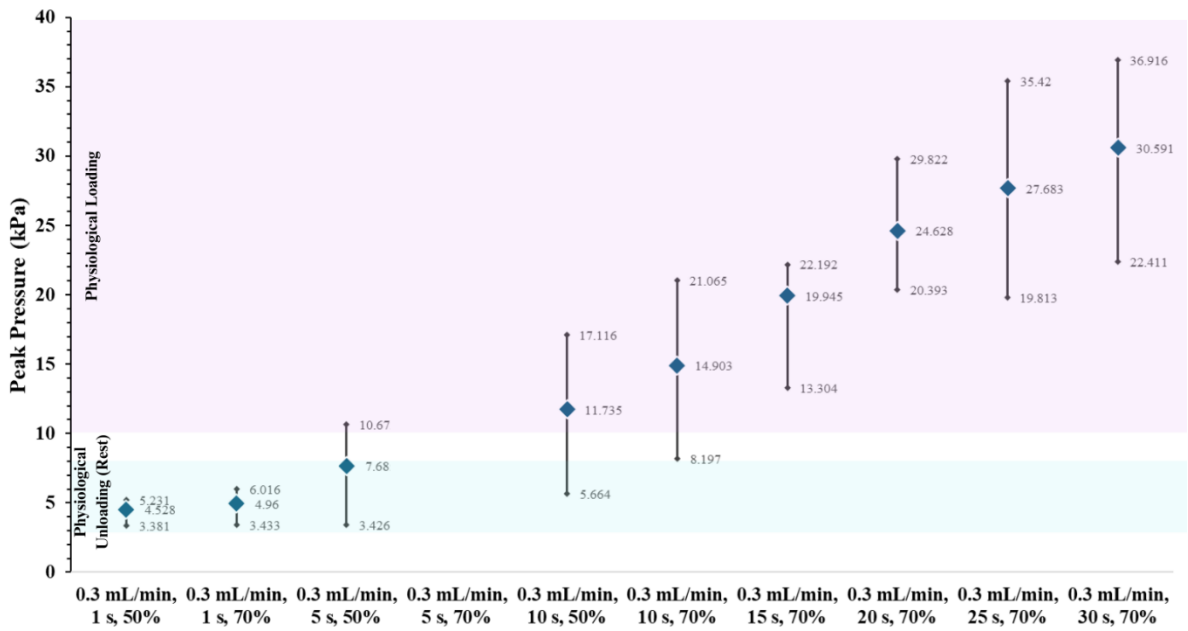

Figure 5.2. Peak pressure values achieved by solenoid-actuated pinch valve falling within physiological unloading and physiological loading ranges. Peak pressure values (kPa) measured using pressure sensors (HJK Sensoren) for a solenoid-actuated pinch valve (Cole Parmer GmbH). The x-axis shows the settings of the upgraded automated perfusion bioreactor: flow rate (mL/min) for perfusion, in addition to period (s) and duty cycle (%) of the pinch valve. Characterizations were performed using P3S3 scaffolds loaded with 150 µL PureCol EZ Gel solution (Merck).

5.4.3 Cell viability and infiltration within the P3S3 scaffolds under dynamic culture conditions simulating a rehabilitation program

When BM-MSCs cultured within P3S3 scaffolds were subjected to a new dynamic culture condition, incorporating fluid flow-induced shear stress and hydrostatic pressure simulating physiological loading, the resazurin reduction assay indicated that the introduction of the new mechanical stimulus did not adversely affect cell viability. On the contrary, hydrostatic pressure resulted in a significant increase in the metabolic activity of BM-MSCs compared to the control group (BM-MSCs exposed to fluid flow-induced shear stress alone), with a p-value < 0.05 (p-value = 0.037) **(Figure 5.3)**.

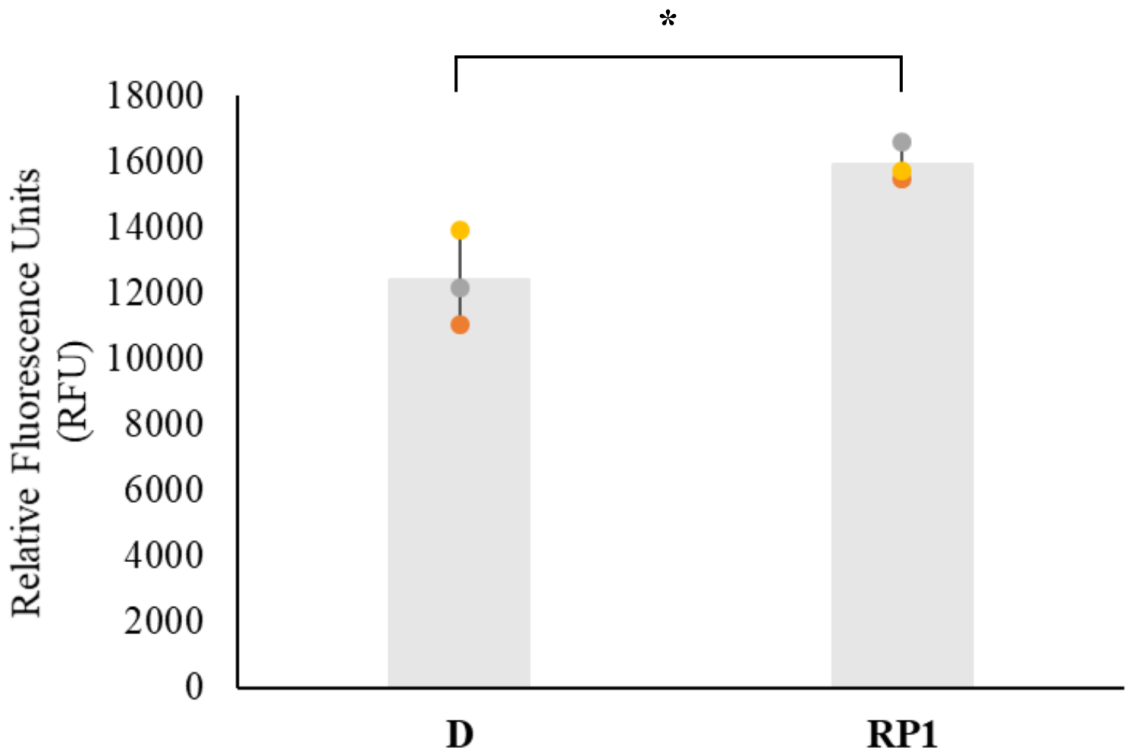

Figure 5.3. *In vitro* cytocompatibility assessment using resazurin reduction assay. Metabolic activity of bone marrow-derived mesenchymal stem cells (BM-MSCs) cultured within P3S3 scaffolds for 14 days under two conditions: direct perfusion providing fluid flow-induced shear stress (D) and a rehabilitation program providing fluid flow-induced shear stress with hydrostatic pressure of 15 kPa simulating physiological loading for 2 h per day (RP1) (*p-value < 0.05).

5.4.4 Gene expression analysis of cells within the P3S3 under dynamic culture conditions simulating a rehabilitation program

The introduction of a hydrostatic pressure of 15 kPa, simulating physiological loading for 2 hours per day over a total duration of 10 days (excluding weekends), induced only slight upregulation in the evaluated genes **(Figure 5.4)**. In details, the upregulations of osteogenesis-related genes were ~1.4 fold-change for RUNX2, ~2.2 fold-change for ALP, ~0.7 fold-change for OPN, ~1 fold-change for OCN, ~2.3 fold-change for MMP3, and ~0.8 fold-change for MMP9. The cation channel, PIEZO1, was upregulated by ~1.6 fold-change. The integrins (ITGAV and ITGA5) as well as the transcriptional coactivators (YAP1 and TAZ1) were upregulated to the same extent, and the values are ~1.2 fold-change and ~2 fold-change, respectively. Members of the RhoA/ROCK signaling pathway and TGFβ/Smad signaling pathway were upregulated by ~1 fold-change, except for SMAD7 whose fold-change is ~1.6. JAK1 was upregulated by ~2.7 fold-change, while MAPK1 by ~2 fold-change. WNT5A and CTNNB1 of the Wnt/β-catenin signaling pathway were upregulated by ~2 fold-change and ~1.6 fold-change, respectively. Finally, NOTCH3 and FZD8 representing genes involved in both cell-cell connections were upregulated by ~1.4 fold-change.

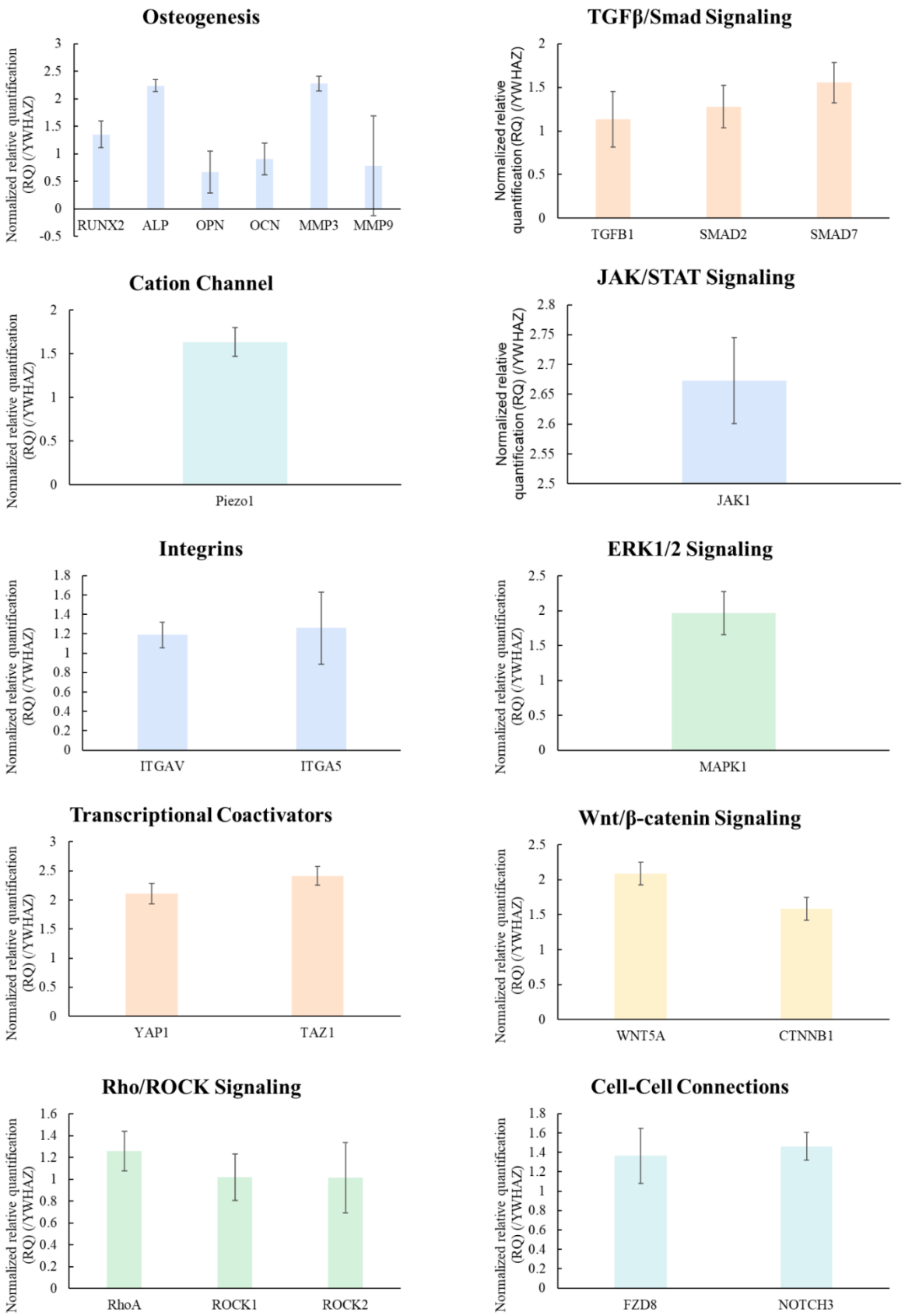

Figure 5.4. Gene expression analyses of bone marrow-derived mesenchymal stem cells (BM-MSCs) cultured within P3S3 scaffolds for 14 days. The relative expressions of various

mRNAs in BM-MSCs cultured under fluid flow-induced shear stress with hydrostatic pressure of 15 kPa simulating physiological loading for 2 h per day (RP1) in comparison to those cultured only under fluid flow-induced shear stress (D) are represented. The relative expressions of the mRNAs were analyzed by reverse transcription-quantitative PCR (RT-qPCR) and were calculated by the $2^{-\Delta\Delta CT}$ method with normalization to the levels of Tyrosine 3-monooxygenase/tryptophan 5-monooxygenase (YWHAZ). Bars represent the mean fold change of three biological replicates +/− standard error of the mean (SEM).

5.5 Discussion

Successful cell seeding onto 3D scaffolds is a critical step in tissue engineering. Initial cell density and seeding efficiency significantly influence osteogenesis, cell viability and cell distribution within the scaffold [28]. In this study, we investigated the efficacy of a 0.5% cell-releasing collagen to seed BM-MSCs within P3S3 scaffolds, a cell seeding method previously shown to result in optimal cell viability, infiltration, and distribution (References to Chapters 2, 3, and 4).

Our findings demonstrate that this method is effective in maintaining cell viability and promoting cell infiltration into the P3S3 scaffolds, in both static and dynamic culture conditions. Furthermore, the novel dynamic culture condition, combining fluid flow-induced shear stress with hydrostatic pressure simulating physiological loading, did not compromise cell viability. These findings are significant as they suggest that the P3S3 scaffolds and the cell seeding method are compatible with the upgraded perfusion bioreactor, which is essential for recapitulating the mechanical environment of native bone tissues.

It is well-established that mechanical stimuli can directly stimulate bone formation by inducing the osteogenic lineage commitment of stem cells [29]. To delve deeper into this phenomenon, we investigated physiological loading-induced osteogenesis by evaluating the expression levels of genes associated with osteogenesis. Our findings revealed that the application of a 15 kPa hydrostatic pressure for 2 h daily over 10 days resulted in a modest upregulation of various genes involved in osteogenesis. Although modest, the upregulation of RUNX2, ALP, OPN, OCN, MMP3, and MMP9 indicates a potential stimulation of osteoblast differentiation and bone matrix mineralization. This finding suggests that while the tested settings of hydrostatic pressure can stimulate cellular responses, the extent of stem cell activation may be influenced by the intensity and duration of the stimulus.

This is consistent with previous studies, which have shown that higher levels of mechanical stress are required to elicit significant increases in bone formation. In a recent study by Ghasemzadeh-Hasankolaei et al. (2023), human adipose-derived MSCs in suspension were exposed to hydrostatic pressure ranging between 5 and 250 for 10 min or 1 h, while encapsulated ones were exposed to cyclic hydrostatic pressure (6 cycles of 10 min each) at 5 or 50 MPa for three times per week, up to three weeks. The results showed that osteogenic differentiation process is magnitude-dependent, and the authors obtained better osteogenic differentiation with the 50 MPa group [30]. Similar outcomes were obtained by Stavenschi et al. (2018), who exposed human BM-MSCs to cyclic hydrostatic pressure of 10 kPa, 100 kPa and 300 kPa magnitudes at frequencies of 0.5 Hz, 1 Hz and 2 Hz for 1 h, 2 h and 4 h of stimulation. The authors concluded that osteogenic differentiation of stem cells depends on the intensity and frequency of the stimulation, and that higher intensity and frequency (300 kPa, 2 Hz) led to the strongest bone-forming response. However, even lower-intensity stimulation (10 kPa) was sufficient to promote collagen production and mineral deposition [31]. Cheng et al. (2022) applied hydrostatic pressure of a magnitude of 30 kPa for 1 h per

day for up to 12 days to placenta-derived multipotent cells (PDMCs), and showed that these settings of the hydrostatic pressure were able to enhance calcium deposition and facilitate osteogenic differentiation [32].

When Neßler et al. (2016) explored how applied hydrostatic pressure with 0-279 kPa and a frequency of 0.005-2 Hz affects mineral deposition by comparing simulation results with experimental data, they concluded that bone cells respond to pressure in two ways: (1) through a mechanism of "cell memory," which allows cells to remember past pressure exposure, influencing their current mineralization behavior, and (2) through a process of "cell recovery," suggesting that cells need time to recover from periods of intense mineralization [33]. The same pressure and frequency values were evaluated by Henstock et al. (2013) on organotypically cultured *ex vivo* chick fetal femurs, and also concluded that cyclic, rather than static, hydrostatic pressure plays a crucial role in bone growth and remodeling [34]. Other authors also highlighted the importance of applying cyclic hydrostatic pressure rather than static ones, which were unable to induce osteogenic differentiation of human MSCs in 3D collagen hydrogel cultures even at magnitudes as high as 280 kPa [35].

Beyond understanding how cells react to physical forces, it is critical to unravel the underlying molecular mechanisms of bone growth and repair. This knowledge will not only help us understand normal and abnormal bone responses to mechanical stress but also pave the way for new treatments for bone diseases. Emerging research is shedding light on the intricate molecular mechanisms underlying mechanotransduction, revealing several key molecules and pathways involved in this process. Effectors of mechanotransduction include the Piezo channels (Piezo1 and Piezo 2), integrins, and transcriptional coactivators (mainly YAP1 and TAZ1); whereas, signaling pathways include RhoA/ROCK signaling pathway, TGFβ/Smad signaling pathway, JAK/STAT signaling pathway, Wnt/β-catenin signaling pathway, and ERK1/2 signaling pathway [36,37].

For this reason, in our study, we evaluated the gene expression levels of various molecules involved in mechanotransduction. The upregulation of PIEZO1, a mechanosensitive ion channel, suggests its potential role in transducing hydrostatic pressure signals into cellular responses. The activation of integrins and YAP/TAZ, known players in mechanotransduction, further supports this notion. The upregulation of molecules involved in the RhoA/ROCK, TGFβ/Smad, JAK/STAT, and Wnt/β-catenin signaling pathways suggests their involvement in mediating the effects of hydrostatic pressure on MSCs. These pathways are known to regulate a variety of cellular processes, including proliferation, differentiation, and apoptosis [36]. The upregulation of NOTCH3 and FZD8, implicated in cell-cell communication, suggests that hydrostatic pressure may also influence cell-cell interactions.

Yet, the upregulation of the evaluated genes was not significant. This can be linked to the modest upregulation in the genes involved in osteogenesis, as explained above. Although we did not observe significant differential expression of the genes examined, previous studies have identified alterations in these genes under different conditions. Sugimoto et al. (2017) exposed a variety of cells (e.g. primary BM-MSCs, immortalized BM-MSCs and osteoblasts) as well as

medaka fish to 0.01 MPa (10 kPa) hydrostatic loading for 10 days. The authors showed that continuous induction with hydrostatic loading induced osteogenic differentiation, and also highlighted the role of hydrostatic pressure in activating PIEZO1, which in turn induced the expression of bone morphogenetic protein 2 (BMP2). Moreover, the authors showed that ERK1/2 and p38 mitogen-activated protein kinase signaling, but not transient receptor potential cation channel subfamily V member 4 (TRPV4), c-Jun N-terminal kinase (JNK), and Smad signaling pathway are also involved in the mechanosensitive cell fate determination in multipotent stem cells [38]. However, in their study, the authors exposed cells to continuous hydrostatic pressure simulating physiological loading, while in our study, physiological loading was simulated for 2 h per day.

While many studies have explored the impact of mechanical forces on cellular function and molecular mechanisms involved in bone regeneration, the findings are often inconsistent. This inconsistency can be attributed to various factors, such as cell type, culture conditions, and substrate properties. Additionally, the precise nature of the mechanical force applied, including its frequency, intensity, and duration, can significantly influence cellular responses [39]. In contrast to previous studies, which examined cells in diverse environments, our study uniquely combined hydrostatic pressure with fluid flow-induced shear stress and employed 3D models that mimic trabecular bone. Thus, to fully understand how mechanical forces affect stem cells, it is important to carefully control these factors and study them one at a time.

5.6 Conclusions

This study successfully demonstrated the feasibility of seeding BM-MSCs onto PLA scaffolds mimicking the human trabecular bone architecture in physiological conditions and resembling the morphological features of bones, specifically the ulna, tibia, and femur (referred to in this Chapter as P3S3), using 0.5% cell-releasing collagen. The viability of BM-MSCs within the scaffolds was not influenced by the administration of mechanical stimuli, which are fluid flow-induced shear stress and hydrostatic pressure simulating physiological loading. The application of a 15 kPa hydrostatic pressure for 2 h daily over a 10-day period resulted in a modest upregulation of genes associated with osteogenesis and mechanotransduction in BM-MSCs cultured on the P3S3 scaffolds. While these findings suggest that hydrostatic pressure can stimulate cellular responses, further research is needed to optimize the magnitude and duration and of the stimulus to maximize bone formation.

5.7. Fundings

This study was carried out within the BIGMECH project – funded by the European Union – Next Generation EU within the PRIN 2022 program (D.D. 104 - 02/02/2022 Ministero dell'Università e della Ricerca). This manuscript reflects only the authors' views and opinions and the Ministry cannot be considered responsible for them.

5.8 Acknowledgments

I would like to thank Dr. Eleonora Zenobi and Dr. Elisa Scateno for kindly providing the 3D-printed PLA scaffolds, as well as Prof. Diana Massai, Dr. Stefano Gabetti, and Dr. Beatrice Masante for kindly providing the upgraded perfusion bioreactor. I would also like to thank Prof. Lia Rimondini and Prof. Andrea Cochis for their supervision.

5.9 References

1. Turunen, M.J., Prantner, V., Jurvelin, J.S., Kröger, H., and Isaksson, H. (2013) Composition and microarchitecture of human trabecular bone change with age and differ between anatomical locations. *Bone*, **54** (1), 118–125.
2. Diederichs, G., Link, T.M., Kentenich, M., Schwieger, K., Huber, M.B., Burghardt, A.J., Majumdar, S., Rogalla, P., and Issever, A.S. (2009) Assessment of trabecular bone structure of the calcaneus using multi-detector CT: Correlation with microCT and biomechanical testing. *Bone*, **44** (5), 976–983.
3. Paschalis, E.P., Mendelsohn, R., and Boskey, A.L. (2011) Infrared Assessment of Bone Quality: A Review. *Clin Orthop Relat Res*, **469** (8), 2170.

4. Fonseca, H., Moreira-Gonçalves, D., Coriolano, H.J.A., and Duarte, J.A. (2014) Bone quality: The determinants of bone strength and fragility. *Sports Medicine*, **44** (1), 37–53.
5. Dalle Carbonare, L., and Giannini, S. (2004) Bone microarchitecture as an important determinant of bone strength. *J Endocrinol Invest*, **27** (1), 99–105.
6. Robling, A.G., and Turner, C.H. (2009) Mechanical Signaling for Bone Modeling and Remodeling. *Crit Rev Eukaryot Gene Expr*, **19** (4), 319.
7. Zhang, P., Hamamura, K., and Yokota, H. (2008) A Brief Review of Bone Adaptation to Unloading. *Genomics Proteomics Bioinformatics*, **6** (1), 4–7.
8. Turner, C.H. (1998) Three rules for bone adaptation to mechanical stimuli. *Bone*, **23** (5), 399–407.
9. Wang, X., Wang, Y., Gou, W., Lu, Q., Peng, J., and Lu, S. (2013) Role of mesenchymal stem cells in bone regeneration and fracture repair: A review. *Int Orthop*, **37** (12), 2491–2498.
10. Liao, X., Lu, S., Zhuo, Y., Winter, C., Xu, W., Li, B., and Wang, Y. (2011) Bone Physiology, Biomaterial and the Effect of Mechanical/Physical Microenvironment on MSC Osteogenesis: A Tribute to Shu Chien's 80th Birthday. *Cell Mol Bioeng*, **4** (4), 579.
11. Karageorgiou, V., and Kaplan, D. (2005) Porosity of 3D biomaterial scaffolds and osteogenesis. *Biomaterials*, **26** (27), 5474–5491.
12. Ma, Q., Miri, Z., Haugen, H.J., Moghanian, A., and Loca, D. (2023) Significance of mechanical loading in bone fracture healing, bone regeneration, and vascularization. *J Tissue Eng*, **14**.
13. Yeatts, A.B., and Fisher, J.P. (2011) Bone tissue engineering bioreactors: Dynamic culture and the influence of shear stress. *Bone*, **48** (2), 171–181.
14. Chen, H.C., and Hu, Y.C. (2006) Bioreactors for tissue engineering. *Biotechnol Lett*, **28** (18), 1415–1423.
15. Gustin, P., and Prasad, A. (2024) EnduroBone: A 3D printed bioreactor for extended bone tissue culture. *HardwareX*, **18**, e00535.
16. Dua, R., Jones, H., and Noble, P.C. (2021) Designing and validation of an automated ex-vivo bioreactor system for long term culture of bone. *Bone Rep*, **14**, 101074.
17. Smith, L.J., Li, P., Holland, M.R., and Ekser, B. (2018) FABRICA: A Bioreactor Platform for Printing, Perfusing, Observing, & Stimulating 3D Tissues. *Scientific Reports 2018 8:1*, **8** (1), 1–10.
18. Viveen, J., Perilli, E., Zahrooni, S., Jaarsma, R.L., Doornberg, J.N., and Bain, G.I. (2023) Three-dimensional cortical and trabecular bone microstructure of the proximal ulna. *Arch Orthop Trauma Surg*, **143** (1), 213–223.
19. Bolbos, R.I., Zuo, J., Banerjee, S., Link, T.M., Benjamin Ma, C., Li, X., and Majumdar, S. (2008) Relationship between trabecular bone structure and articular cartilage morphology and relaxation times in early OA of the knee joint using parallel MRI at 3T. *Osteoarthritis and cartilage / OARS, Osteoarthritis Research Society*, **16** (10), 1150.
20. Pecci, R., Baiguera, S., Ioppolo, P., Bedini, R., and Del Gaudio, C. (2020) 3D printed scaffolds with random microarchitecture for bone tissue engineering applications: Manufacturing and characterization. *J Mech Behav Biomed Mater*, **103**, 103583.
21. James, S., Fox, J., Afsari, F., Lee, J., Clough, S., Knight, C., Ashmore, J., Ashton, P., Preham, O., Hoogduijn, M., Ponzoni, R.D.A.R., Hancock, Y., Coles, M., and Genever, P. (2015) Multiparameter Analysis of Human Bone Marrow Stromal Cells Identifies Distinct

Immunomodulatory and Differentiation-Competent Subtypes. *Stem Cell Reports*, **4** (6), 1004–1015.
22. Schmittgen, T.D., and Livak, K.J. (2008) Analyzing real-time PCR data by the comparative CT method. *Nature Protocols 2008 3:6*, **3** (6), 1101–1108.
23. Livak, K.J., and Schmittgen, T.D. (2001) Analysis of Relative Gene Expression Data Using Real-Time Quantitative PCR and the 2−ΔΔCT Method. *Methods*, **25** (4), 402–408.
24. R: The R Project for Statistical Computing.
25. Posit | The Open-Source Data Science Company.
26. Wickham, H., Averick, M., Bryan, J., Chang, W., McGowan, L.D., François, R., Grolemund, G., Hayes, A., Henry, L., Hester, J., Kuhn, M., Pedersen, T.L., Miller, E., Bache, S.M., Müller, K., Ooms, J., Robinson, D., Seidel, D.P., Spinu, V., Takahashi, K., Vaughan, D., Wilke, C., Woo, K., and Yutani, H. (2019) Welcome to the Tidyverse. *J Open Source Softw*, **4** (43), 1686.
27. Gurkan, U.A., and Akkus, O. (2008) The mechanical environment of bone marrow: A review. *Ann Biomed Eng*, **36** (12), 1978–1991.
28. Bouet, G., Marchat, D., Cruel, M., Malaval, L., and Vico, L. (2015) In vitro three-dimensional bone tissue models: from cells to controlled and dynamic environment. *Tissue Eng Part B Rev*, **21** (1), 133–156.
29. Chen, J.C., and Jacobs, C.R. (2013) Mechanically induced osteogenic lineage commitment of stem cells. *Stem Cell Res Ther*, **4** (5), 1–10.
30. Ghasemzadeh-Hasankolaei, M., Pinto, C.A., Jesus, D., Saraiva, J.A., and Mano, J.F. (2023) Effect of high cyclic hydrostatic pressure on osteogenesis of mesenchymal stem cells cultured in liquefied micro-compartments. *Mater Today Bio*, **23**, 100861.
31. Stavenschi, E., Corrigan, M.A., Johnson, G.P., Riffault, M., and Hoey, D.A. (2018) Physiological cyclic hydrostatic pressure induces osteogenic lineage commitment of human bone marrow stem cells: A systematic study. *Stem Cell Res Ther*, **9** (1), 1–13.
32. Cheng, C.C., Chung, C.A., Chang, C.J., Cheng, Y.C., Huang, C.J., Chien, C.C., and Lin, H.T. (2022) Hydrostatic pressure facilitates calcium deposition and osteogenic gene expression in the osteoblastic differentiation of placenta-derived multipotent cells. *Taiwan J Obstet Gynecol*, **61** (2), 270–276.
33. Neßler, K.H.L., Henstock, J.R., El Haj, A.J., Waters, S.L., Whiteley, J.P., and Osborne, J.M. (2016) The influence of hydrostatic pressure on tissue engineered bone development. *J Theor Biol*, **394**, 149–159.
34. Henstock, J.R., Rotherham, M., Rose, J.B., and El Haj, A.J. (2013) Cyclic hydrostatic pressure stimulates enhanced bone development in the foetal chick femur in vitro. *Bone*, **53** (2), 468–477.
35. Henstock, J.R., Price, J.C.F.A., and El Haj, A.J. (2024) Determining Which Hydrostatic Pressure Regimes Promote Osteogenesis in Human Mesenchymal Stem Cells. *Tissue Eng Regen Med*, **21** (8), 1141.
36. Di, X., Gao, X., Peng, L., Ai, J., Jin, X., Qi, S., Li, H., Wang, K., and Luo, D. (2023) Cellular mechanotransduction in health and diseases: from molecular mechanism to therapeutic targets. *Signal Transduction and Targeted Therapy 2023 8:1*, **8** (1), 1–32.
37. Sun, Y., Wan, B., Wang, R., Zhang, B., Luo, P., Wang, D., Nie, J.J., Chen, D., and Wu, X. (2022) Mechanical Stimulation on Mesenchymal Stem Cells and Surrounding

Microenvironments in Bone Regeneration: Regulations and Applications. *Front Cell Dev Biol*, **10**, 808303.

38. Sugimoto, A., Miyazaki, A., Kawarabayashi, K., Shono, M., Akazawa, Y., Hasegawa, T., Ueda-Yamaguchi, K., Kitamura, T., Yoshizaki, K., Fukumoto, S., and Iwamoto, T. (2017) Piezo type mechanosensitive ion channel component 1 functions as a regulator of the cell fate determination of mesenchymal stem cells. *Scientific Reports 2017 7:1*, **7** (1), 1–14.
39. Goetzke, R., Sechi, A., De Laporte, L., Neuss, S., and Wagner, W. (2018) Why the impact of mechanical stimuli on stem cells remains a challenge. *Cellular and Molecular Life Sciences 2018 75:18*, **75** (18), 3297–3312.

Conclusion & Future Prospective

Notwithstanding the limitations inherent to our specific experimental models, the underlying principles and conclusions have broader implications.

In **Chapter 1**, we described the development of a perfusion bioreactor that offers a powerful investigation tool for *in vitro* bone biology research. Its versatility in delivering customizable biomechanical and biophysical stimuli, combined with automated control, enables precise investigation of the effects of fluid flow-induced shear stress and pulsed electromagnetic field (PEMF) stimulation on bone cell differentiation and tissue formation.

In **Chapter 2**, the automated perfusion bioreactor was used for culturing 3D-printed polylactic acid (PLA) scaffolds mimicking the human trabecular bone architecture in physiological condition and the morphological features of the iliac crest (referred to as PLA600). We were able to demonstrate that 0.5% cell-releasing collan is optimal for efficient cell seeding and basal medium rather than osteogenic medium allows the detection of the effects of PEMF stimulation on bone marrow-derived mesenchymal stem cells (BM-MSCs) cultured in a more physiologically relevant environment.

In **Chapter 3**, transcriptomic analysis revealed the complex molecular mechanisms underlying the response of BM-MSCs to PEMF stimulation. The identified gene signatures provide valuable insights into the potential of PEMF as a therapeutic tool for bone regeneration.

In **Chapter 4**, PLA600 seeded with BM-MSCs using 0.5% collagen were tested in the upgraded automated perfusion bioreactor that enables the delivery of controllable fluid flow-induced shear stress and hydrostatic pressure simulating physiological unloading and loading. We were able to demonstrate that fluid flow-induced shear stress and hydrostatic pressure simulating physiological unloading, did not compromise cell viability, and as such, this platform enables a more accurate understanding of bone cell behavior and tissue formation.

In **Chapter 5**, we applied the upgraded automated perfusion bioreactor with a new PLA scaffold mimicking the human trabecular bone architecture in physiological conditions and resembling the morphological features of bones, specifically the ulna, tibia, and femur (referred to in this Chapter as P3S3). After culturing BM-MSCs seeded on these scaffolds under fluid flow-induced shear stress in the absence and presence of hydrostatic pressure simulating physiological loading (2 h per day, 10-day period) modest upregulation in genes involved in osteogenesis and mechanotransduction were detected. The study demonstrated that hydrostatic pressure can stimulate osteogenic differentiation of BM-MSCs, yet, further optimization of pressure parameters is needed to maximize bone formation.

Future experiments will aim to optimize rehabilitation programs simulated using the upgraded automated perfusion bioreactor. These programs will be progressive, with the magnitude of hydrostatic pressure increasing weekly. Additionally, PEMF stimulation will be integrated into the simulated rehabilitation program.

Overall, many obstacles are still in the way of a complete integration of advanced technologies for the optimization of *in vitro* experiments aimed at studying biophysical stimulation. However, this and other works provide important insights on how challenges can be addressed and workflows adapted to reap the benefits of advanced technologies for the *in vitro* study of complex biological processes, which is crucial to reduce the use of animals in research.

Fundings

This study was carried out within the BIGMECH project – funded by European Union – Next Generation EU within the PRIN 2022 program (D.D. 104 - 02/02/2022 Ministero dell'Università e della Ricerca). This manuscript reflects only the authors' views and opinions and the Ministry cannot be considered responsible for them.

Acknowledgments

Thank you to all the wonderful people at CAAD for their support and guidance during my time here. I am especially grateful to my colleagues, PhD students, and technicians who patiently answered my questions and helped me learn new techniques, as well as to Daiana and Giovanni for their warm welcome every day.

I would also like to express my sincere appreciation to the collaborators who provided essential tools and resources for our research. Eleonora Zenobi and Elisa Scatena generously supplied the scaffolds, while Professors Diana Massai, Beatrice Masante, Stefano Gabetti, and Simone Israele provided the bioreactor.